NASA CONTRACTOR REPORT

NASA CR-1593

DEVELOPMENT OF AN ACTIVE OPTICS CONCEPT USING A THIN DEFORMABLE MIRROR

by Hugh J. Robertson

Prepared by
THE PERKIN-ELMER CORPORATION
Norwalk, Conn.
for Langley Research Center

NATIONAL AERONAUTICS AND SPACE ADMINISTRATION • WASHINGTON, D. C. • AUGUST 1970

NASA CR-1593

DEVELOPMENT OF AN ACTIVE OPTICS CONCEPT USING A THIN DEFORMABLE MIRROR

By Hugh J. Robertson

116 p.
Refs p 116
1. Telescopes

Prepared under Contract No. NAS 1-7103 by
THE PERKIN-ELMER CORPORATION
Norwalk, Conn.

for Langley Research Center

NATIONAL AERONAUTICS AND SPACE ADMINISTRATION

For sale by the Clearinghouse for Federal Scientific and Technical Information
Springfield, Virginia 22151 – CFSTI price $3.00

CONTENTS

Page

LIST OF ILLUSTRATIONS

DEVELOPMENT OF AN ACTIVE OPTICS CONCEPT

USING A THIN DEFORMABLE MIRROR

By Hugh J. Robertson
The Perkin-Elmer Corporation, Norwalk, Conn.

SUMMARY

The large booster capability developed by the National Aeronautics and Space Administration has made it possible to place large astronomical telescopes in orbit where they should be able to perform considerably better than can ground based telescopes, which are limited by atmospheric turbulence. To take full advantage of the better seeing conditions above the atmosphere requires a telescope capable of diffraction-limited performance. The optical surfaces in such a telescope must be maintained to very close tolerances and this is particularly difficult with the primary mirror because of its size, if conventional telescope construction techniques are employed.

As a new approach, differing from traditional telescope construction methods, Perkin-Elmer introduced the concept of Active Optics which consists of measuring the surface shape, or figure, of a telescope primary mirror, computing the necessary electronics control signals, and physically aligning the mirror to its theoretical design figure. The merit of the Active Optical approach is that system performance is not limited by uncertainties in manufacturability and in thermal and temporal dimensional stability.

The Active Optics concept was first applied to the development of a 20-inch mirror composed of three segments whose alignment was controlled automatically to diffraction-limited tolerances.

This report describes the design, construction and test results of an active control experiment with a 30-inch diameter thin flexible mirror whose surface was aligned by straining the mirror with an array of actuators distributed across its back. Sixty-one points of force application were used to provide a test of the servo response characteristics of a high order, multi-

loop control system with the strong interactions that would be encountered in a very large flexible primary mirror.

The initial figure error of the 30-inch mirror, which was greater than 1/2 wavelength rms, was decreased by active alignment to less than 1/50 wavelength rms, which betters the requirement for diffraction-limited performance.

OBJECTIVES

It has now become feasible to orbit large optical systems for astronomical research. Large-aperture telescopes with diffraction-limited performance are desired to provide the optical resolution made possible in the absence of atmospheric turbulence. It will be difficult to obtain and preserve the close tolerances required for diffraction-limited performance of the large elements of such a telescope if these elements are constructed and mounted with the techniques traditionally applied to ground-based telescopes. The Active Optics approach makes use of recent developments in interferometric figure sensing and servo-mechanical control techniques to provide a new technique for obtaining the desired optical performance.

Segmented Active Optics

The fundamental concept of Active Optics consists of measuring the surface shape (or figure) of a telescope primary mirror, computing the necessary electronic control signals, and physically aligning the mirror to its original design figure. The basic building blocks of the active system are shown in figure 1 and include an interferometric figure sensor for detection of errors of the mirror surface figure, actuators to provide the precise mechanical displacement of the mirror surface required, and electronics for converting the errors observed by the figure sensor, controlling voltages, and applying those voltages to the appropriate actuators to make error corrections. The initial experiment performed at Perkin-Elmer to demonstrate the feasibility of the concept consisted of measuring and correcting the alignment of individual elements of a segmented mirror (refs. 1 and 2). The specific ob-

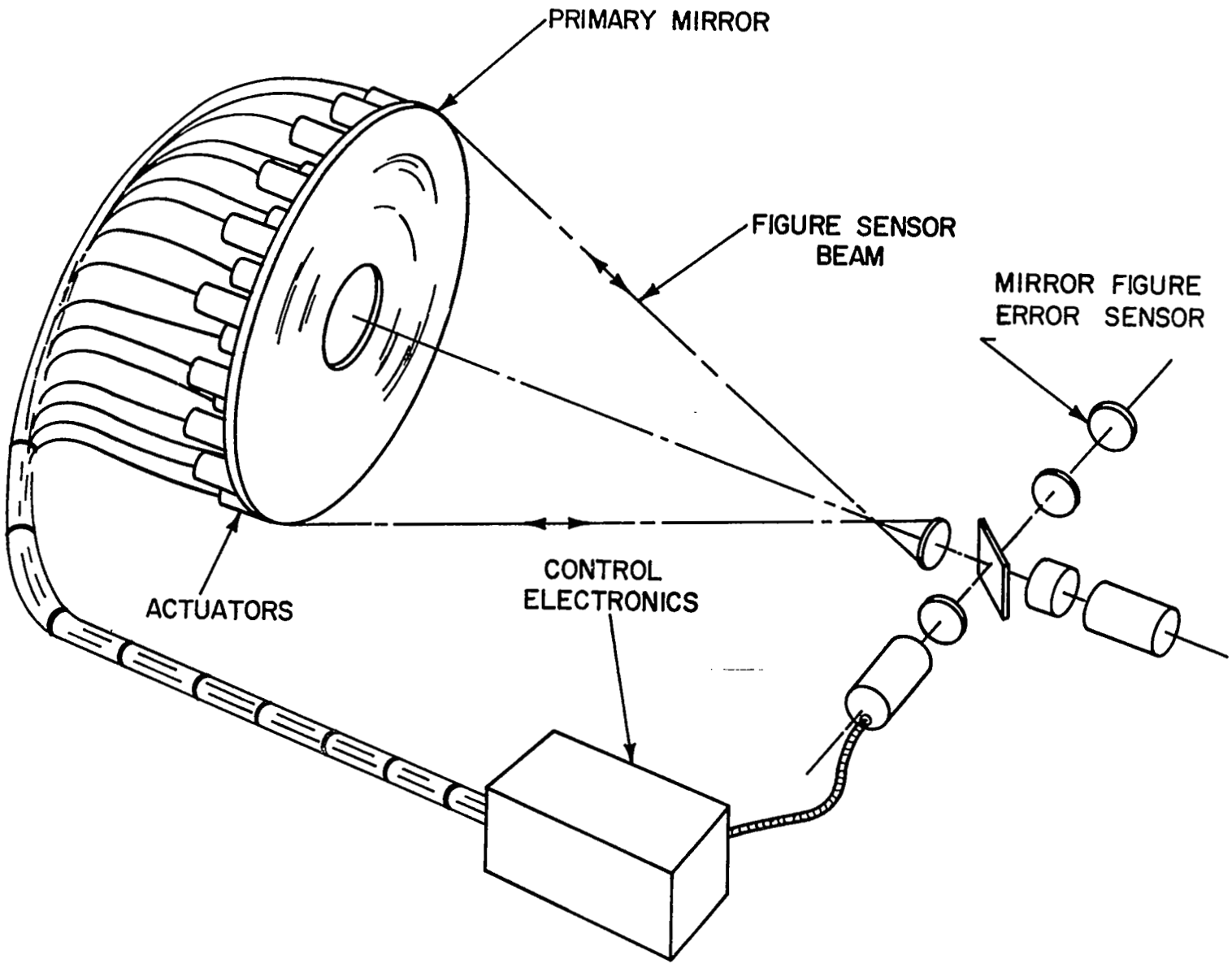

Figure 1. Deformable Mirror Active Optics Concept

jective of the experiment was to automatically align and maintain closed-loop control of a 20-inch, three-segment mirror to within 1/20 wavelength rms of the design figure.

The experiment was most successful. Diffraction-limited performance was obtained, as proven by several independent optical tests. The composite figure of the segmented mirror assembly with closed-loop control was measured to deviate from the design figure by less than 1/40 of a wavelength rms.

Deformable Active Optics

The next logical step in the development of the Active Optics Concept was to determine the relative merits of a servo stressed flexible mirror approach.

The objective of the program, which is the subject of this report, was to investigate, analytically and experimentally, the feasibility of obtaining diffraction-limited optics for space application by actively stressing a thin flexible mirror into the proper shape. For the purpose of this project, the reference shape was spherical.

The program was divided into two phases.

In Phase I the specific objectives were:

(a) To analytically determine the parameters for a thin mirror as follows:

(1) Optimum thickness-to-diameter ratio.

(2) Optimum placement and type of actuator to be used.

(3) Required figure accuracy prior to active control, i.e., manufacturing tolerance to achieve a final 1/20 λ rms error.

(4) Effect of mirror interactions, including discontinuities in the mirror surface, such as the boundaries imposed by a finite radius and a hole in the center of the mirror.

(5) Predicted rms figure error during active control of the mirror.

(b) To design, fabricate, and evaluate an actuator of the type determined by the above analysis, for use in the thin mirror control system.

(c) To design the control system in sufficient detail to show its feasibility.

(d) To fabricate and test a 30-inch-diameter, thin, fused-silica mirror. (The 30-inch diameter was chosen as appropriate for use in the existing vacuum tank facility.) Accuracy of figure, thickness and f/number of the mirror were to be those determined by the above analysis as the most appropriate for the magnitude and scale of corrections to be made. The tests were to be of a quantitative nature and of sufficient accuracy to allow comparison of the mirror before and after stressing.

In Phase II the specific objectives were:

(a) To fabricate a suitable mounting assembly with actuators to provide the forces and displacements required to strain the thin mirror and produce the necessary figure corrections to achieve the design goal figure accuracy of 1/20 λ rms.

(b) To design and fabricate the electronics required to generate control signals for the individual actuators from the figure sensor developed under NASA Contract NAS1-5198 (i.e., the segmented mirror experiment).

(c) To combine the figure sensor, electronics, actuators, and mirror into an automatic control system, the design objective of which was to maintain the figure error to within 1/20 λ rms or better. Sequencing and programming could be done manually.

(d) To evaluate the closed-loop operation of the control system to determine the accuracy of operation, employing the knife-edge test, the point source test, and scans of the mirror surface with the phase measurement interferometer.

Summary of Results

(a) The mirror was fabricated from fused silica to the following dimensions:

Diameter	- 30 inches
Thickness	- 0.50 inch
Radius of Curvature	- 178 inches

(b) A force application arrangement of 61 points located hexagonally (figure 2) on 3.75-inch centers was selected to remove errors of the spatial frequency expected and to test predictions for response of a high-order interacting control system.

(c) A theoretical approach for synthesizing a stable high-order interacting control system was developed. Predicting stability required knowledge of the mirror reaction to the multiple forces used to maintain the desired mirror figure. A structural analysis program was used to obtain estimates of the static deflections of a point-loaded, thin, shallow, spherical mirror. The calculated deflections were compared to experimentally measured deflections and the results were reported in reference 3. The analytical program was used to determine the properties of the 30-inch-diameter mirror, from which it was possible to predict that a stable control system could be designed.

A control system was designed and built employing parallel analog control channels and using a matrix of feedforward elements to counteract the effect of the mirror interaction and hence improve servo response. From the analysis of the mirror interaction, feedforward network values were determined.

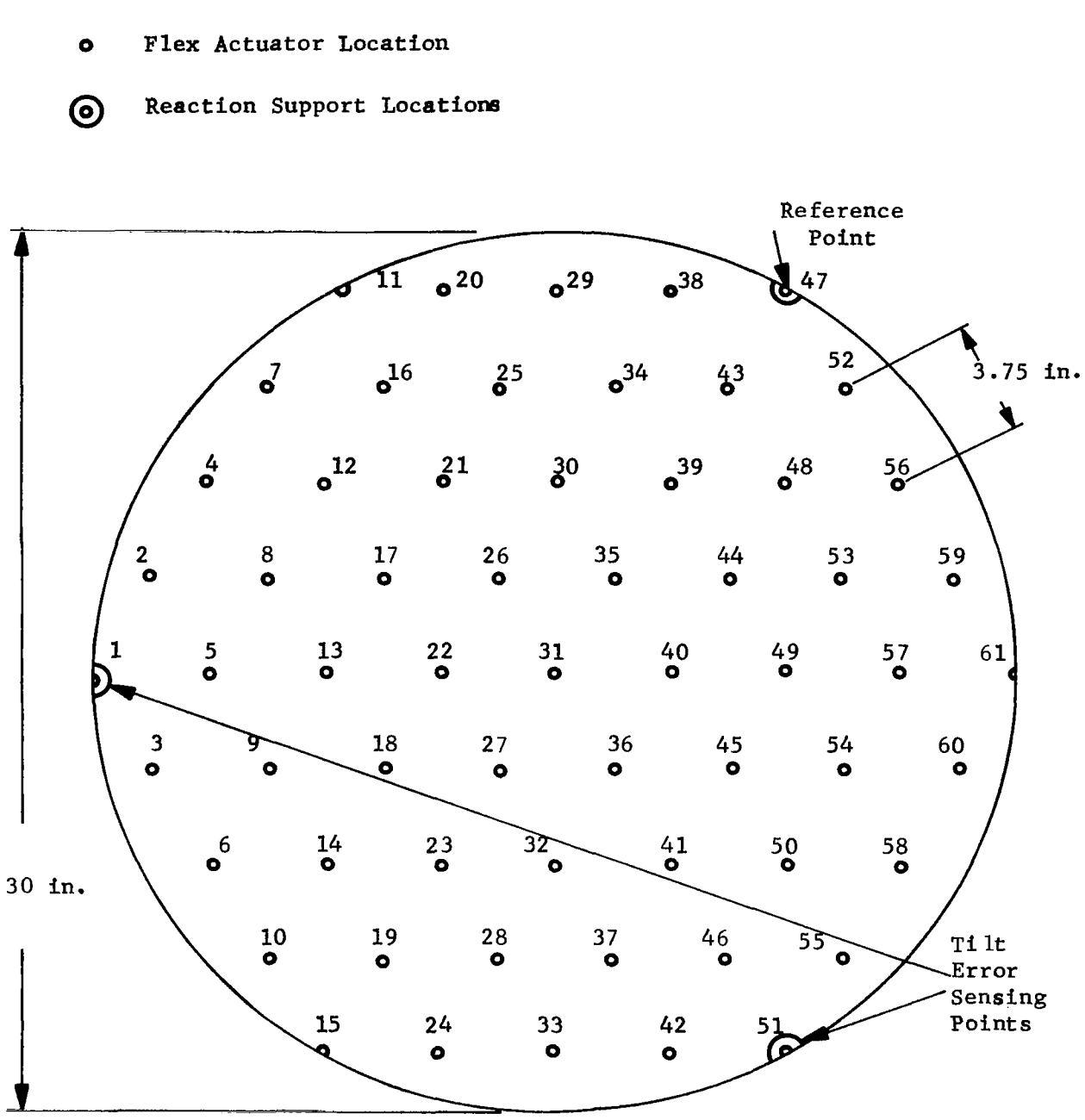

Figure 2. Actuator and Reaction Support Locations on Thin Deformable Mirror

(d) Differential spring type actuators capable of applying forces with a range of plus or minus two pounds and producing local displacements of a wavelength were designed and built.

(e) A mirror support system to minimize the external stresses on the mirror due to the mounting arrangement itself was designed and constructed.

(f) The existing phase measurement interferometer figure sensor was modified for use with the thin mirror control system by adding tilt and focus control and a photodiode matrix for parallel sensing of the 61 mirror image points corresponding to the actuator locations.

(g) The mirror, actuators, and support system were assembled and mounted in a vacuum tank.

(h) The mirror was aligned, and the accuracy of alignment and the precision and response of the control system were tested with the following results:

(1) The final mirror figure with a near optimum mirror-to-figure-sensor spacing was measured to be better than $\lambda/50$ rms by analysis of interferograms and profile scans, and this performance was qualitatively confirmed by pinhole tests.

(2) The control system response to step disturbances verified the theoretical predictions, and the control precision was observed to be better than 1/150 wavelength rms, from repeatibility measurements made with the profile scan test.

SYSTEM STEADY STATE PERFORMANCE

Alignment Accuracy

Four measurement techniques were employed to obtain a quantitative, as well as a qualitative evaluation of the accuracy and precision of the mirror alignment during control. Information was obtained about the amplitude of departure of the controlled surface from ideal (both locally and rms), the precision and repeatability of the control system, and the dynamic range of the system (i.e., its ability to remove large errors).

Interferograms.- One of the most graphic techniques for obtaining mirror figure accuracy is by recording the output of a test interferometer photographically. In this case, the test interferometer was already set up and aligned as the figure sensor in the Active Optics control loop. This test shows the local deformations of the mirror quantitatively to within the accuracy of the errors introduced by the interferometer itself, which were previously shown to be less than 1/50 λ peak (ref. 4). For a spherical mirror the interferograms are very easy to interpret. Figure 3 shows an interferogram of the mirror in a relaxed state before alignment. Each fringe indicates a 1/2-wavelength change in figure error with respect to a perfect sphere.

Figure 4 shows an interferogram of the mirror after alignment by the Active Optics control system. In this case, the wavefront in one arm of the interferometer was tipped relative to the wavefront in the other arm in order to obtain a set of parallel straight-line fringes. The deviation of these fringes from a straight line and from uniform spacing is proportional to the deformation at the mirror, again, within the accuracy allowed by any errors introduced by the interferometer.

Models of the figure error before and after alignment as measured from the interferograms are shown in figure 5. Departure from a best-fit sphere is shown to the same scale in both models. Each level in the before-alignment model represents 1/2 wavelength at 6328Å or approximately 12 microinches. Each level in the after-alignment model represents 1/40 wavelength or approximately 5/8 microinch.

Figure 3. Interferogram of 30-Inch Mirror Before Alignment, Supported with Optical Axis Horizontal (Weight supported at the 58 actuation points and at the 3 reaction support points)

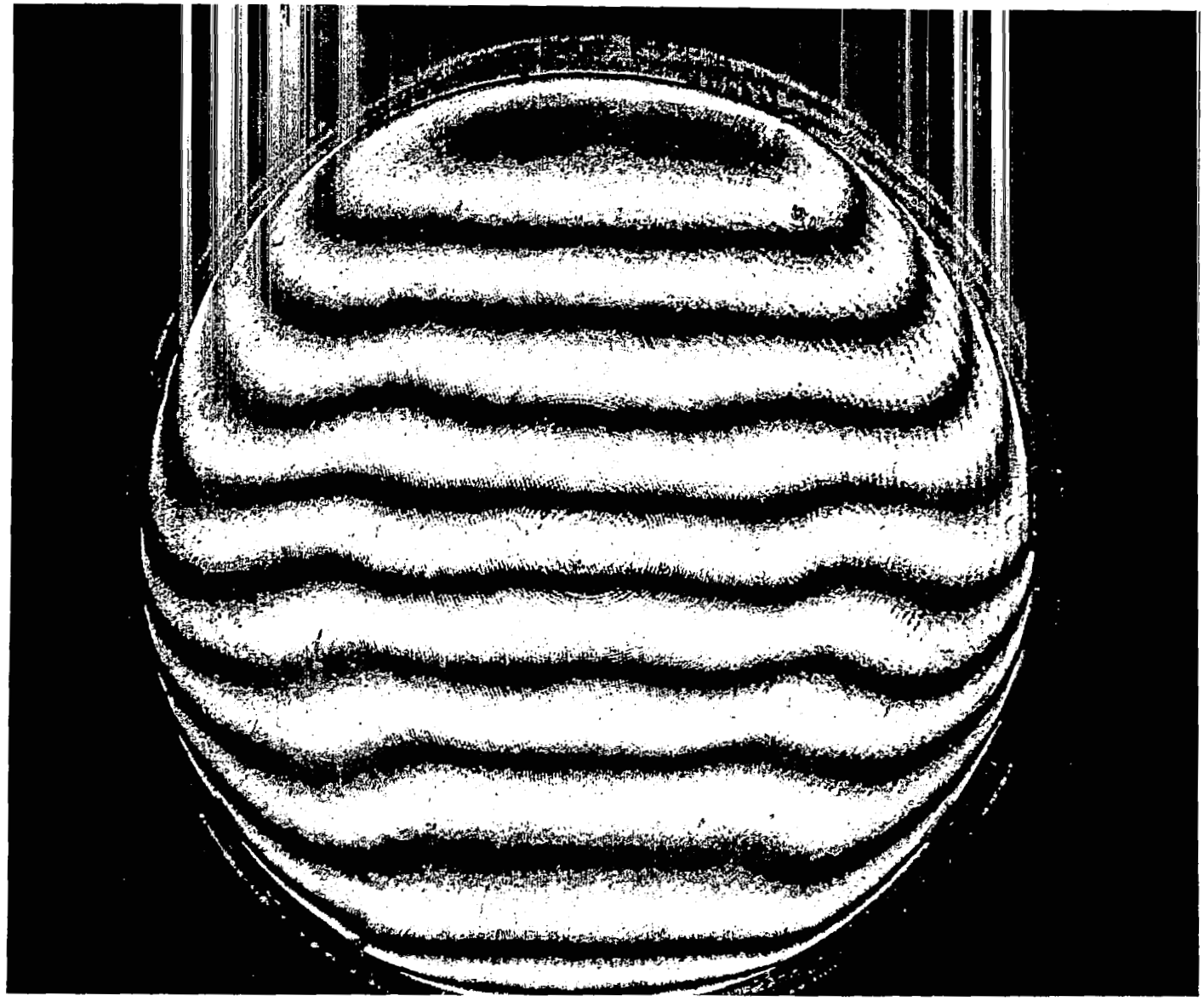

Figure 4. Interferogram of 30-Inch Mirror After Alignment with Active Optics Control System (Wavefront tilted to obtain straight line fringes)

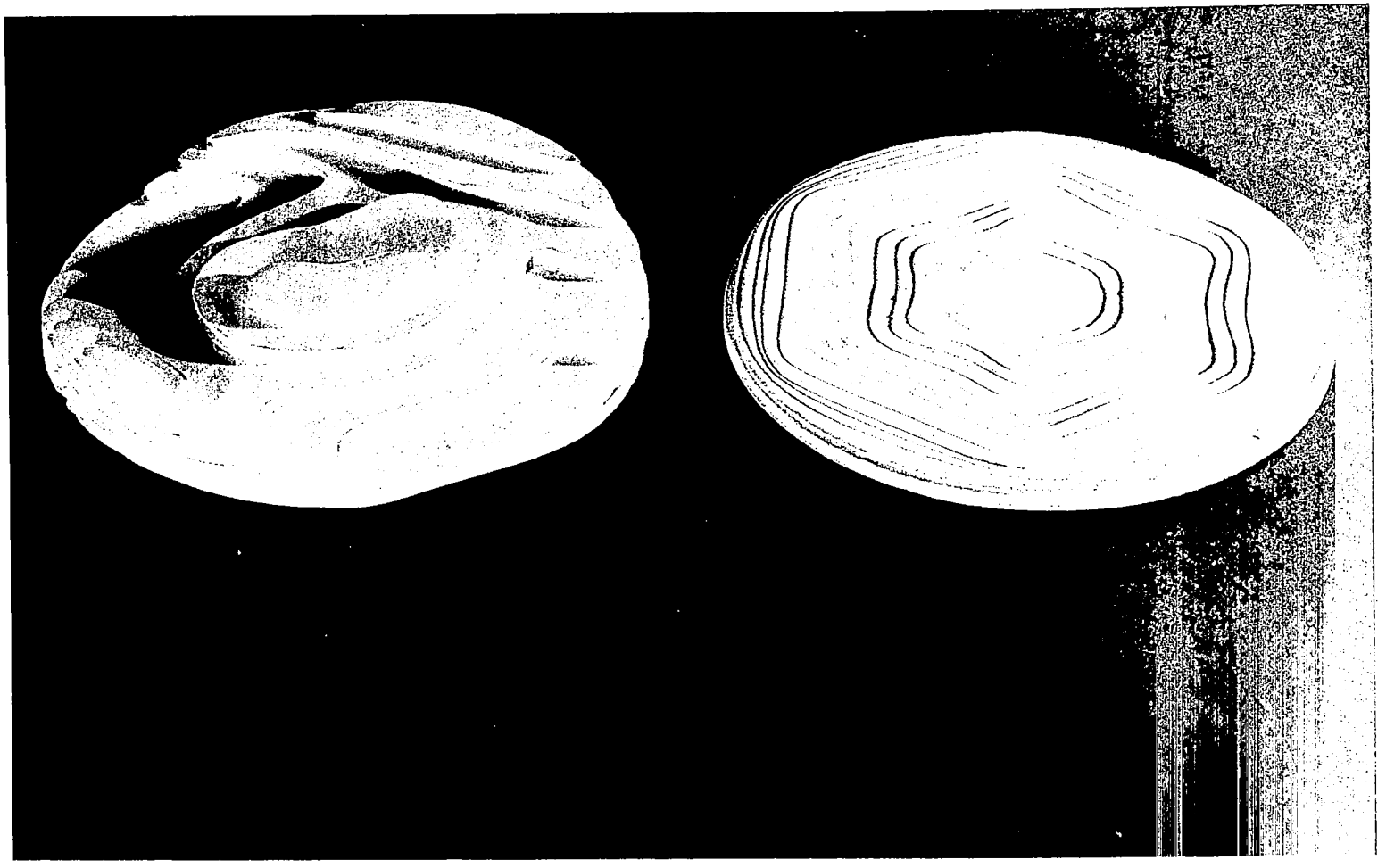

Before Alignment

After Alignment

Figure 5. Contour Models of Departure of 30-Inch Mirror from a Best-Fit Sphere, Before and After Active Alignment (Each level is equivalent to 1/2 wavelength in the before-alignment model and 1/40 wavelength in the after-alignment model)

Figure 6 shows an interferogram of the aligned mirror at a mirror-to-figure-sensor spacing approximately 0.160 inch larger than that used for figure 4. The mirror curvature can be maintained at any given radius within the range of the actuators by keying the "focus" control to the value of the output voltage of the position-indicating potentiometer of one of the flex actuators for that position. It is apparent that the radius selected for figure 6 is closer to optimum than is the radius used in figure 4. The residual deformations measured for the two cases were 1/30 wavelength rms and 1/50 wavelength rms, respectively.

Profile scans.- The interferograms described in the previous paragraph have the disadvantage that the control system must be turned off to record them. This did not seriously degrade their accuracy as the mirror figure was observed to maintain itself very well after thermal equilibrium had been reached; however, it was desired to obtain similar quantitative information about the mirror surface under control to determine the precision and repeatability of the control system.

Figure 7 shows a set of profile scans obtained by scanning the output of the phase measurement interferometer using the Image Dissector and applying the output of the phase detector to an X-Y recorder. This gives a set of curves very similar in appearance to the interference fringes observed in figure 6. The mirror was scanned twice so that each curve consists of a double trace. The variations between traces give an indication of the precision of the control system. The repeatability is within 1/30 wavelength everywhere, indicating that the precision error introduced by the control system is less than 1/150 wavelength rms.

In figure 8 the areas between the profile scans and the zero error reference lines have been filled in to show the mirror deviation from a best-fit sphere.

Pinhole test.- A pinhole source 0.0001 inch in diameter was located approximately 1/8 inch to one side of the center of curvature of the mirror and the image formed by the mirror was observed through a microscope. The pinhole test does not contain errors from the interferometer or control elec-

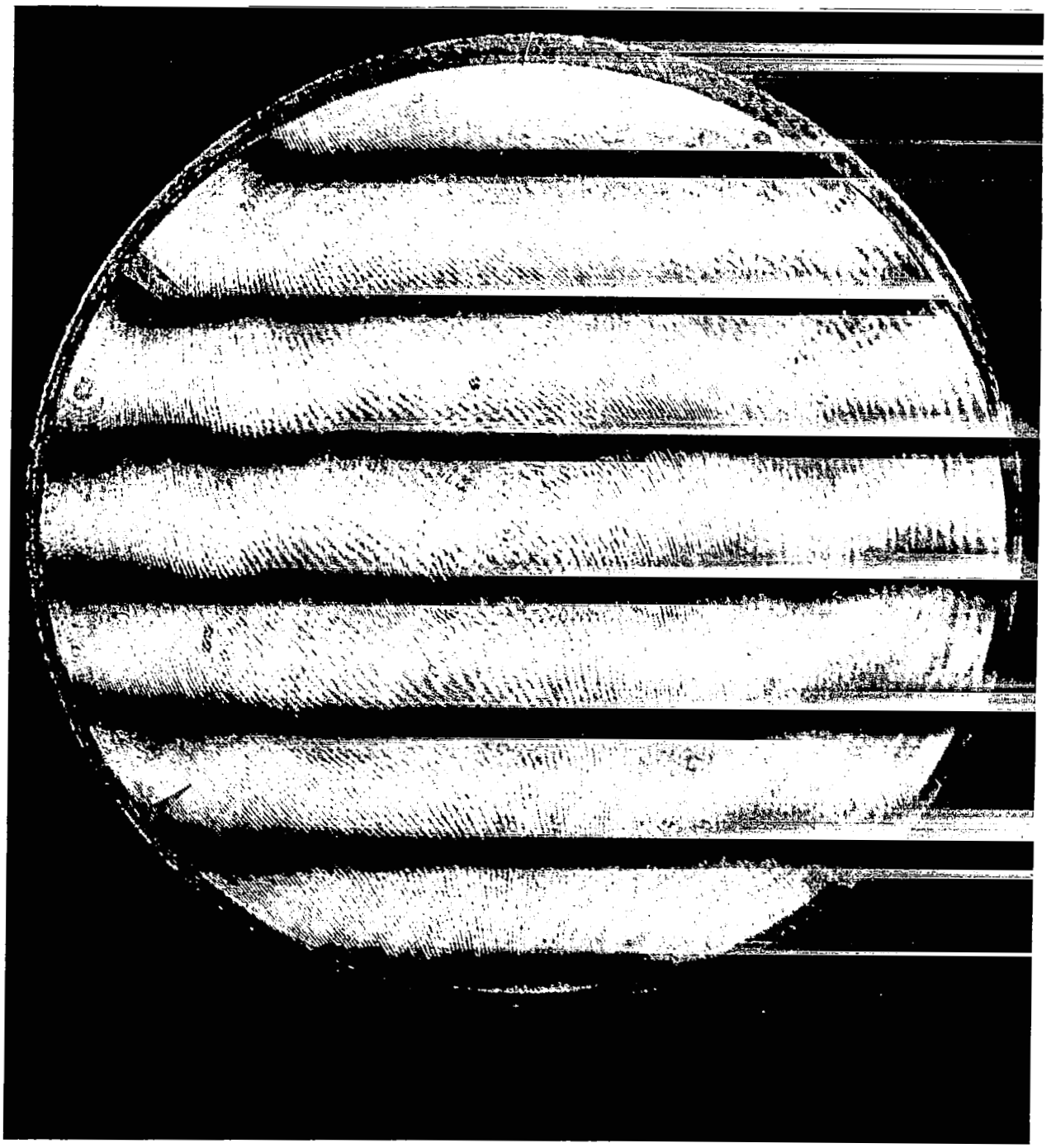

Figure 6. Interferogram of 30-Inch Mirror After Alignment with Active Optics Control System (Mirror-to-figure-sensor distance adjusted for close to optimum mirror figure)

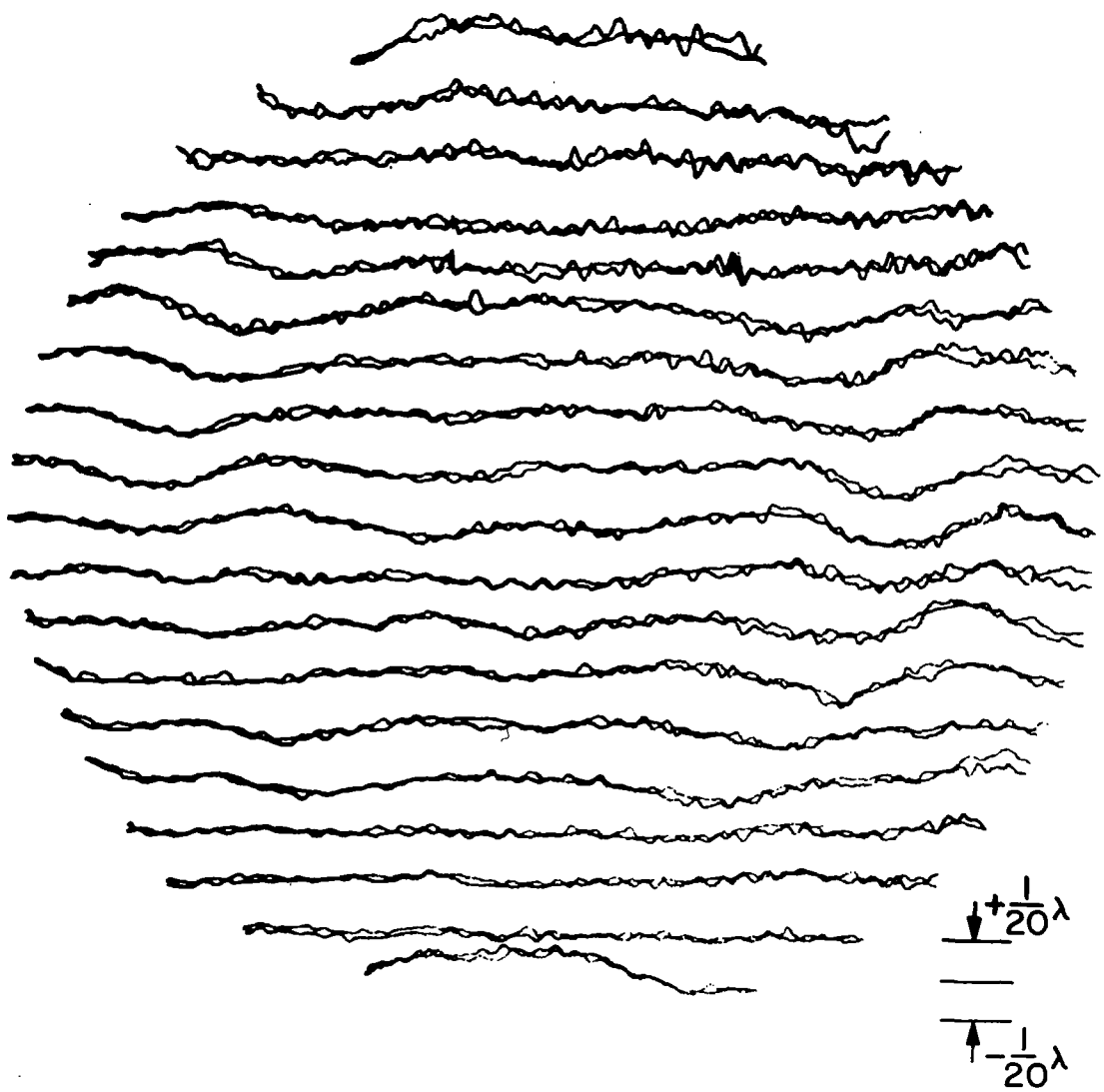

Figure 7. Mirror Figure Profile Scans from Phase Detector Output During Active Control

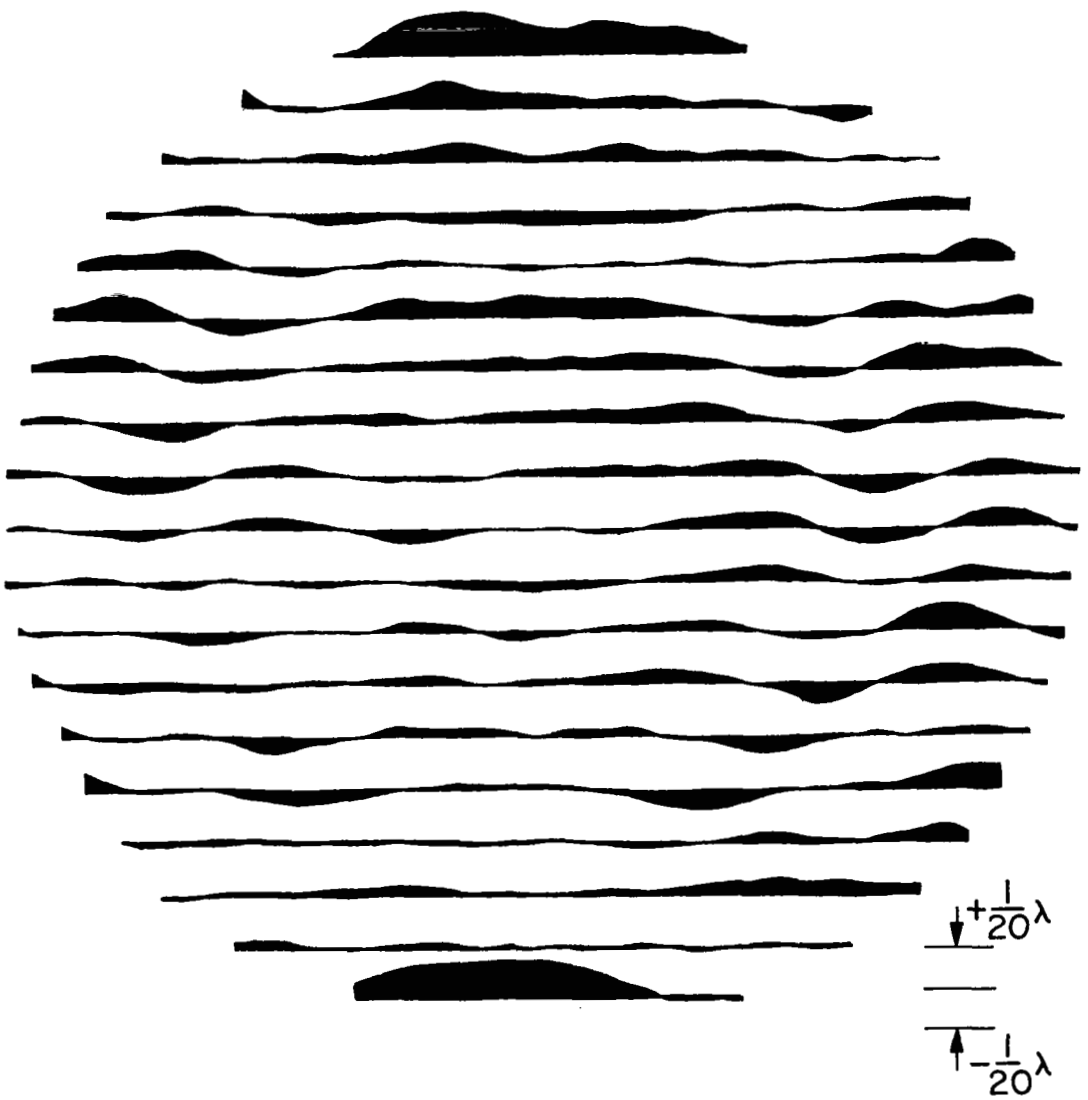

Figure 8. Mirror Figure Profile Showing Deviations from a Best-Fit Sphere (Shaded areas represent deviations)

tronics and directly tests the ability of the mirror to perform the function for which it is designed, that is, to form an image. Therefore, the pinhole test is a very useful and necessary, as well as graphic, cross-check on the performance of the system. Analysis of the pinhole image can give quantitative information about the rms figure error but it cannot be correlated with specific local areas of the mirror. Figure 9 is a photograph of the image for the mirror before alignment and after alignment in the position used to obtain the interferogram of figure 10. The first dark ring is 0.00025 inch in diameter in the actual pinhole image with the aligned mirror, so that the photograph is a 2000X enlargement. The uniformity and symmetry of the first dark ring and the first bright ring outside the Airy disc are quite good and indicate that the alignment accuracy is indeed close to the 1/50 λ rms indicated by an analysis of figure 6.

Foucault knife-edge test.- The knife-edge test is a traditional test that is useful for showing the location of mirror errors but from which it is very difficult to obtain good quantitative information about error amplitude, especially for near-diffraction-limited systems. A sample of a knife-edge photograph is shown in figure 10. The knife-edge test does not include errors introduced by the interferometer optics, but, as previously noted, these are small.

System Transient Response

The laboratory system was tested, both with and without crossfeed resistors, to determine the measured step response of given channels as well as the resulting interaction at adjacent channels. While only preliminary results are presently available, their agreement with theoretical predictions is quite good. The following paragraphs present the comparisons along with relevant discussion of the hardware and theory where thought necessary.

The laboratory equipment incorporates a minor (tachometric feedback) loop around the lead-screw drive motor to obtain an integration characteristic; i.e.,

$$\text{MINOR LOOP TRANSFER FUNCTION} = \frac{16.7}{S} \quad \frac{\text{rad/sec}}{\text{volt}} \quad .$$

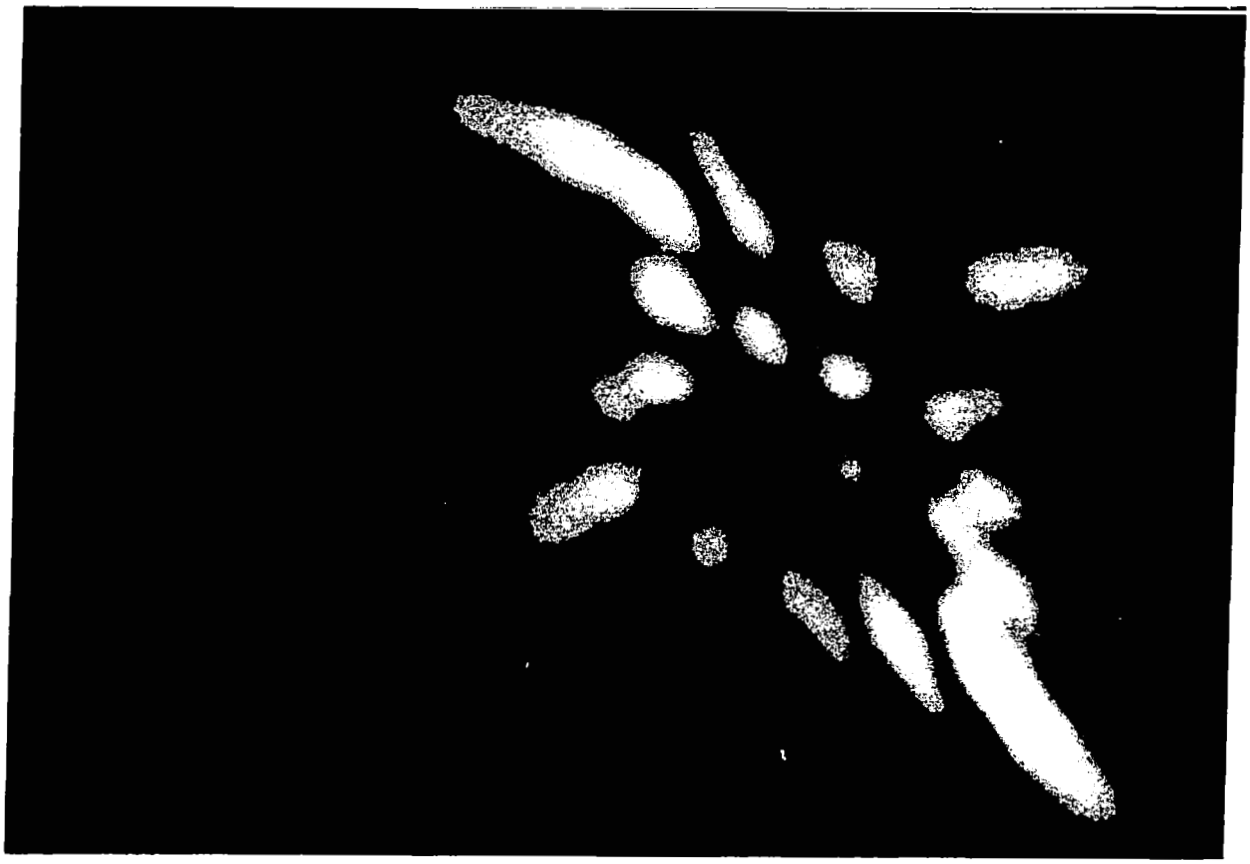

(a)

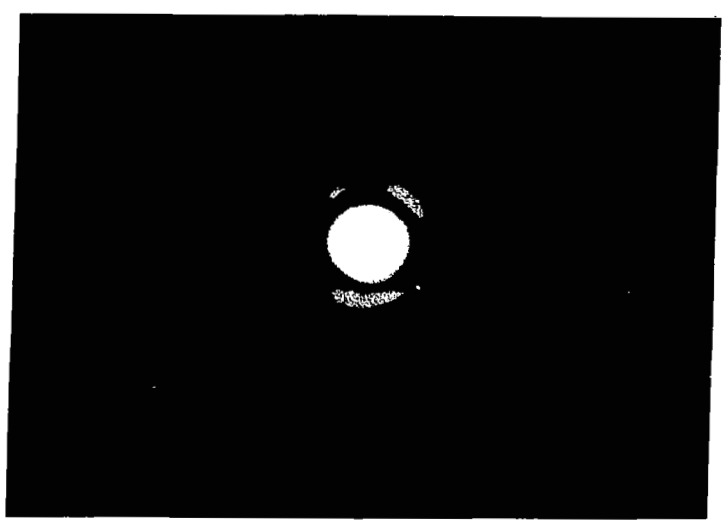

(b)

Figure 9. Image of 0.0001-Inch Pinhole Source at Mirror Center of Curvature (a) Before and (b) after alignment (2000X Enlargement)

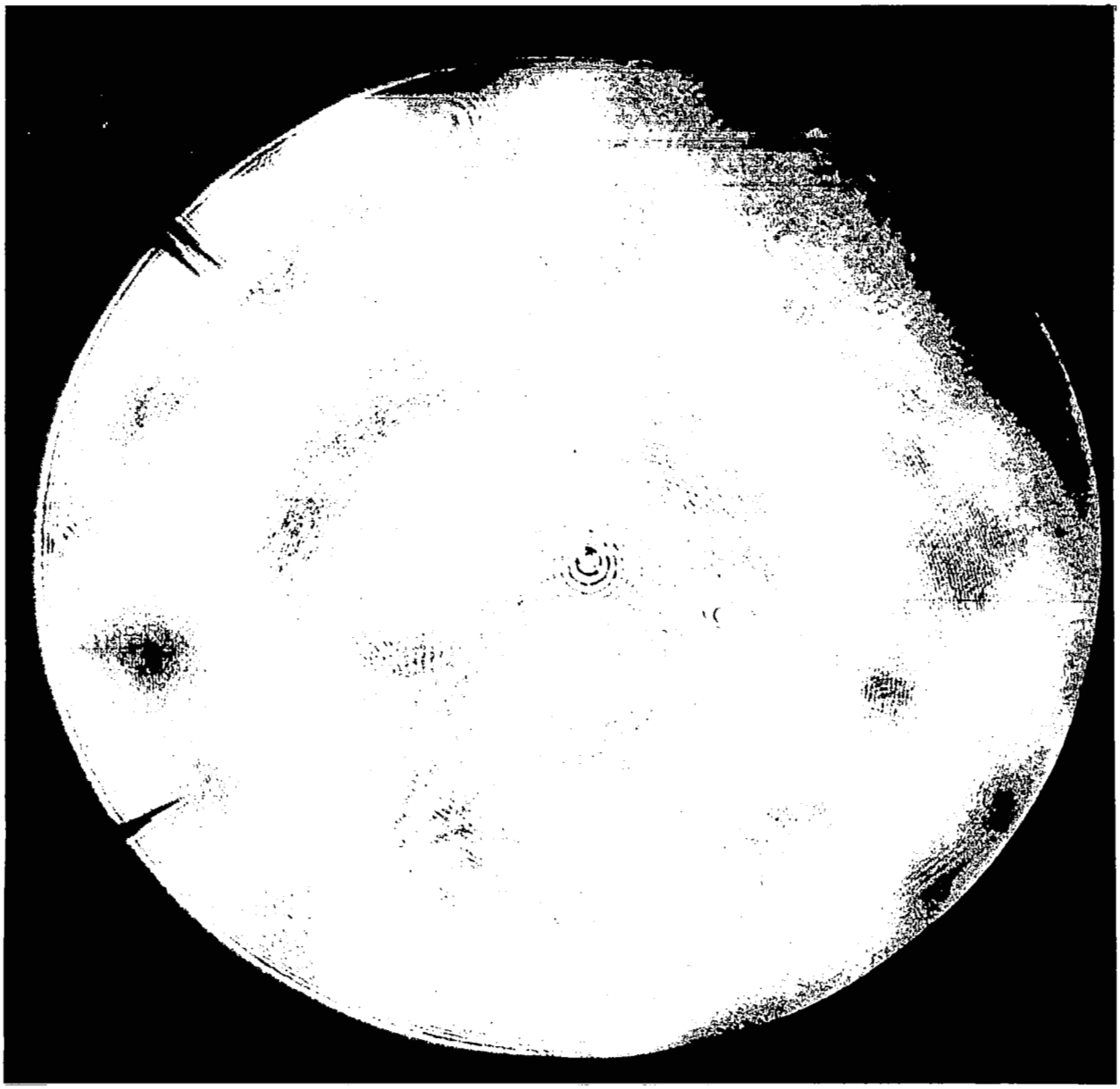

Figure 10. Foucault Knife Edge Test of 30-Inch Mirror After Alignment

This forward loop function is derived as shown in figure 11 and is used in the major loop analysis as presented in figure 12, which, it should be noted, is relevant to both the coupled and decoupled cases.

In the coupled case, the feedforward gain is unity and the nature of the response at a given mirror point, due to a step at the same or a different point, is determined from the mirror matrix and the other transfer functions comprising the loop(s). A stable system ensues only when all the roots of the system's characteristic equation are well-behaved (have positive damping), a condition that prevails when the locus of the actuator characteristic avoids encircling all of the critical points. This is determinable via Nyquist plane analysis or, equivalently, by resort to Bode analysis as is described in subsequent section, "Control Loop Design". In the former case, the denominator of the response expression was in the form

$$\prod \left(\frac{1}{\lambda_i} + G\right)$$

where $\frac{1}{\lambda_i}$ are the critical points, all of which must be avoided by choice of G if all denominator factors are to generate only well behaved roots. For Bode analysis, the denominator would be written in the form

$$\prod(1 + \lambda_i G)$$

and each $G\lambda_i$ would be treated in fashion analogous to the single loop approach. Only if all such $G\lambda_i$ plots indicate positive gain and phase margin will all roots be well-behaved and a stable system result.

For the present system, with its λ_i range of 1 to 3224 microinches per pound, the Bode plot would be as shown in figure 13. The phase margin, which depends upon the actual crossover frequency (and hence the actual gain), varies from a maximum of near 90° for λ_i = 1 microinch per pound to a minimum of about 25° for λ_i = 3224 microinches per pound. The system is thus expected to be stable and to have response components with time constants less than

$$\tau_c = \frac{1}{0.001(2\pi)} = 159 \text{ seconds},$$

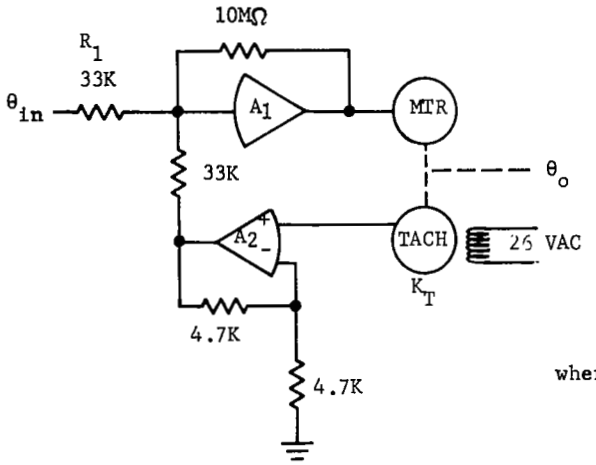

$$\frac{\theta_o}{\theta_{in.}} = \frac{\frac{AK_m}{JS^2+RS}}{1+\frac{AK_mK_TA_FS}{JS^2+RS}} = \frac{AK/S}{1+AKK_TA_F+\tau S}$$

$$\frac{\theta_o}{\theta_{in.}} = \frac{AK}{1+AKK_TA_F} \times \frac{1}{S\left(1+\frac{\tau S}{1+AKK_TA_F}\right)}$$

where A_F = tachometer amplifier gain = 2

A = 10M/33K = 300

$K_m = \frac{0.55 \text{ in.oz.}}{26 \text{ VAC}} = 1.320 \times 10^{-3}$ lb. in/volt

$R = \frac{0.55 \text{ in.oz.}}{5500 \text{ rpm}} = 60 \times 10^{-6}$ $\frac{\text{lb.in.}}{\text{rad/sec}}$

$\frac{K_m}{R} \triangleq K$

$K = 22 \frac{\text{rad/sec}}{\text{volt}}$

$J = 7.7 \text{ gm cm}^2 = 6.75 \times 10^{-6}$ lb in.sec^2

$\tau = \frac{J}{R} = 0.113$ sec

$K_T = 1.21 \times 10^{-3}$ volt/rad/sec

Open Loop Gain = $\frac{AK_mK_TA_F}{JS+R} = \frac{AKK_TA_F}{1+\tau S} = \frac{300x22x1.21x10^{-3}x2}{1+.113S} \approx 1.0$ @ F = 22.5 Hz

$\therefore \frac{\theta_o}{\theta_{in.}} \approx \frac{AK_T}{(1+AKK_TA_F)S} \approx \frac{1}{K_TA_FS}$ at frequencies $\ll$ 22.5 Hz

$\frac{\theta_o}{\theta_{in.}} = \frac{10^3}{2.42S} = \frac{413}{S}$ $\frac{\text{rad/sec}}{\text{volt}}$; with R_1 = 33K

and $\frac{\theta_o}{\theta_{in}} = \frac{33}{820} \times \frac{413}{S} = \frac{16.7}{S}$ $\frac{\text{rad/sec}}{\text{volt}}$; with R_1 = 820K

Figure 11. Minor Loop Analysis

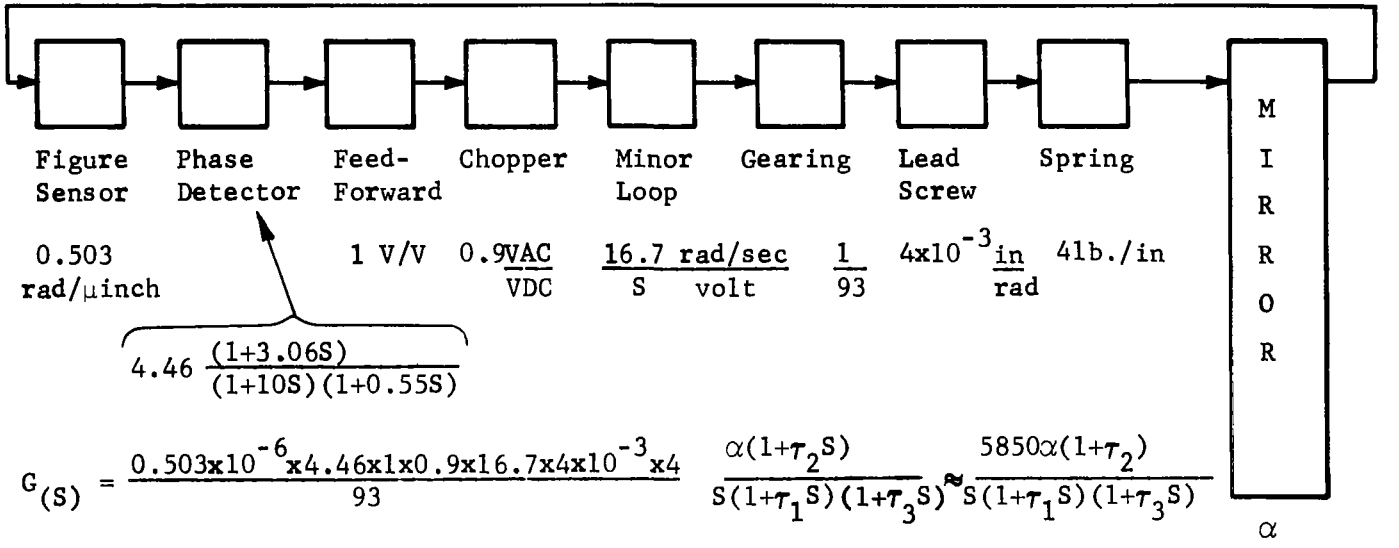

If α = 1 x 10^{-6} inch/lb and 3224 μinch/lb, as in coupled case with extreme eigenvalues, then

$$G_{(S)} = \frac{5.8\times10^{-3}(1+\tau_2 S)}{S(1+\tau_1 S)(1+\tau_3 S)}$$ which becomes unity at f = 0.000925 Hz when $\tau_j = 0$

and

$$G_{(S)} = \frac{18.700(1+\tau_2 S)}{S(1+\tau_1 S)(1+\tau_3 S)}$$ which becomes unity at f = 2.98 Hz when $\tau_j = 0$

If α = 5 x 10^{-6} inch/lb as for channels 31 and 43 in the decoupled case, then with a feedforward gain of 0.5

$$G_{(S)} = \frac{14.5\times10^{-3}(1+\tau_2 S)}{S(1+\tau_1 S)(1+\tau_3 S)}$$ which becomes unity at f = 0.0023 Hz.

Figure 12. Major Loop Analysis

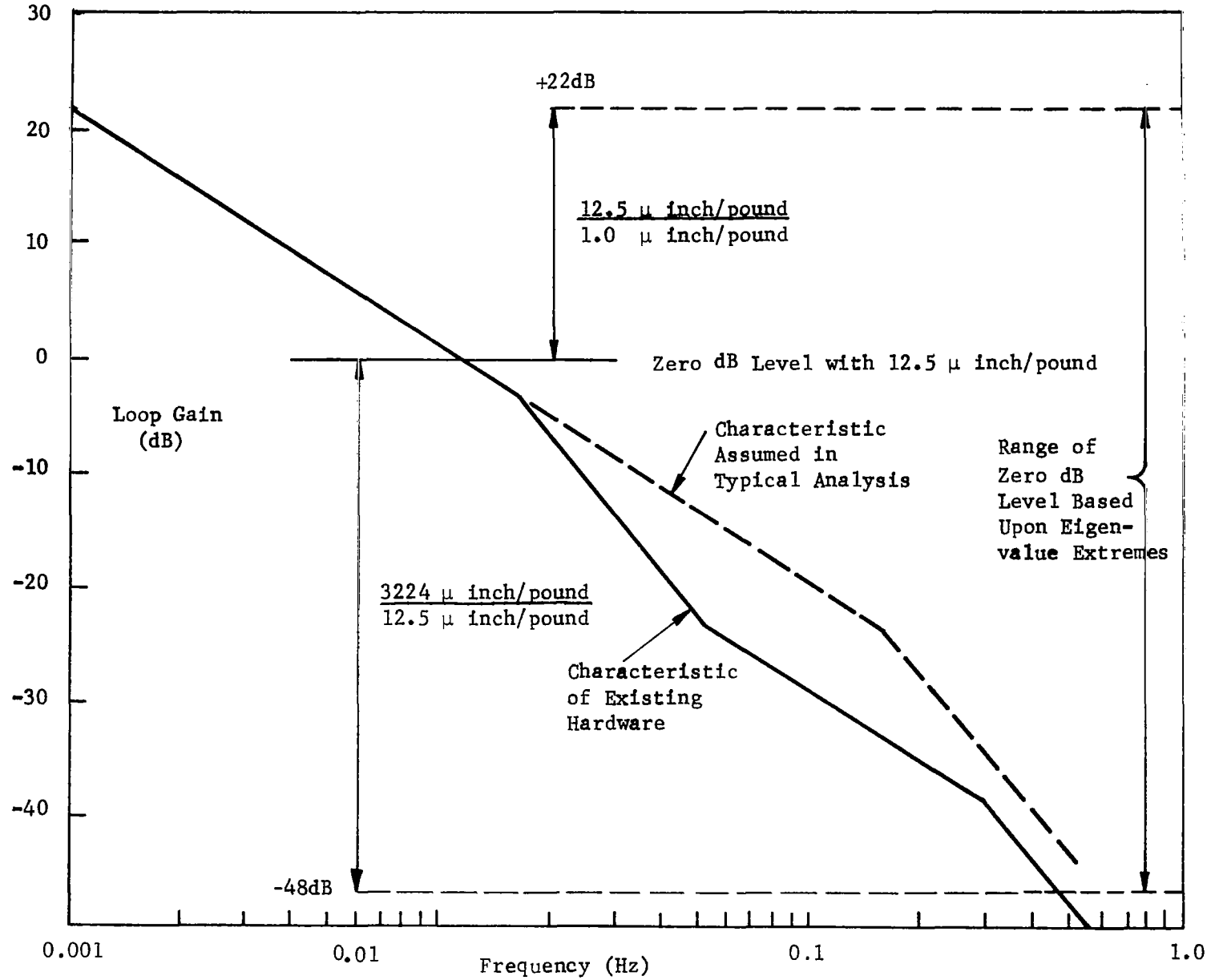

Figure 13. Coupled System Major Loop Characteristic

and resonant frequencies not in excess of approximately 0.5 Hz. As was pointed out previously, the actual response consists of on the order of n terms, each of which may be of significant amplitude. The exact solution for step function response is more involved than obtaining the mirror numerical matrix eigenvalues and therefore has not been attempted. However, figure 14 shows the nature of the response when a step error is introduced* into channel 31, corresponding to the center actuator. (See figure 2 for channel numbering code.) The significant points to be noted from the figure are:

- Measured time constants are on the order of 40 and 87 seconds**, values that are within the 159-second maximum predicted value.
- Responses at all adjacent (six) actuator points are essentially the same. This is to be expected with the symmetrical arrangement of the actuators.
- Points farther removed (viz, the second ring and more distant actuators) show decreasing response with distance due to decreased coupling between more remote points.

A step function introduced, on the other hand, into channel 61, corresponding to an unsupported actuator array corner, displays different measured time constants. This is shown in figure 15. The interactions at the symmetrically arrayed points 59 and 60 are nearly equal, being 28.6° and 22° peak amplitude, respectively, with time constants of 72 and 75 seconds. The inboard point 57 exhibited about one half this response due to interaction. It should be noted that the 88° step input was nearly equal to 90°, corresponding to an eighth wave of mirror deformation.

---

*Measurement technique is shown in figure 18.

**Time constant values given represent the time required for the error to be completely removed based upon the slope of the curve at the point considered. Such a computation is completely valid for a single time constant response. In the event that several exponential components are present, the method is, at best, only approximate but tends to improve for points on the trailing edge of the response where the shorter time constant terms have decreased significantly. This places the largest time constant in greatest evidence.

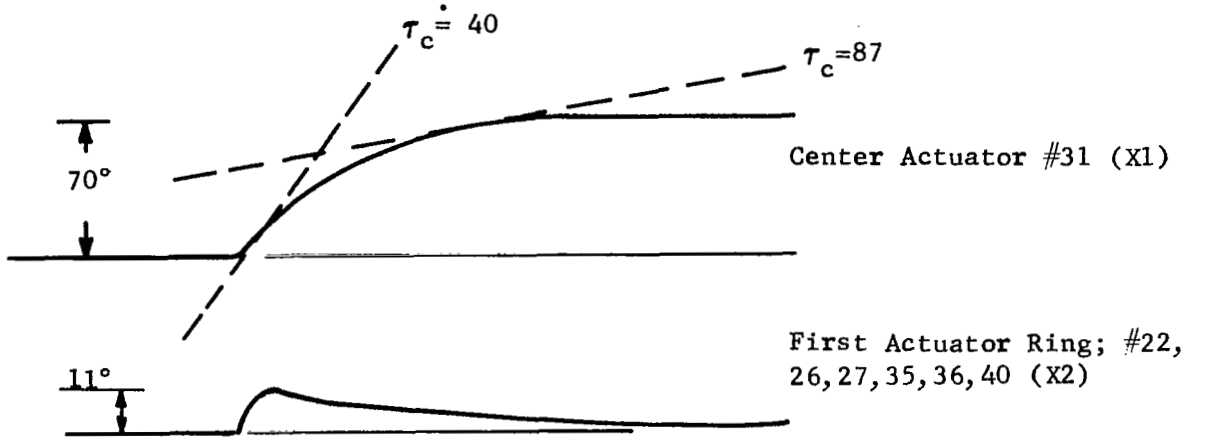

Notes: 1. Time Scale ⟷ 1.5 min ⟷

2. $90° = \frac{\lambda}{8}$ Mirror Deformation

Figure 14. Coupled Response

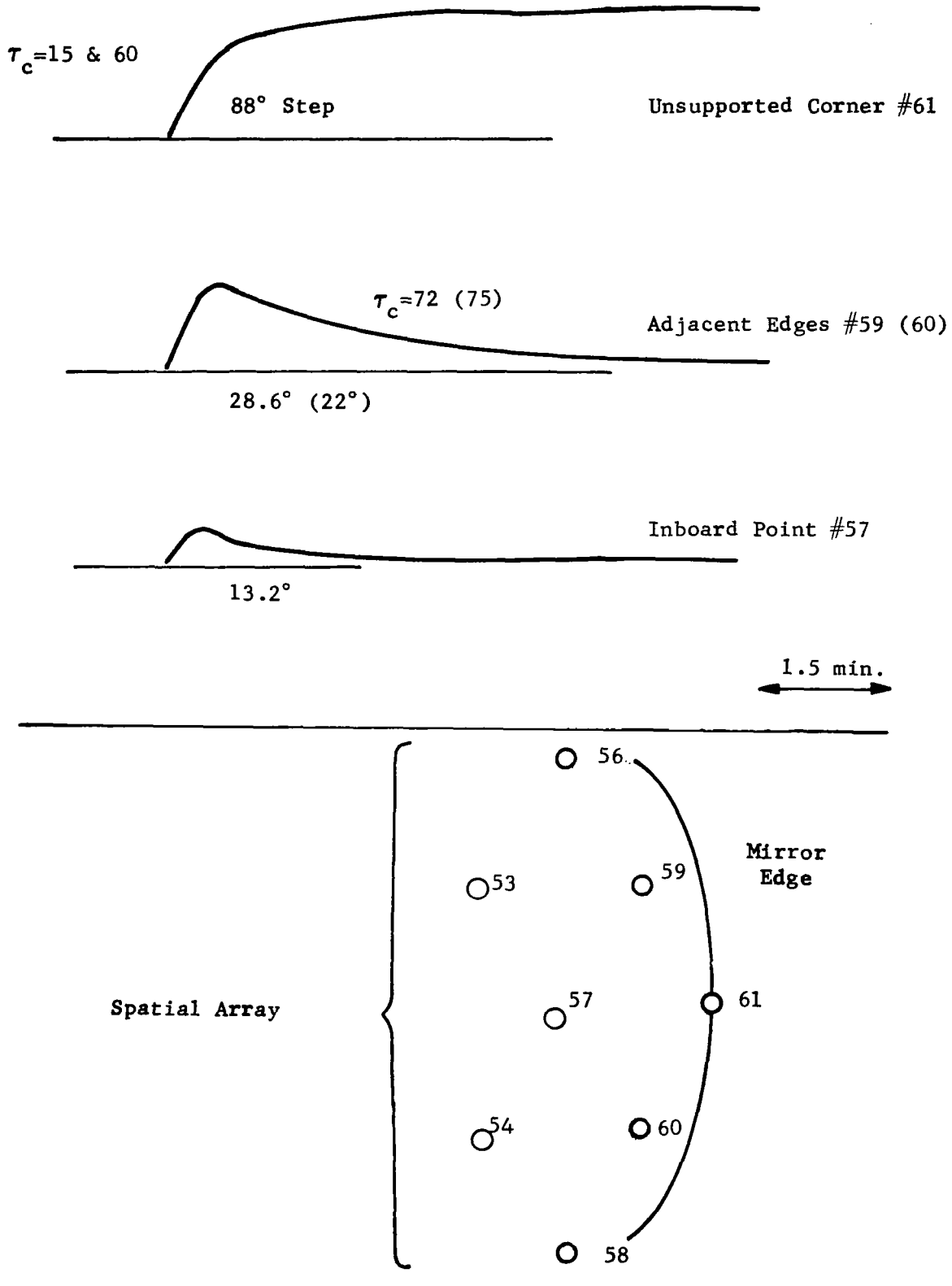

Figure 15. Coupled Response

The information of figure 12 also leads to the Bode curve of figure 16 for the decoupled case. In this configuration the crossfeed resistors (between channels) act to hold the surrounding points fixed as the forced channel operates through its associated resistor to correct the error introduced. The latter resistor is on the order of 20 kilohms for channel 31 corresponding to a feedforward gain of 1/2 for this channel. The decoupled mirror compliance as measured at points 31 and 43 is nearly 0.2λ mirror deformation per pound of applied force, the other points being effectively fixed positionwise. The measured step response of channel 43 is shown in figure 17 for both the coupled and decoupled cases. It is evident from the curves that the feedforward network was very effective in avoiding interaction response at adjacent actuators, the trace of response at actuator number 34 being attributed to non-perfect decoupling resistors. Moreover, the response of channel 31 was found to be essentially the same as for channel 43 for step errors introduced into each. This is as expected since all channels should display identical step responses in the decoupled configuration.

A word of explanation is in order regarding the apparent double valued nature of channel 43 initial response when decoupled. The dashed curve is the measured error response rate from which the solid error response curve was estimated, the direct measurement of error response being precluded by the particular hardware arrangement. Figure I8 indicates the general nature of the measurement techniques.

For the coupled case, a unity feedback condition prevails and the step responses as measured are equivalent to the responses produced by actual mirror step displacement errors. For the decoupled case, the unit feedback arrangement was not conveniently possible since the filtering action of the shaping amplifier was desired for the measured signal to remove phase detector noise and, in addition, dc step inputs at subsequent points could not be readily introduced.

A reasonable comparison between measured and predicted response is a comparison of time constants. This is true since the open loop gain characteristic in the region of unity gain is essentially -6 dB/octave, for which a nearly exponential response results; i.e.,

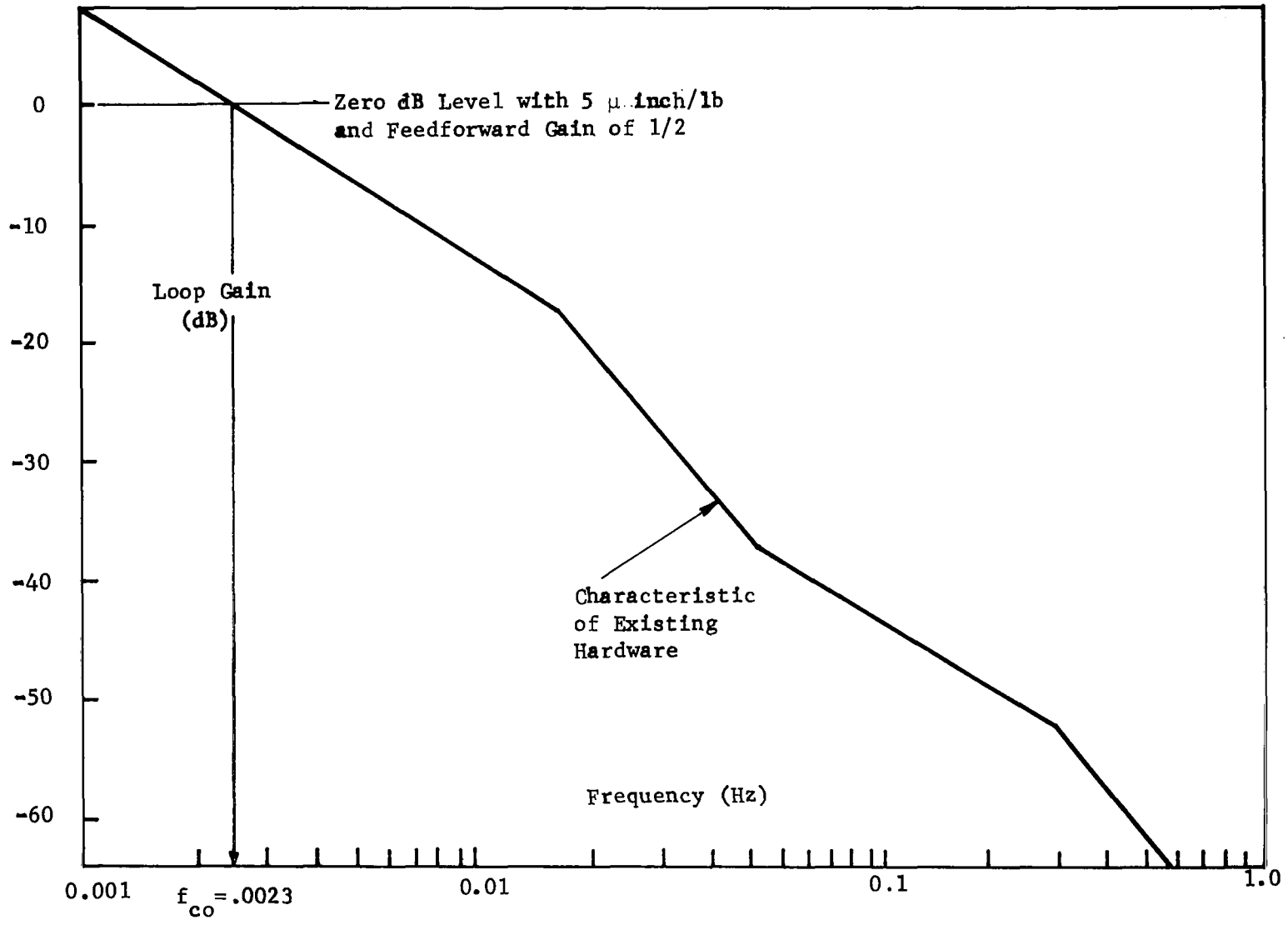

Figure 16. Decoupled System Major Loop Characteristic

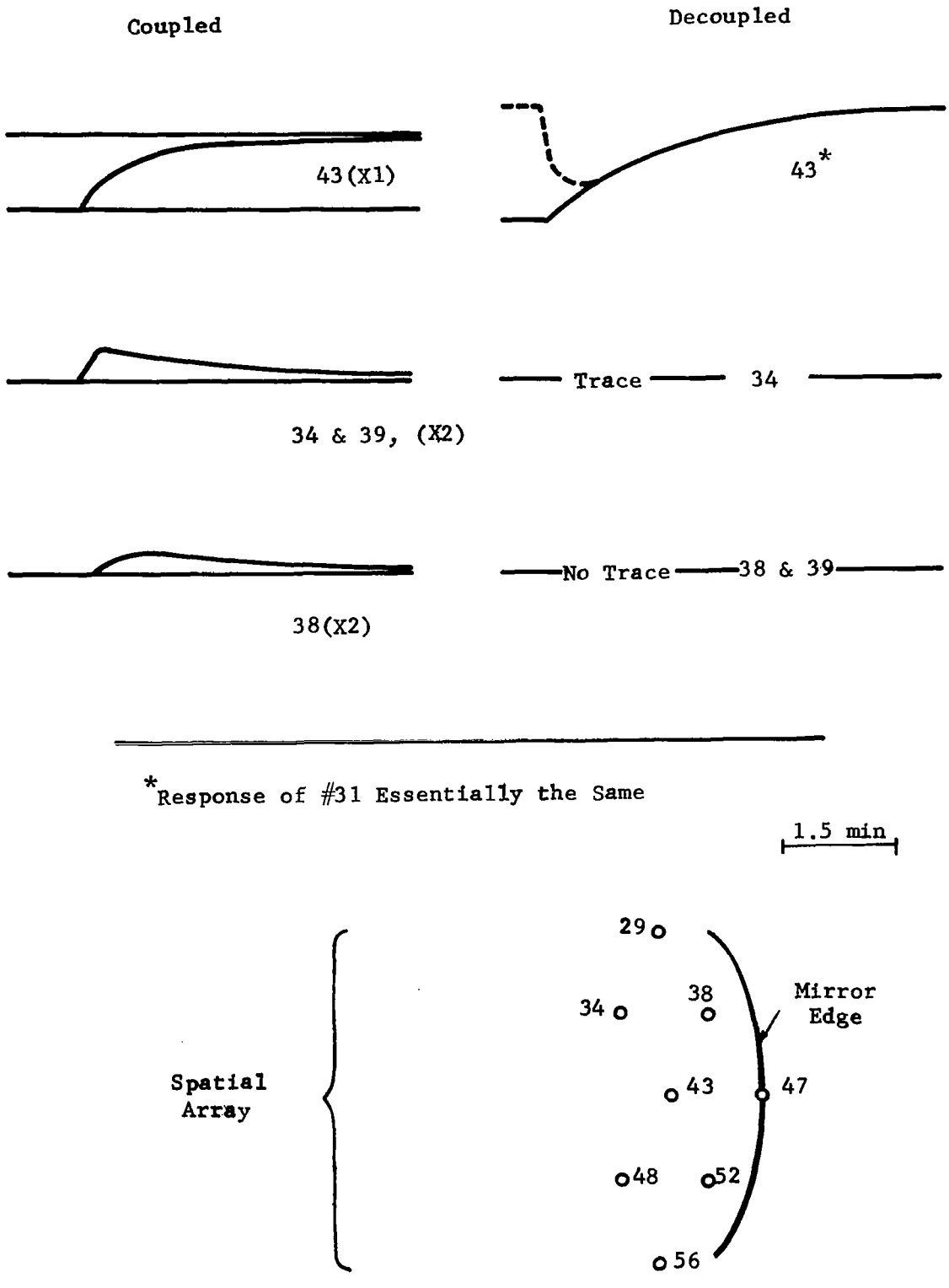

Figure 17. Decoupled Response

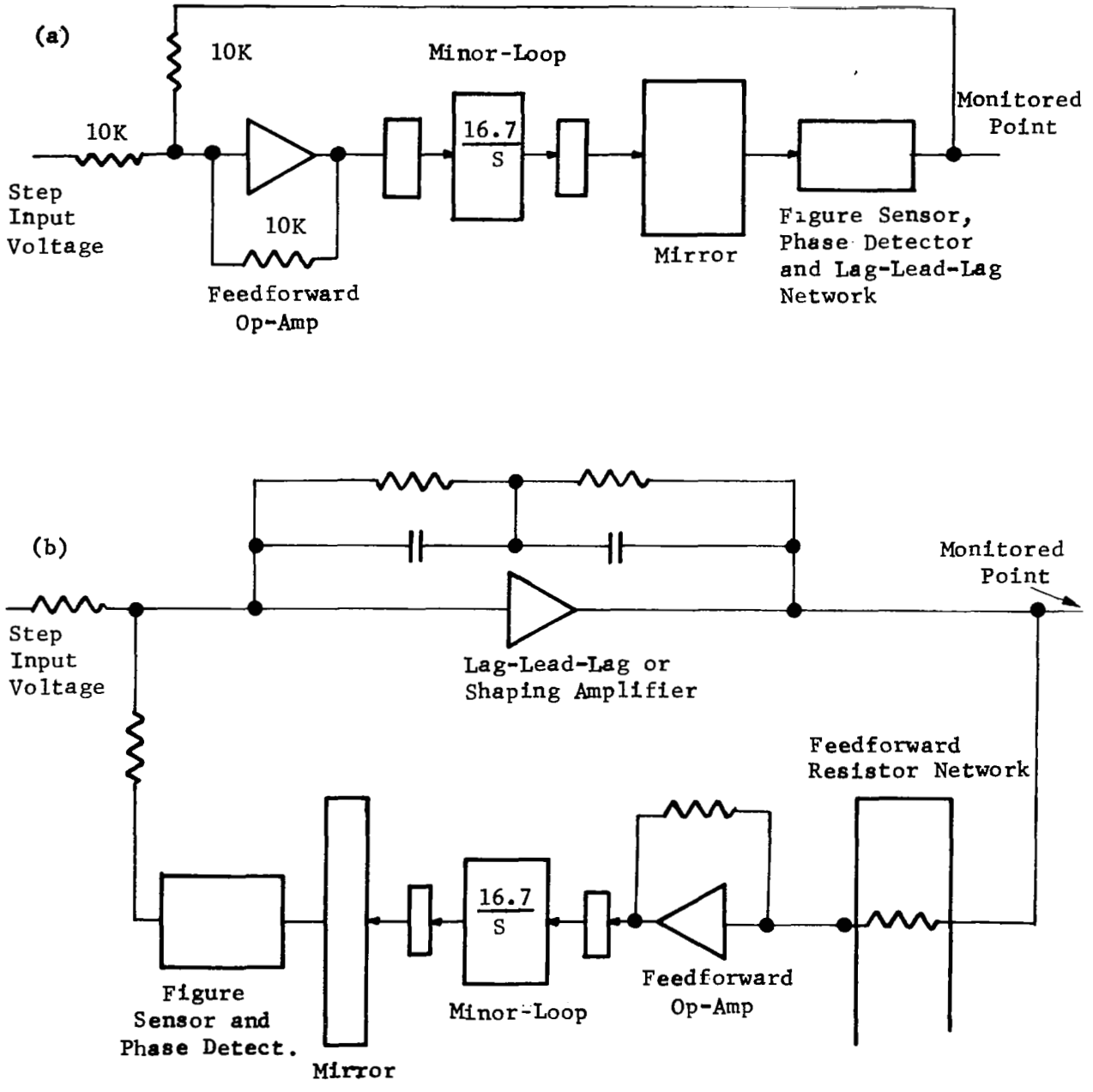

Figure 18. Measurement Techniques for (a) Coupled Case and (b) Decoupled Case

$$\tau_c \approx \frac{1}{2\pi f_{co}} = \frac{1}{2\pi(0.0023)} = 69 \text{ seconds}$$

Moreover, the derivative of an exponential response is in itself exponential

$$\frac{d(K[1-e^{-at}])}{dt} = Kae^{-at}$$

A measured time constant for the decoupled response of channel 31 is on the order of 90 seconds, a value close enough to substantiate predictions.

ANALYTICAL STUDY

The basic concept of Active Optics applied to a thin mirror is deceptively simple. In principle, the mirror figure error is measured and the mirror is stressed to remove the error. In practice, there were several difficult problems to be solved. There were the questions of what kinds of errors had to be accommodated, how thick the mirror should be, whether force or displacement correction was to be used, and how the mirror should be mounted. The key problem was finding a systematic relationship between what could be measured and the types of figure control that were possible (subsequently referred to as the control system). Therefore, it was necessary to spend the first several months in an analytical study to answer these questions. In the following paragraphs, the principal sources of error and possible approaches to the selection of a control system are discussed briefly.

Determination Of Mirror Parameters

Mirror diameter and radius of curvature. - The 30-inch diameter was determined at the start as the largest size that would conveniently fit into the vacuum tank purchased for the previous contract (Contract NAS1-5198). The radius of curvature was selected as approximately 180 inches to locate the mirror, mirror support system, and actuator system near one end of the tank to allow convenient access to the assembly. This also provided an f/3 mirror

which required an f/6 cone of illumination from the figure sensor at the center of curvature, and this was the maximum the existing figure sensor could provide without redesign.

Actuator spacing and placement.- The spacing of the actuators and the amplitude of correction that they are required to make depend upon the mirror aberrations, which are due to fabrication tolerances, gravitational environment, thermal environment, spontaneous stress release, and dynamic loading to be removed.

It was initially predicted that the figure deformations of the 30-inch thin mirror at the conclusion of the fabrication process employed would be less than 1 wavelength peak overall and less than 1/10 wavelength peak over any area with a diameter of 6 inches. The actual errors exceeded these estimates (see subsequent section "Thin Mirror Fabrication"), but were still well within the capability of the control system. It would certainly be desirable, however, to produce, from the standpoint of long term reliability in an orbiting system, a figure accuracy that minimizes the number of actuators required to remove deformations and to make the mirror diffraction limited. Initial calculations indicate that, for a given actuator spacing, a local amplitude of deformation of approximately 1/2 wavelength can be removed without leaving a residual ripple of greater than 1/40 wavelength peak. A residual ripple of ±1/40 wavelength would introduce an rms error of approximately 1/50 wavelength. This implies that the amplitude of a deformation with the highest spatial frequency that can be corrected should be no greater than 1/2 wavelength.

The actuator spacing should be determined ideally by the highest spatial frequency of the deformations that might be expected from all sources. A large diffraction-limited mirror, such as the 36-inch Stratoscope mirror modeled in figure 19, illustrates the type of residual deformations that may be expected after figuring. The deviation from a best-fit parabola is shown in the model in an extremely exaggerated scale, the largest difference between maxima and minima being equivalent to less than 1/10 wavelength or 2.5 millionths of an inch.

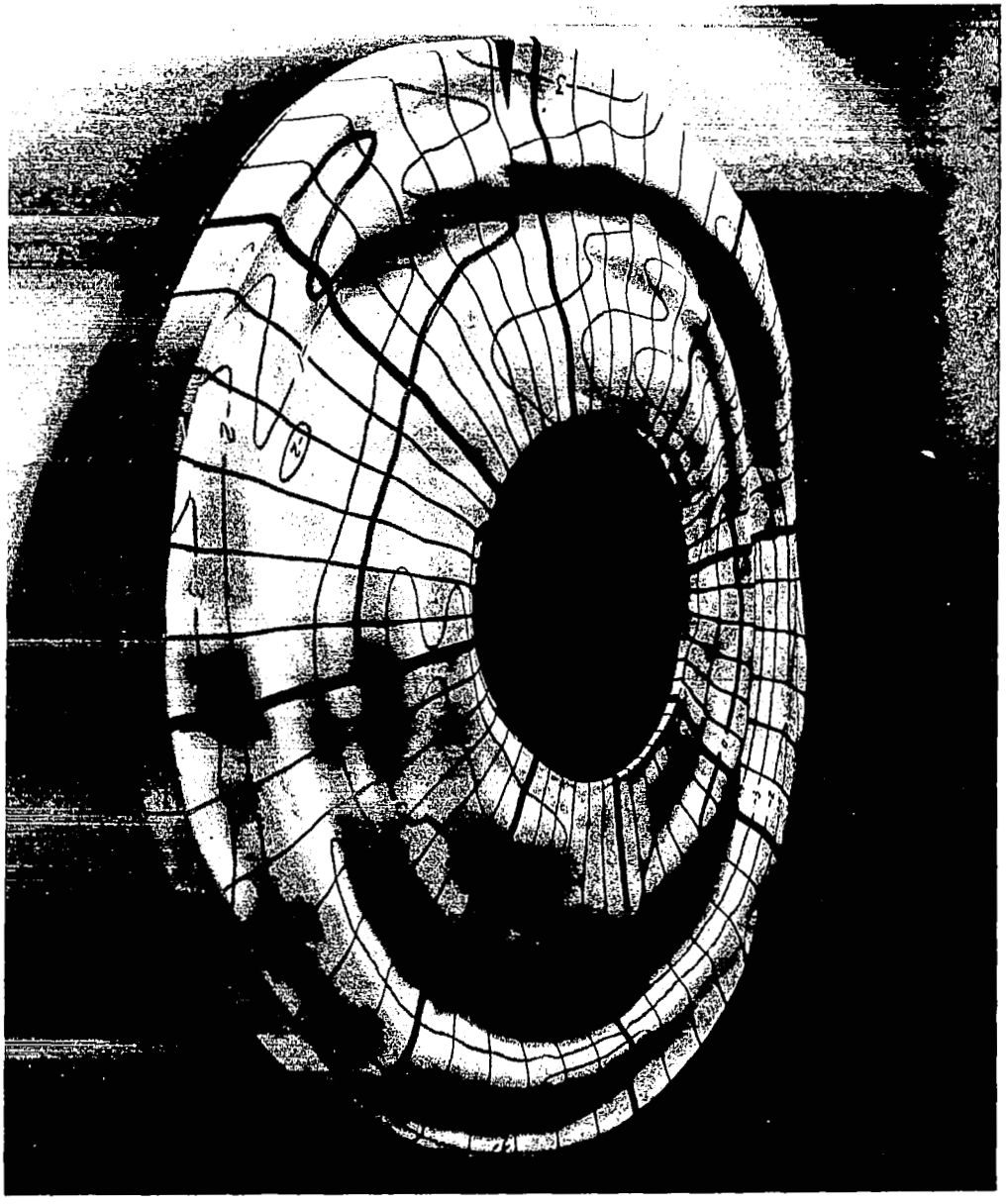

Figure 19. Model of Residual Deformations in 36-Inch Diffraction-Limited Stratoscope Mirror (rms error = 1/50 λ)

For space operation, the change from a gravity to gravity-free environment may cause significant mechanical distortion. However, after correct alignment and operation have been established, thermal effects will probably predominate. As was expected, thermal effects were not the limiting factors determining correction range. The principal sources of figure error for the laboratory experiment were those introduced during fabrication and by the stresses introduced by the mounting structure and these may be primary sources of error in a large spaceborne system also. However, the range of correction that the system is capable of making indicates that it will be possible to design a system of this sort that will be capable of performing in and adapting to the environment in which it is to operate.

The actuator placement chosen gives uniform spacing of the actuators over the entire mirror (see figure 2). Each actuator is symmetrically surrounded by other actuators except those near the edge discontinuity. This is not necessarily the optimum arrangement of actuators. For instance, when more is known about the distribution of stresses due to the space environment, it might be desirable to vary the actuator density as a function of radial position or to add a few actuators near the unsupported segments of the mirror's edge. For the present, however, the evenly distributed arrangement shown was considered adequate to demonstrate the control system feasibility and to produce the desired final figure accuracy.

The maximum spatial frequency of the deformation that can be removed is 7.5 inches per cycle based upon an actuator spacing of 3.75 inches and the fact that at least three points of contact are required to generate a non-plane figure change. The 58-actuator distribution shown gives a degree of control over static deformations with a high spatial frequency component such as the residual deformations observed in the Stratoscope mirror (figure 19). In the present case, it also demonstrates the ability of a multiple-loop control system to operate in a stable mode with the number of actuator points to be expected in a larger mirror system.

Mirror thickness.- Figure 20 shows the force required to obtain a localized mirror deflection of 1 wavelength as a function of mirror thickness when the actuator spacing is fixed at 3.75 inches. Also shown is the maximum stress

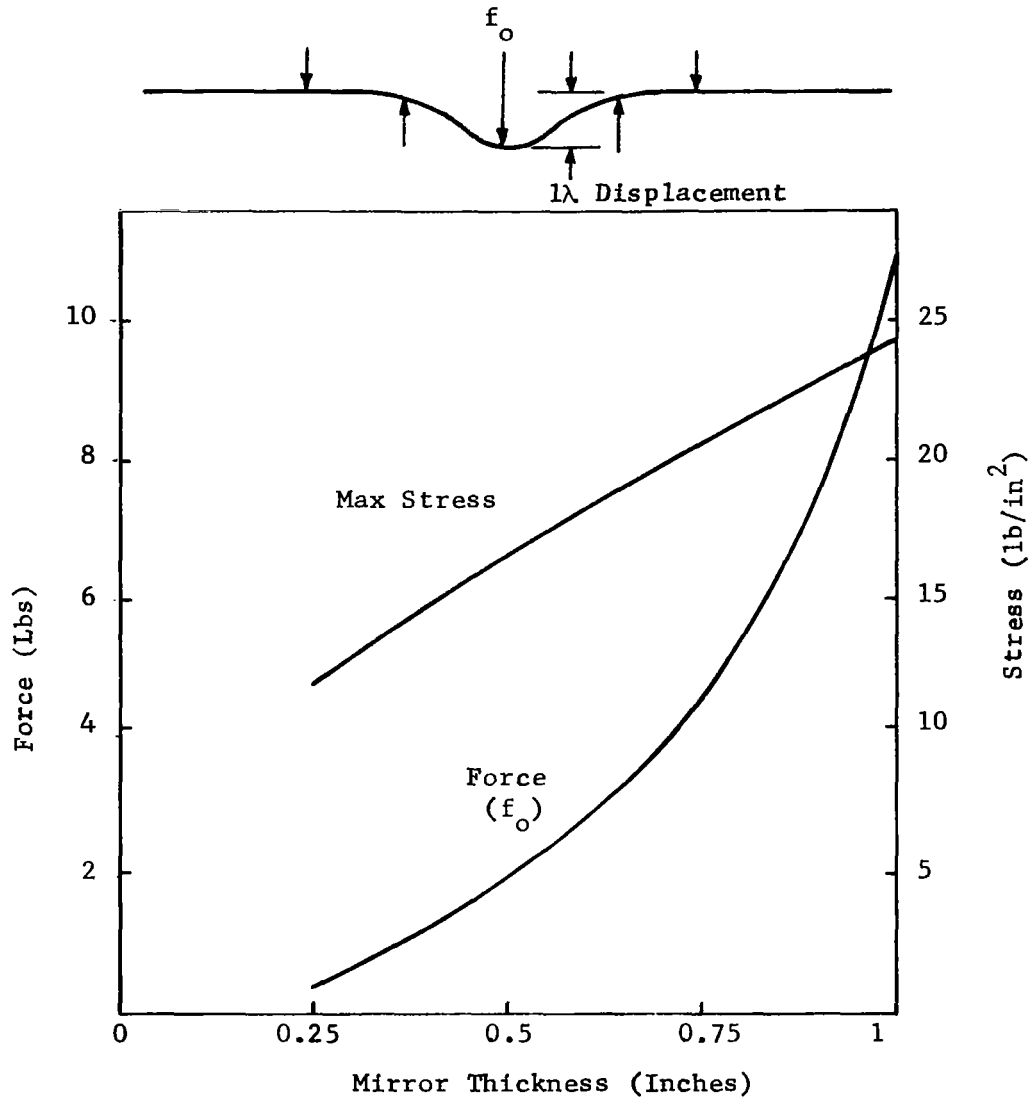

Figure 20. Force and Stress as a Function of Mirror Thickness for 3.75-Inch Actuator Spacing and a Localized Displacement of 1 Wavelength

that is developed by the 1-wavelength displacement. Since the deflection is a linear function of the applied force, the readings may be multiplied by an appropriate factor to give the force required to obtain other small deflections.

It would appear from these considerations that it is desirable to minimize the mirror thickness, not only to reduce the stress exerted against the mirror but also to minimize the force requirements on the actuator. However, a limit can be placed on the minimum thickness-to-diameter ratio that can practically be achieved by the problems that arise in the fabrication, in the support and measurement of the mirror in the normal gravitational environment, and from the stresses generated in launch. For the 30-inch diameter mirror, a 1/2-inch thickness was selected as a compromise between amplitude of force required for deflection, and difficulty of fabrication. For larger mirrors, the forces required to obtain the same amplitude local deflections increase with the linear dimension for the same diameter-to-thickness ratio and the same number of actuators. For example, a 120-inch mirror, 2 inches thick with 15-inch actuator spacing, would require an actuator to exert approximately 8 pounds to obtain a local deflection of 1 wavelength.

Effects of discontinuities on system parameters.- Discontinuities have not had a first-order effect on the considerations leading to the actuator spacing or thickness determination for the 30-inch mirror. However, there is a definite effect other than making the influence coefficients more difficult to find analytically. It can be shown that there is always a unique set of forces that can maintain the displacements constant at all the actuator points except at the actuator being programmed to move. Because a deformation can be removed by removing its local components, every actuator point can be made to fit the reference sphere if the system is stable. This does not imply, however, that the slope of the surface at each actuator point is zero or that all the points between the actuators fit the reference sphere. By making the figure sensor average the error over the surrounding territory of each actuator,

the average displacement over the entire mirror surface can be zeroed since each actuator will null an error signal that is proportional to the average displacement.

The deviation of the surface from a best-fit sphere, which occurs as a ripple between the actuators, can therefore be made to have an average value of zero, but its rms value will still be finite. The amplitude of the ripples produced will be proportional to the amplitude of the local displacement removed by the actuators if the spacing remains constant. The peak value of the ripple introduced by each actuator has been measured to be approximately 1/20th of the local displacement of each actuator in the experimental arrangement for determining mirror interactions. If the mirror were unbounded, the ratio of amplitudes of the ripple and the local displacement would be relatively independent of the mirror thickness and the actuator spacing. Since the mirror has discontinuities, the relative amplitude of the ripple will increase somewhat for actuators adjacent to a free boundary (as opposed to a clamped boundary). The effect will be "worse" (i.e., larger relative amplitude of ripple) for the discontinuity of the outside mirror edge than for that of a center hole. In either case the remedy is the same. The ripple can be reduced by applying a restraining moment at the edge to control the slope, but a simpler remedy is to decrease the actuator spacing near the discontinuity if the ripple is objectionable. In the present experiment, no adjustment was made to the actuator spacing near the discontinuity since the increase in ripple amplitude was expected to be small and the spacing was considered adequate to remove the deformations and maintain the residual ripple below the goal of 1/20 wavelength rms.

Stability Considerations

A conventional approach in the synthesis of a control system is to select or tailor the servo frequency characteristic, open-loop gain versus frequency, so that the minus one point in the Nyquist plane is not encircled. The minus one point can thus be thought of as a critical point for a single loop controller. While this technique is not directly applicable in the case of

n interacting loops, such as encountered with the deformable mirror control system, an analogous approach is possible. The method, evolved early in the program, involves the selection of an actuator characteristic that avoids encirclement of n critical points whose locations are determined by the mirror and support system under consideration. A present necessary assumption in the approach is that all actuators in the system have the same characteristic.

An alternate approach to system stability is to decouple the n actuator control loops so that they do not interact. Performance under such ideal conditions is that which prevails with n separate control loops, and standard synthesis techniques may be applied. The decoupling can be realized with an electrical network which, in effect, mechanizes the inverse of the matrix describing mirror displacements due to applied forces. These two approaches to stability shall now be discussed to serve as a review of previous work. The intent here is not mathematical rigor but rather the presentation of basic ideas that enable a better understanding of system stability and the measured results presented elsewhere in this report.

The laboratory system features spring-type actuators designed to apply forces to the mirror, which itself is a spring-mass system. For a single actuator system, the arrangement is as shown in figure 21, where the actuator force F produces acceleration of mirror mass M, overcomes any damping forces ($D\dot{\delta}$) present, and overcomes the spring constant of the mirror. The compliance is denoted by X so that the spring constant is the inverse of this, while mirror deflection is represented by δ. The equation expressing this fact

$$F = M\ddot{\delta} + D\dot{\delta} + \frac{1}{X}\delta$$

can be rearranged to obtain the mirror transfer function

$$\frac{\delta(S)}{F(S)} = \frac{1}{MS^2 + DS + \frac{1}{X}}$$

where S is the Laplacian operator (or $j\omega$ in the case where only steady state solution or performance is of interest).

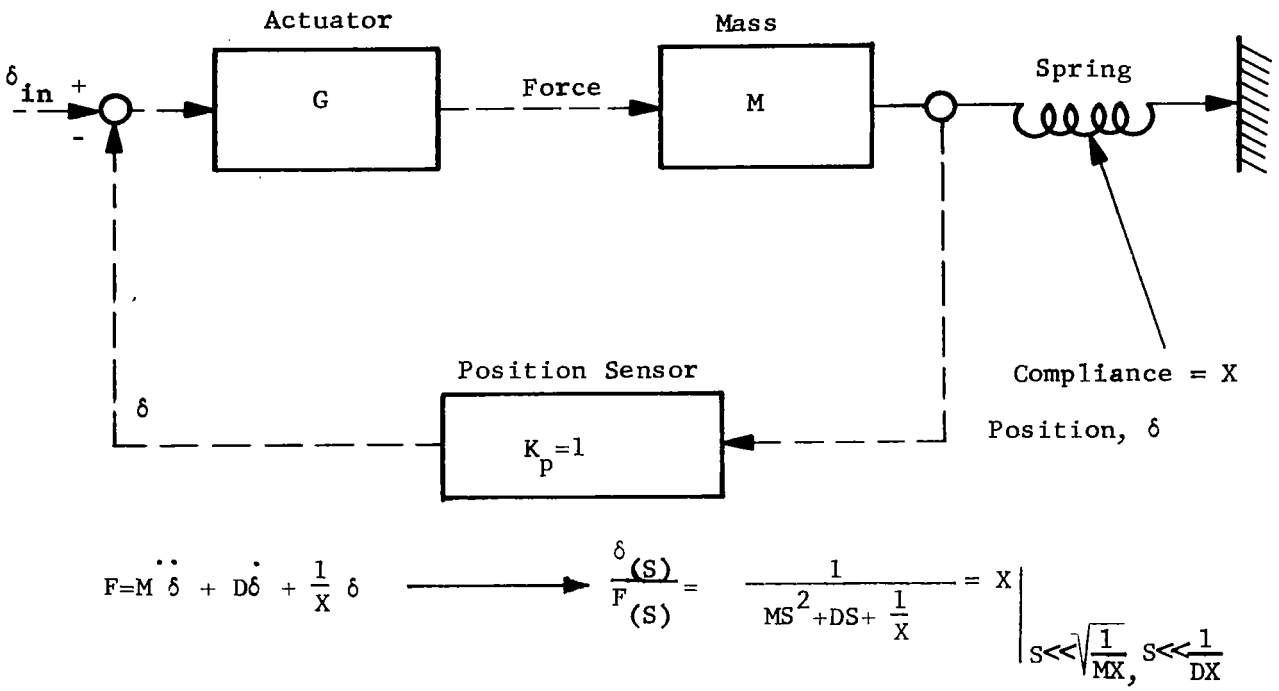

$$F=M\ddot{\delta}+D\dot{\delta}+\frac{1}{X}\delta \longrightarrow \frac{\delta(S)}{F(S)}=\frac{1}{MS^2+DS+\frac{1}{X}}=X\Big|_{S\ll\sqrt{\frac{1}{MX}},\ S\ll\frac{1}{DX}}$$

$$\therefore \delta = FX, \text{ And } \frac{\delta}{\delta_{in}}=\frac{GX}{1+GX}=\frac{AX/S}{1+AX/S}\ ;\ \text{When } G = A/S$$

Stability When Minus is Not Encircled By Since Roots of Denominator Have Negative Real Parts

Figure 21. Single Actuator Loop

The response to a force input is, in general, seen to be a complex one involving both amplitude and phase, except at very low frequencies. In this domain, where S is much smaller than $\sqrt{\frac{1}{MX}}$ and $\frac{1}{DX}$, the transfer function reduces to

$$\frac{\delta_{(S)}}{F_{(S)}} = X$$

which means that deflection is related to applied force by the numerical constant X, the mirror compliance (viz, inches deflection per pound of force). The laboratory demonstration model of the deformable mirror control system is operated at very low frequency, compared to mirror natural vibrational frequencies and, therefore, is well within the two frequency constraints given above. Hence, the deflection δ_{ij} at point i, due to an applied force F_j at point j, can be expressed as

$$\delta_{ij} = X_{ij}F_j$$

In general, the deflections at the n applied force points due to the n applied forces are representable in matrix notation as

$$\begin{bmatrix} \delta_1 \\ \delta_2 \\ \delta_3 \\ \vdots \\ \delta_n \end{bmatrix} = \begin{bmatrix} X_{11} & X_{12} & X_{13} \cdots X_{1n} \\ X_{21} & X_{22} & X_{23} \cdots X_{2n} \\ X_{31} & X_{32} & \cdots X_{3n} \\ \vdots & \vdots & \vdots \quad \vdots \\ X_{ni} & X_{n2} & \cdots X_{nn} \end{bmatrix} \begin{bmatrix} F_1 \\ F_2 \\ F_3 \\ \vdots \\ F_n \end{bmatrix}$$

or

$$[\delta] = [X]\,[F]$$

or, more simply, with matrix notation

$$\delta = XF$$

For the special case where n = 1 the mirror transfer function is

$$\frac{\delta}{F} = X$$

and the expression relating output, δ, and input, δ_{in}, positions of a single loop actuator controller is

$$\frac{\delta}{\delta_{in}} = \frac{\text{FORWARD LOOP GAIN}}{1+\text{OPEN LOOP GAIN}} = \frac{GX}{1 + GX}$$

Such a loop is obtained, as shown by figure 21, with the addition of a position sensor (there shown with unity transfer function for convenience) and an actuator with transfer function G. Stability prevails in such a system when the Nyquist plot of the open-loop gain, GX, does not encircle the minus 1 point. This criterion insures that the roots of the denominator are well behaved, i.e., lie in the left half S plane and have positive damping. Non-well-behaved roots, such as those indicating output for zero input and therefore instability, are thus avoided.

Two points are now worth noting as an aid in following subsequent discussion. First, if the denominator had been [2 + GX], well-behaved roots would have been obtained with a GX locus which does not encircle the minus 2 point. Second, if the denominator had consisted of two, rather than one such factor (viz,[1 + GX][2 + GX], two constraints for stability would have been required; that is, well-behaved roots would have been generated (from the first term) if GX did not encircle the minus 1 point and (from the second term) if GX did not encircle the minus 2 point. Here there are two critical points, the minus 1 and the minus 2 points, where each corresponds to or arises from a separate denominator factor.

If in the single loop case the actuator characteristic is of the integrating type, A/S, stability should be expected since the A X/S locus does not encircle the minus 1 point. This is depicted by figure 22 from which it is also evident that many other candidate choices for G will provide a stable system.

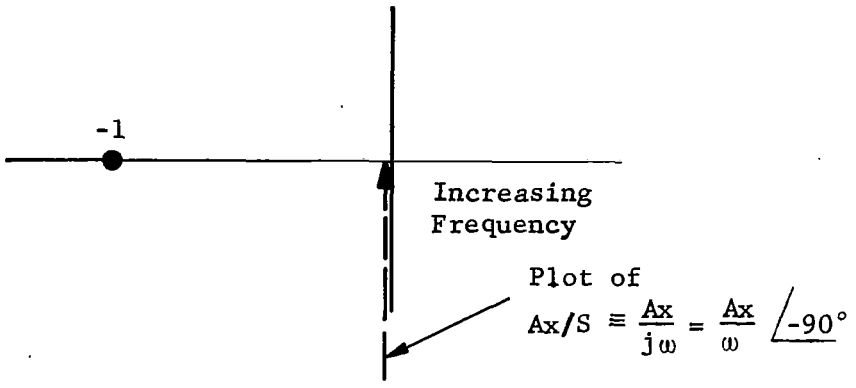

Figure 22. Nyquist Diagram

A typical implementation for this system would be as shown in figure 23. Here a position sensor detects displacement errors δ_{11} at point 1 and provides an actuator input signal for generation of corrective force F_1. For a two actuator arrangement, obtained by adding a second sensor and actuator (shown with dashed lines), the situation is a bit more complex in that one must also consider the effect of deflection δ_{21} introduced at point 2 due to force F_1 and vice versa.

A representative block diagram for this case would be as shown in figure 24 where the total deflection δ, at point 1 has components F_1X_{11} and F_2X_{12} due to forces at F_1 and F_2, respectively. The total deflection at point 2 is similarly related via X_{21} and X_{22} to forces F_1 and F_2. As shown, the errors E_1 and E_2 at points 1 and 2 are determined by the total deflections plus possibly some disturbances (or forcing functions) represented by D_1 and D_2. The figure sensor will be assumed to have a transfer function sign of minus to obtain negative feedback, and an amplitude of unity so that the actuator characteristic can be expressed as G. It should be noted again that G is a function of S (or $j\omega$), while the mirror matrix factors, X_{ij}, are simply real numbers.

Now let this two actuator system, rather than the actual N array, be considered in order to derive a stability criterion or synthesis constraint analogous to non-encirclement of the minus 1 Nyquist point.

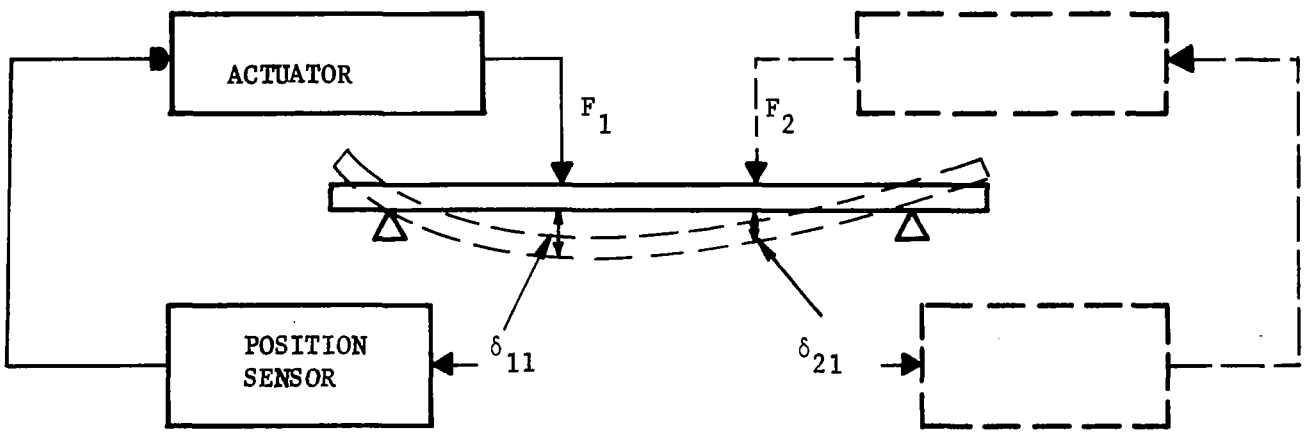

Figure 23. Typical System Arrangement

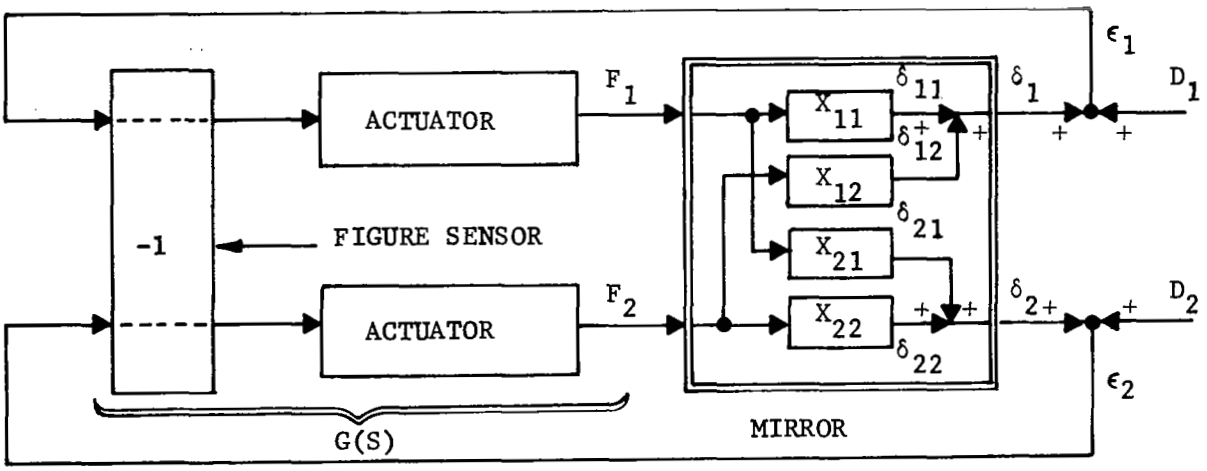

Figure 24. Two-Loop Block Diagram

The equations characterizing the system are

$$X_{11}F_1 + X_{12}F_2 + D_1 = E_1 = -\frac{F_1}{G_1}$$

$$X_{22}F + X_{22}F_2 + D_2 = E_2 = -\frac{F_2}{G_2}$$

A standard method of solution is to arrange and group terms containing F_i as indicated below

$$\left[X_{11} + \frac{1}{G_1}\right] F_1 + X_{12}F_2 = -D_1$$

$$X_{21}F_1 + \left[X_{22} + \frac{1}{G_2}\right] F_2 = -D_2$$

and express the solution for F_i as the ratio of determinants: viz,

$$F_1 = \frac{\det\begin{bmatrix} -D_1 & X_{12} \\ -D_2 & \left(X_{22} + \frac{1}{G_2}\right) \end{bmatrix}}{\det\begin{bmatrix} \left(X_{11} + \frac{1}{G_1}\right) & X_{12} \\ X_{21} & \left(X_{22} + \frac{1}{G_2}\right) \end{bmatrix}}$$

The denominator is the determinant formed from the coefficients of F_1 and F_2, while the numerator determinant is identical except that the coefficients of F_i are replaced by the forcing functions minus D_1 and minus D_2.*

*This solution is obtained, using matrix analysis, as follows

$$[X][F] = [-D]$$

$$\therefore [F] = [X^{-1}][-D]$$

where $$[X^{-1}] = \begin{bmatrix} \left(X_{22} + \frac{1}{G_2}\right) & -X_{12} \\ -X_{21} & \left(X_{11} + \frac{1}{G_1}\right) \end{bmatrix} \div \det \begin{bmatrix} \left(X_{11} + \frac{1}{G_1}\right) & X_{12} \\ X_{21} & \left(X_{22} + \frac{1}{G_2}\right) \end{bmatrix}$$

and stability is usually indicated by the roots of the characteristic equation formed by setting the denominator determinant equal to zero.

The resulting form for the solution of F_i is thus seen to consist of a numerator function P involving the disturbances, some of the coefficients X_{ij}, and the actuator characteristic; i.e.,

$$F_i = \frac{P\,(D_1,\ D_2,\ X_{ij}\ X_{ii},\ G_2)}{\left(\frac{1}{G}\right)^2 + \left(\frac{1}{G}\right)\left(X_{11} + X_{22}\right) + \left(X_{11}X_{22} - X_{12}X_{21}\right)}$$

More importantly, the denominator is seen to be a polynominal in G, or more precisely 1/G, and the numerical factors of the mirror compliance matrix. Here, all the actuators have been assumed to have equal transfer functions in order to obtain the indicated form of the denominator. For simplicity, now assume that $X_{11} = X_{22} = 1$, in which case

$$F_1 \approx \frac{P}{\left(\frac{1}{G}\right)^2 + \left(\frac{1}{G}\right)\ 2 + \left(1 - (X_{12}X_{21})\right)}$$

or equivalently

$$F_i = \frac{P}{\left(\frac{1}{G} + 1 + \sqrt{X_{12}X_{21}}\right)\left(\frac{1}{G} + 1 - \sqrt{X_{12}X_{21}}\right)}$$

where the denominator has been factored.

In the special case where the actuators are of the integrating type ($G = \frac{1}{S}$), the denominator roots are clearly well behaved, having negative real parts and therefore positive damping, as long as $\sqrt{X_{12}X_{21}} < 1$. More specifically, the roots are

$$S = -1 - \sqrt{X_{12}X_{21}},\ -1 + \sqrt{X_{12}X_{21}}$$

Hence, it can be concluded that a two loop system utilizing actuators of characteristic 1/S will be stable as long as $\sqrt{X_{12}X_{21}} < 1$. This is all very well and good, but a more important question to answer is what other characteristics also lead to a stable situation. The answer to this becomes more evident if both the numerator and denominator of the previous equation for F_i are multiplied by G^2 (or G^n in the more general case) to obtain

$$F_i = \frac{PG^2}{\left[1 + \left(1 + \sqrt{X_{12}X_{21}}\right)G\right]\left[1 + \left(1 - \sqrt{X_{12}X_{21}}\right)G\right]}$$

and then, similarly, both divided by the product of the G coefficients,

$$\left[1 + \sqrt{X_{12}X_{21}}\right]\left[1 - \sqrt{X_{12}X_{21}}\right] \triangleq C$$

to yield

$$F_i = \frac{PG^2C^{-1}}{\left[\frac{1}{1-\sqrt{X_{12}X_{21}}} + G\right]\left[\frac{1}{1+\sqrt{X_{12}X_{21}}} + G\right]}$$

Here the roots are well-behaved if G does not encircle the minus $\frac{1}{1+\sqrt{X_{12}X_{21}}}$ and minus $\frac{1}{1-\sqrt{X_{12}X_{21}}}$ critical points. Non-encirclement of the first point is required to avoid unstable roots from the first denominator term. A similar constraint, represented by the second point, insures stable roots from the second denominator factor. In the general case, where the number of loops is n, there are n denominator factors and therefore n constraints, or critical points that must not be Nyquist encircled when choosing an appropriate G.

The whole point of the above discussion is that the mirror (and structure) numerical compliance matrix terms alone determine the critical points to be avoided when synthesizing the actuator characteristic. Figure 25 represents the two-loop actuator example and shows that the critical points depart from the minus 1 point as interaction between channels is increased. With a moderate amount of coupling ($X_{12}X_{21}<1$) the points are located as shown and G = 1/S will not encircle either. This is not unexpected in light of the previous discussion. However, other suitable choices for G are possible including an integrating type actuator with a lag-lead-lag network in cascade. The laboratory demonstration deformable mirror hardware, it should be noted, has such a G characteristic. This characteristic is also shown in figure 26, a more general diagram applicable to the n actuator case. For such a system the overall effect of interaction or mirror crosstalk can be considered as a breakup of the minus 1 point into an array of critical points. This is indicated in the figure by arrows from the minus 1 point to the critical points shown in the

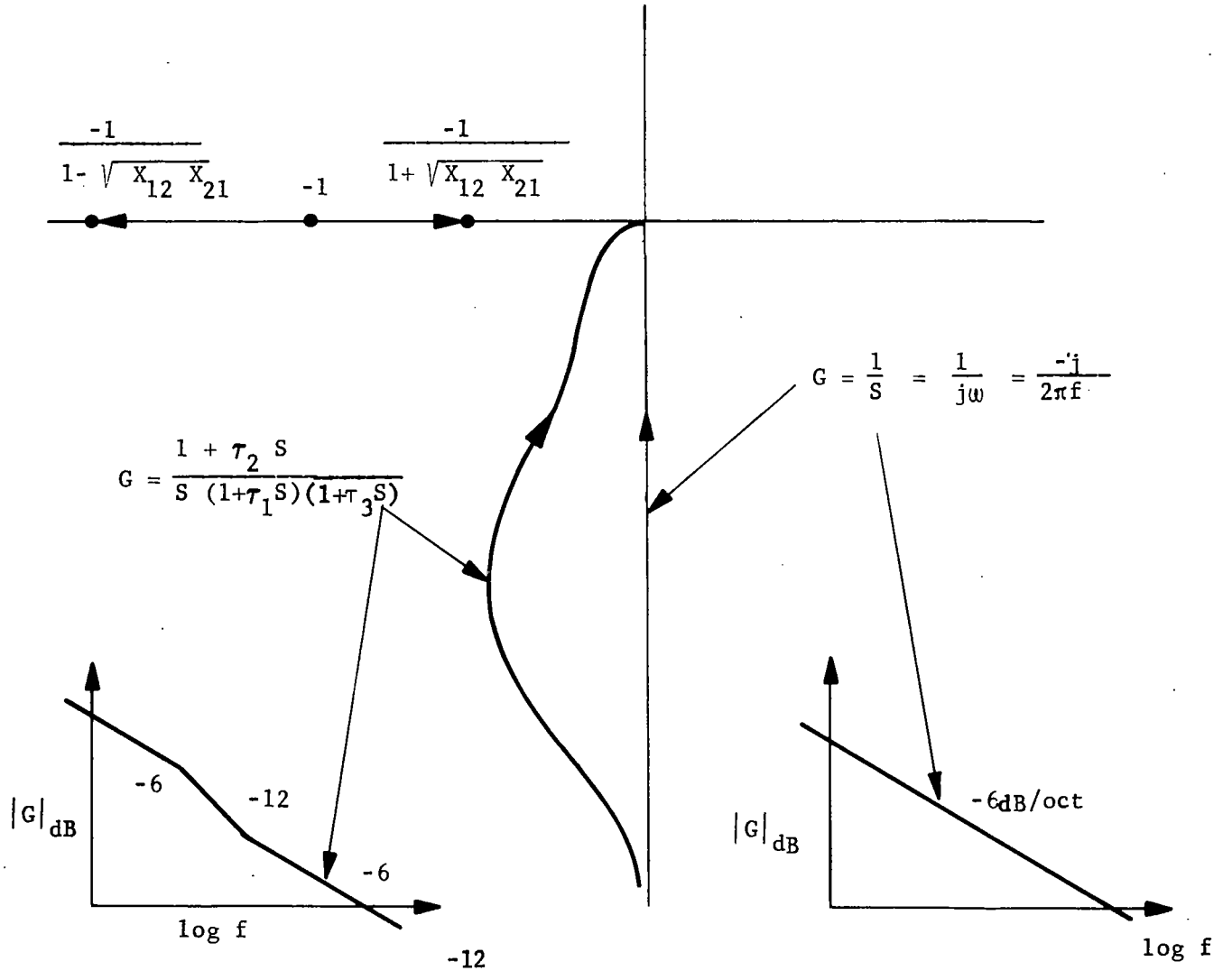

Figure 25. Nyquist Diagram for Two-Actuator System

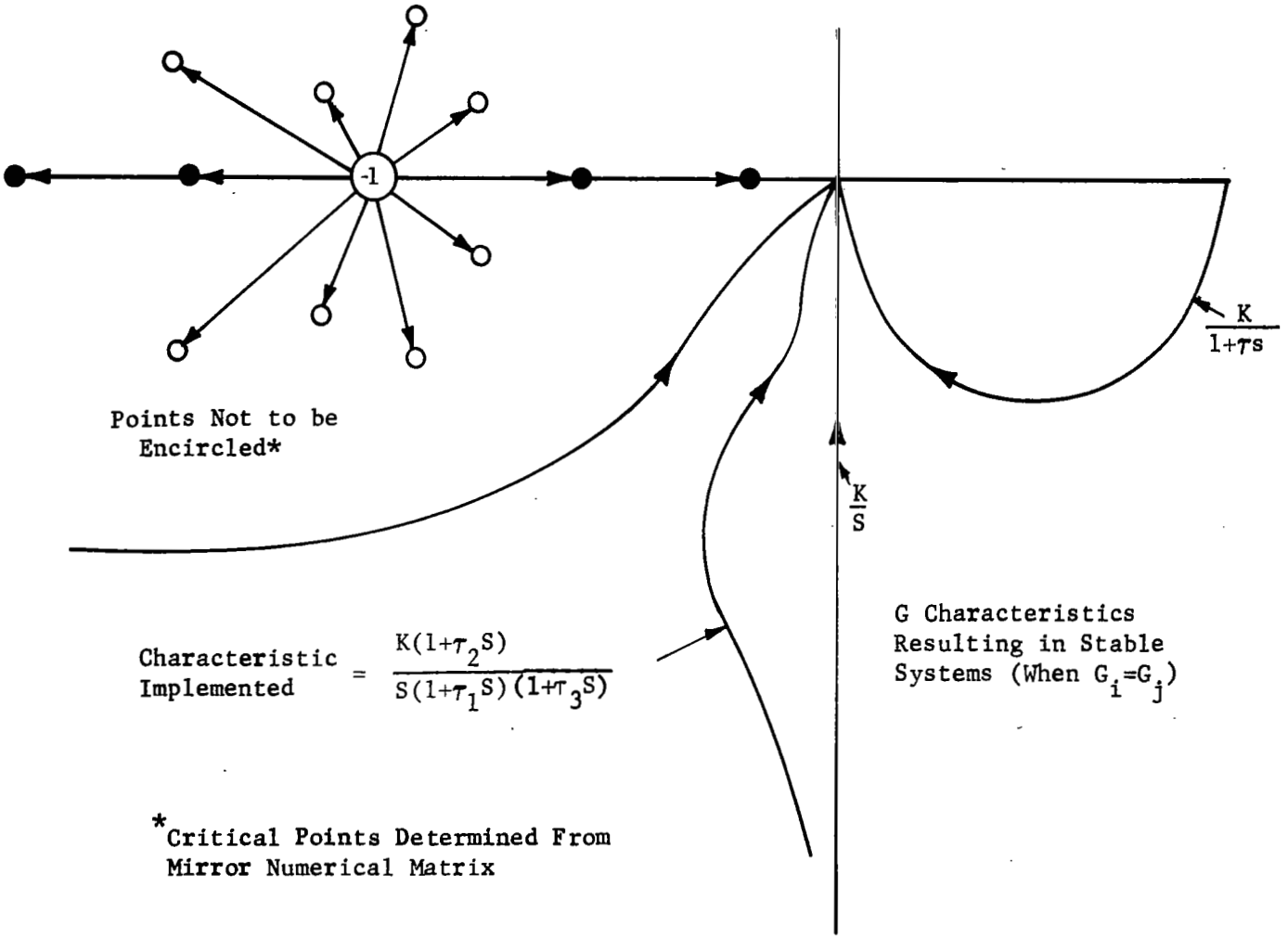

Figure 26. Nyquist Diagram

left half plane. This location is not entirely unexpected since the mirror with supporting structure is passive and stable by itself.

The eigenvalues of the present mirror were found to all lie along the positive real axis and so are represented by the critical points shown by the dots, rather than the circles, in the figure. Hence, possible choices for G include amplification with single lag, integration, and the implemented integration plus lag-lead-lag network. The foregoing approach was utilized to predict that the laboratory model control system would be stable without the decoupling (or crossfeed or feedforward) network. It is worth noting that the critical points are the negative inverse of the eigenvalues of the mirror force-to-displacement matrix, whose terms are real numbers in the low frequency range of control.

An important aspect to the stability discussion above is that the system is an interacting one. Hence, a forcing function such as a step error introduced into the system can produce a response either at this or another point. The prediction of expected responses, it should be noted, thus involves the solution of essentially an nth order determinant, some of whose terms are functions of frequency. The associated amount of effort involved in doing this is significantly greater than determining critical points from the numerical mirror matrix, X.

An alternate approach to stability involves the use of a decoupling network, which in effect implements X^{-1}, the inverse of the mirror matrix X. The attractive features of this approach include non-interaction of channels, similar responses of all channels if desired, and potentially improved stability. Since X is not frequency-sensitive, neither is X^{-1} and its mechanization need involve only resistors (thus avoiding the complication and expense of reactive elements as well). The inverse network can be thought of as a circuit, as shown in figure 27, which for a given ϵ_{iA} generates an array of actuator input driving signals. The particular array generated, moreover, is that which will cause a force array that changes the mirror displacement at point i only. This will be the case if the actuators have equal reaction times (or G characteristics) so that corrective forces are applied in proper relative phase or at the same relative rates, so to speak. Hence, it is concluded that if all G_i

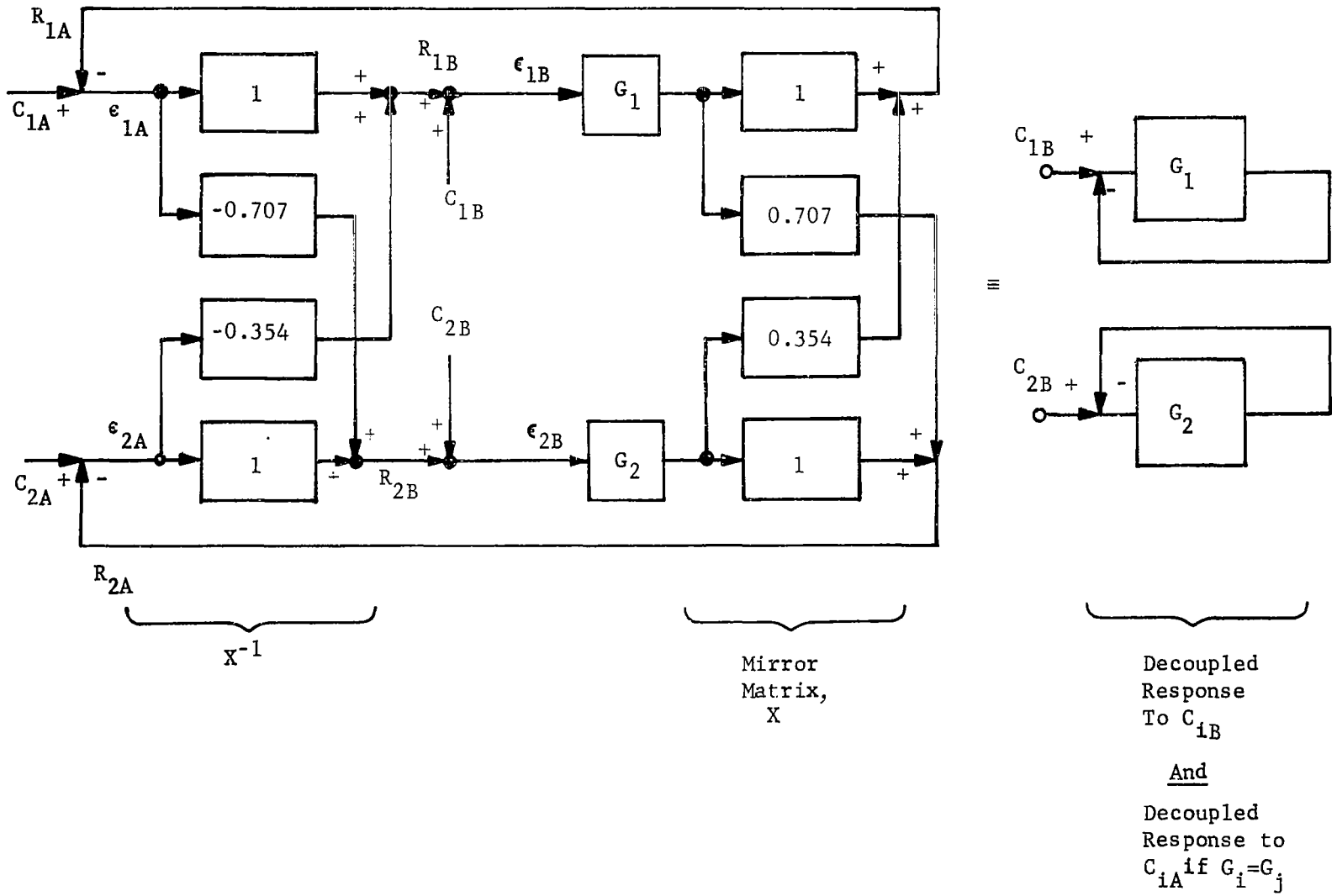

Figure 27. Inverse Matrix (Feedforward) Concept

characteristics are equal, mirror displacement errors at any point will be corrected without effects at other points. However, many actuators will be simultaneously driven to accomplish this end.

An error at ϵ_{iB}, on the other hand, will drive only one actuator and produce an array of errors that act through the network X^{-1} to produce a corrective reaction R_{iB} only at point iB. This occurs whether or not equal G_i characteristics exist since the mirror matrix and its inverse are effectively in cascade, and therefore are equivalent to n straight-through (non-interacting) connections.

The stability of the system can be investigated by considering reactions to either C_{iA} or C_{iB} inputs, i.e., in the first case (and using matrix notation),

$$R_A = XGX^{-1}(C_A - R_A), \text{ or } R_A = \left[1 + XGX^{-1}\right]^{-1} XGX^{-1}C_A$$

while in the second case

$$R_B = -X^{-1}XG(C_B + R_B), \text{ or } R_B = -\left[1 + X^{-1}XG\right]^{-1} X^{-1}XGC_B$$

Each of these expressions involves an inverse matrix having a matrix numerator, determined in standard fashion, plus a determinant in the denominator from which the system stability (roots) is determined. Since the stability of the system should not depend upon where disturbances are introduced, it can be expected that identical roots will evolve from the two denominator determinants,

$$\det\left[1 + X^{-1}XG\right] \quad \text{in the first case and}$$

$$\det\left[1 + XGX^{-1}\right] \quad \text{in the second case.}$$

This can be readily shown since the following relationships hold.

$$XX^{-1} = X^{-1}X = 1$$

$$\det XX^{-1} = \det X^{-1}X = \det 1$$

$$\det X\,[A]\,X^{-1} = \det X \det A \det X^{-1} = \det X^{-1} \det A \det X = \det A$$

Hence

$$\det [1 + X^{-1}XG] = \det [1 + G] = \det [X^{-1}X + G]$$
$$= \det X^{-1} [1 + XGX^{-1}] X$$
$$= \det X^{-1} \det [1 + XGX^{-1}] \det X$$
$$= \det [1 + XGX^{-1}]$$

In both cases, then, the denominator determinant is equal to

$$\det [1 + X^{-1}XG] = \det [1 + G]$$

which is expressible as

$$\prod_{i=1}^{n} (1 + G_i)$$

if the G matrix is a diagonal one. Hence, stability will prevail even with different actuator characteristics as long as all the characteristics chosen do not encircle the minus Nyquist point.

The synthesis procedure reduces then to that involved with n separate servo loops.

Control System Design Considerations

The control system study indicated that it was feasible to control the deformation of a solid thin mirror. After consideration of several approaches, it was decided to proceed with a diagonalized multi-dimensional control system. A diagonalized multi-dimensional control system is one that achieves independent displacement at each actuator despite elastic interaction that takes place within the mirror. This ideal system is achieved by introducing between the channels crossfeeds or interconnections that negate the mirror interactions. Thus, the ideal diagonalized control system has no net interactions between channels.

Provision was also made for controlling the system without crossfeeds so that the response of the system could be observed with and without the decoupling provided by the diagonalization.

Complete diagonalization was not attempted, so that the number of crossfeeds could be limited to a manageable number. The extent of decoupling required for stability was not known; therefore, the number of crossfeeds chosen was somewhat arbitrary for the first experiment. The determination of the crossfeed values is discussed in a subsequent section.

The ideally diagonalized system will always be stable if the independent channels are stable and will track displacement errors until they converge to zero or are negligible. Component variations, tolerances, and ignorance of the mirror's influence coefficients will cause a physically realizable system to have residual interactions, however. These residual interactions decrease the channel independence and become a source of potential instability.

An analysis of the departure of the system parameters from the ideal diagonalized system establishes a limit to the maximum allowable percent variation in the compensating network resistor values. The analysis also shows that, subject to the equal gain blocks in each channel, classical single-loop feedback analysis and synthesis methods may be applied in designing the system to obtain a desired transient performance.

Force and displacement concepts in the selection of a thin mirror flex actuator.- The basic control system configuration is as shown in figure 28. The mirror is a 30-inch diameter, 1/2-inch thick, fused-silica, spherical, F/3 reflector. It is controlled by n actuators where n has been selected as 58.

The thin mirror flex actuator can be idealized in general by defining force and displacement actuators in terms of their relative spring constants. The actuator motor can produce either a force or a displacement. The force or displacement can be considered to be working in parallel with a spring and mass in the mobility analogy (force = current), or in series with a spring and mass in the classical analogy (force = voltage). If the spring's constant is much greater than the other spring constants of the system, the actuator is

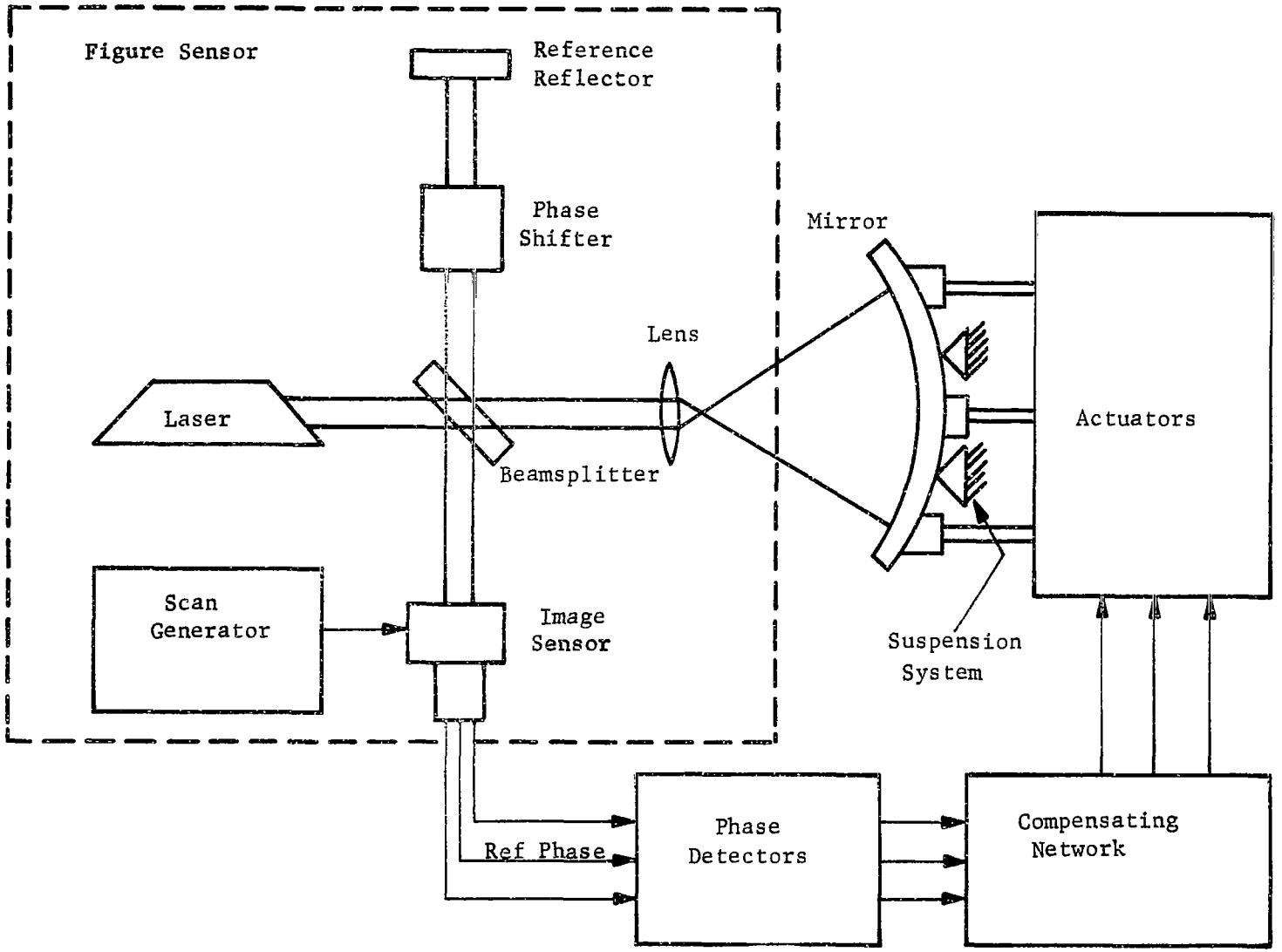

Figure 28. Control System Configuration for Thin Deformable Mirror.

considered to be a "displacement" actuator. A piezoeletric element can be used to provide essentially displacement actuation. If the spring constant is much lower than the other spring constants of the system, the actuator is considered to be a "force" actuator. An example of this type of actuator is a motor-controlled lead screw, which drives a very soft spring. The properties of three actuator types characterized by three different relative spring constants are developed below:

High spring constant (displacement actuator, see figure 29a): In this case a displacement-producing device is approximated by setting the spring constant high with respect to the other spring constants of the system. In this configuration, the displacement step sizes are very nearly equal in size to those displacements that are produced in the mirror, and a displacement produced at one point has relatively little effect on the displacement of other actuator points. The forces applied to the mirror at each actuator point, however, are definitely dependent upon the other actuator displacements. This means that the interaction due to mechanical coupling through the mirror is automatically accommodated so that a local displacement can be obtained at any point by programming a single actuator at that point. It is assumed that the backing plate is very rigid in this case and that a component representing the backing plate rigidity is included in the actuator spring constant.

The highest spring constant in the 0.5-inch-thick mirror is that constant associated with a displacement of a single actuator with all of the other actuators held fixed. The displacement-force relationship for this case is approximately 10 microinches displacement with a 1 pound force for 3.75-inch actuator spacing. This gives a spring constant of 100,000 pounds per inch. If an effective actuator spring constant of at least 10 times this value is desired to approximate a displacement actuator, the actuator and backing plate together must present a spring constant of 10^6 pounds per inch. This requires a backing plate with the rigidity of a 2-inch thick steel plate and actuators with the rigidity of a 1-inch-long by 0.5-inch-diameter glass rod.

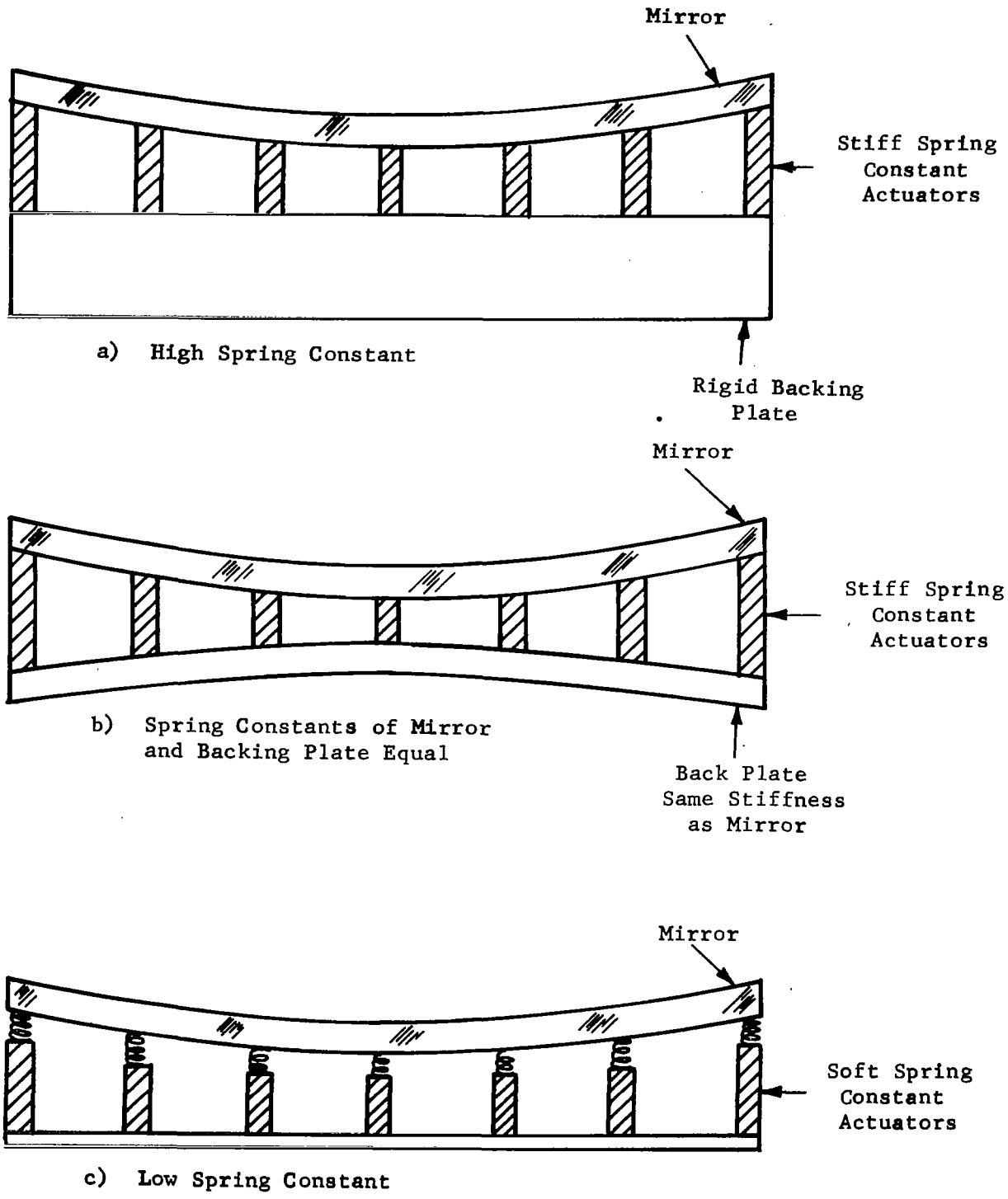

Figure 29. Idealized Actuator Devices

As the size of the mirror increases, the effective thickness of the backing plate will scale approximately proportionally if the number of actuation points remains the same. This would reduce the weight-saving advantage to be obtained with an active optical system utilizing a thin deformable mirror.

Spring constant equal to the approximate magnitude of the other spring constants of the system (see figure 29b): In this case, the displacement step size is larger than the displacements created in the mirror. Both the step size and the applied forces depend strongly upon all the actuators. In general, neither the displacement nor the force applied is a unique function of the drive applied to a particular actuator. One particular configuration, however, does provide the independent displacement characteristic observed in the first case. This configuration uses a very stiff actuator and a backing plate that has the same relative displacement characteristics as the mirror. That is, the shape of the displacement at any point is the same as the corresponding point on the mirror for a given force configuration. The only practical way to obtain this same displacement characteristic is to use a backing plate that is identical to the mirror. (An infinitely rigid backing plate that has the "same" shape but zero amplitude also satisfies this requirement but has already been considered in the first case.) The advantage this system presents is again the automatic localization of the actuator effect (if the actuators themselves are very rigid), as in the first case, without a highly rigid and, consequently, massive backing plate.

The backing plate should be of the same material and geometry as the mirror. The mounting arrangement would be restricted and probably complex in order to maintain the symmetry between mirror and backing plate. The actuators must have the same characteristics required for the first case above.

Low spring constant force actuator (see figure 29c): In this case, a force actuator is approximated by setting the actuator spring constant very low with respect to the other spring constants of the system. In this configuration the size of the actuator displacement step is much larger than the corrections applied to the mirror. The force applied at a given actuator is dependent upon

the control of that actuator and is relatively independent of the forces exerted by the other actuators. The displacement produced, however, is dependent upon the effects of all the actuators. The displacements of the mirror surface are essentially independent of changes in the shape of the backing plate.

Consider, for example, the 30-inch diameter, 0.5-inch-thick mirror having actuators on 3.75-inch centers applied to the mirror through springs that have a rate of 4 pounds per inch. A displacement of the backing plate of 1×10^{-3} inch can give a maximum mirror displacement of 1/100 wavelength for this configuration. This does not represent a very stringent tolerance for the dimensional stability of the backing plate and, consequently, it can be a relatively flexible structure.

The basic advantage of the force actuation approach is that there is no requirement for a relatively massive backing plate and there is no necessity for correction of changes in mirror figure due to the displacements of the backing plate. In the force actuation system, the precision mirror is the natural restraining spring that converts force into displacement; therefore, it appeared worthwhile to develop the force actuator method experimentally since it preserves the weight-saving advantage of the Active Optical approach.

This discussion has been in terms of a mirror plus a backing or reaction plate. In a trestle-arrangement support structure (figure 30), there is no backing plate, and interaction takes place between actuator groups. Actuators can work in overlapping groups to reduce coupling, and the groups of actuators react through the mirror itself. This arrangement was not used for this experiment since it does not allow flexibility in making comparative tests with varying actuator numbers and spacings.

Consideration of the actuator type to be employed led to the choice between force or displacement type output. Very high stiffness actuators have been shown to imply heavy supports. This latter requirement is perhaps unrealistic in a space application where conservation of payload is important. Therefore, a force type actuator was used in this experiment. The major

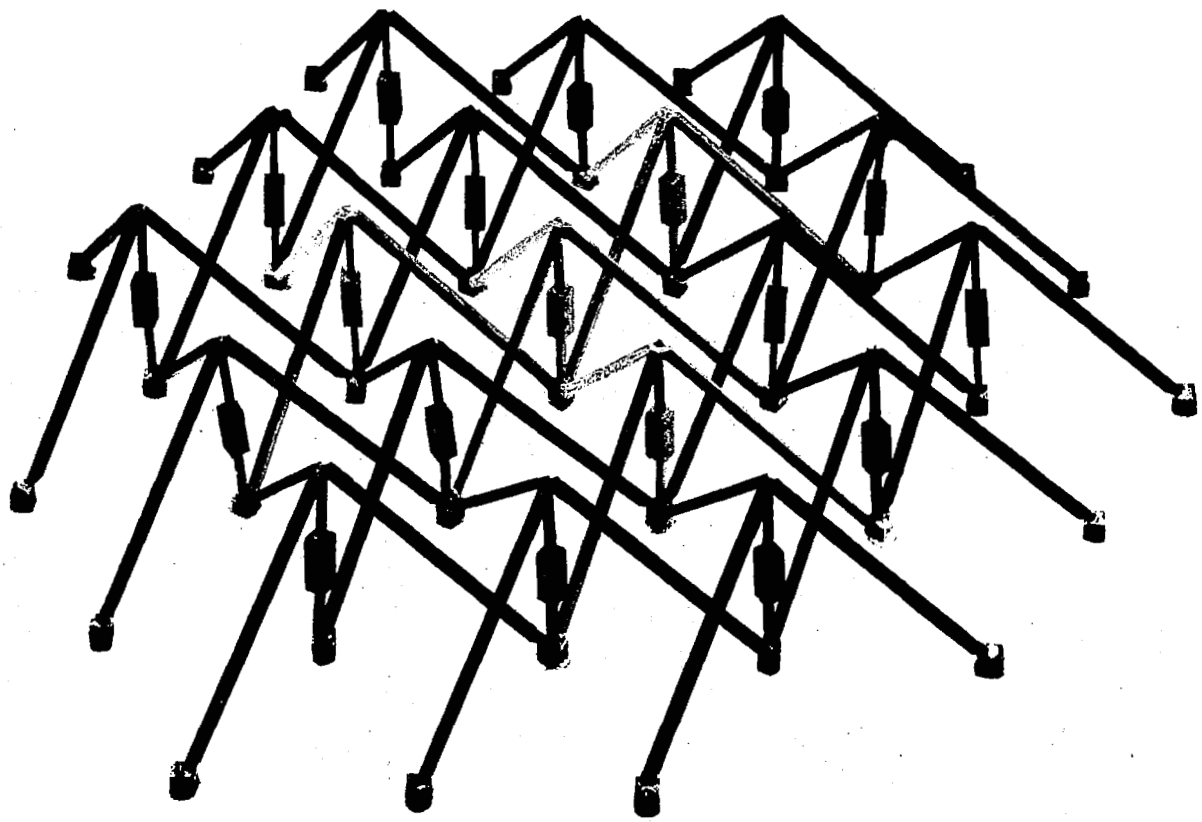

Figure 30. Trestle Actuator Support Mockup

disadvantage of the force output actuator is that displacement interaction within the mirror introduces the possibility of instability in the control system. One of the primary functions of the control system then was to negate the mirror interaction by deliberately introducing interactions in a suitable compensation network.

Control system selection.- The basic control problem was to accurately sense a mirror's figure and to provide a means to deform its shape so as to insure an rms figure error of less than 1/20th of a wavelength.

The main difficulty in achieving this objective was considered to be the mirror's internal displacement interaction. Several possible approaches to obtaining the objective, in spite of the difficulty of mirror internal interaction are:

(a) N independent, continuously-tracking feedback loops

(b) A sampling adaptive system

(c) Optimal control based on minimization of mean square error

(d) Self-organizing control

(e) Modal excitation

It was decided that the first approach was the most straightforward and offered the least complex implementation; therefore, the project design effort was directed toward the first approach. This does not, however, preclude the future consideration of other approaches.

The basic control system data processing approach was selected after evaluating three competitive techniques:

(a) Analog data processing - In the analog approach, the feed-forward resistors, determined from the inverted influence coefficient or stiffness coefficient matrix of the mirror, decouple the parallel channels.

(b) Digital data processing - In the digital approach, the stiffness coefficient matrix is stored in the data-processor memory. The analog error signals in each channel are converted to digital signals, and multiplication with the appropriate stiffness coefficients is accomplished by small general purpose digital computer that is appropriately programmed. The products are summed and distributed to the appropriate actuator channels where they are converted to analog signals again. This data handling is accomplished by the digital computer.

(c) Hybrid digital and analog data processing. This system stores the stiffness coefficient matrix in a digital memory storage unit that is used to control an analog signal multiplier. The multiplier is a binary code ladder that is programmed through switches controlled by the memory.

Various combinations of parallel and sequential operation were considered as subclassifications of these methods of processing. The analog data processing method was selected for implementation in this experiment.

Control system implementation.- The control system concept is based upon a matrix of 61 points or nodes of force application arrayed on the mirror. For the decoupled system, a figure error measured at a particular node is used to generate a constellation of forces that are applied to the back of the mirror in the vicinity of that node. In principle, the constellation of forces is computed so that it generates only a local deformation in a small area centered on that particular node, while all other portions of the mirror are unaffected. Any random figure error profile is then considered to be the sum of many small area errors where the small area size is determined by the actuator spacing. This approach effectively decouples the control channels for each node by the use of crossfeeds in the forward loops, or "feedforwards", that counteract the interactions in the mirror.

The diagram of figure 31 illustrates the general control concept. Interactions between the tilt and focus control loops and the flex control loops are decoupled by keeping the response time of the flex control loops much longer than that of the tilt and focus control loops, i.e., on the order of five to ten times slower. (The flex control loops are those that control the 58 actuators that apply forces to strain or flex the mirror and are sometimes referred to as flex actuators.)

Error signals for control of the flex actuators are developed from information at the output of a diode array. Fifty-eight channels of signal amplification, filtering, hard limiting, and phase detection are used in the figure error detector for parallel operation. Fifty-eight servo amplifiers are used for simultaneous operation of all channels.

Feedforwards, consisting of resistive components between channels, provide an analog multiplication and summing of the error signals. If decoupling were necessary between every pair of channels and no symmetry were present, approximately 3600 resistors would be required. However, a maximum of 19 resistors for each node, or a total of less than a thousand resistors for the full matrix were estimated to be sufficient to insure stability. (See section "Determination of Feedforward Network".)

Control system functions.- The control system functional diagram is shown in figure 32. The 61 control channels are almost identical with some small differences in frequency response, cross coupling, and switching functions between the flex channels and the tilt and focus channels. Each channel takes its signal from a "Fotofet" detector at the output of the phase measurement interferometer. Each signal is compared with a reference signal to obtain phase information. (The phase error is proportional to mirror figure error - see refs. 1 and 2.) The dc voltage at the output of the phase detectors, proportional to the phase difference observed between signal and reference, is applied in appropriate amplitude to the servo amplifiers through the feedforward matrix of resistors. These resistors distribute the signal in the proportion determined by the analysis of the mirror interaction as appropriate to obtain decoupled loop operation.

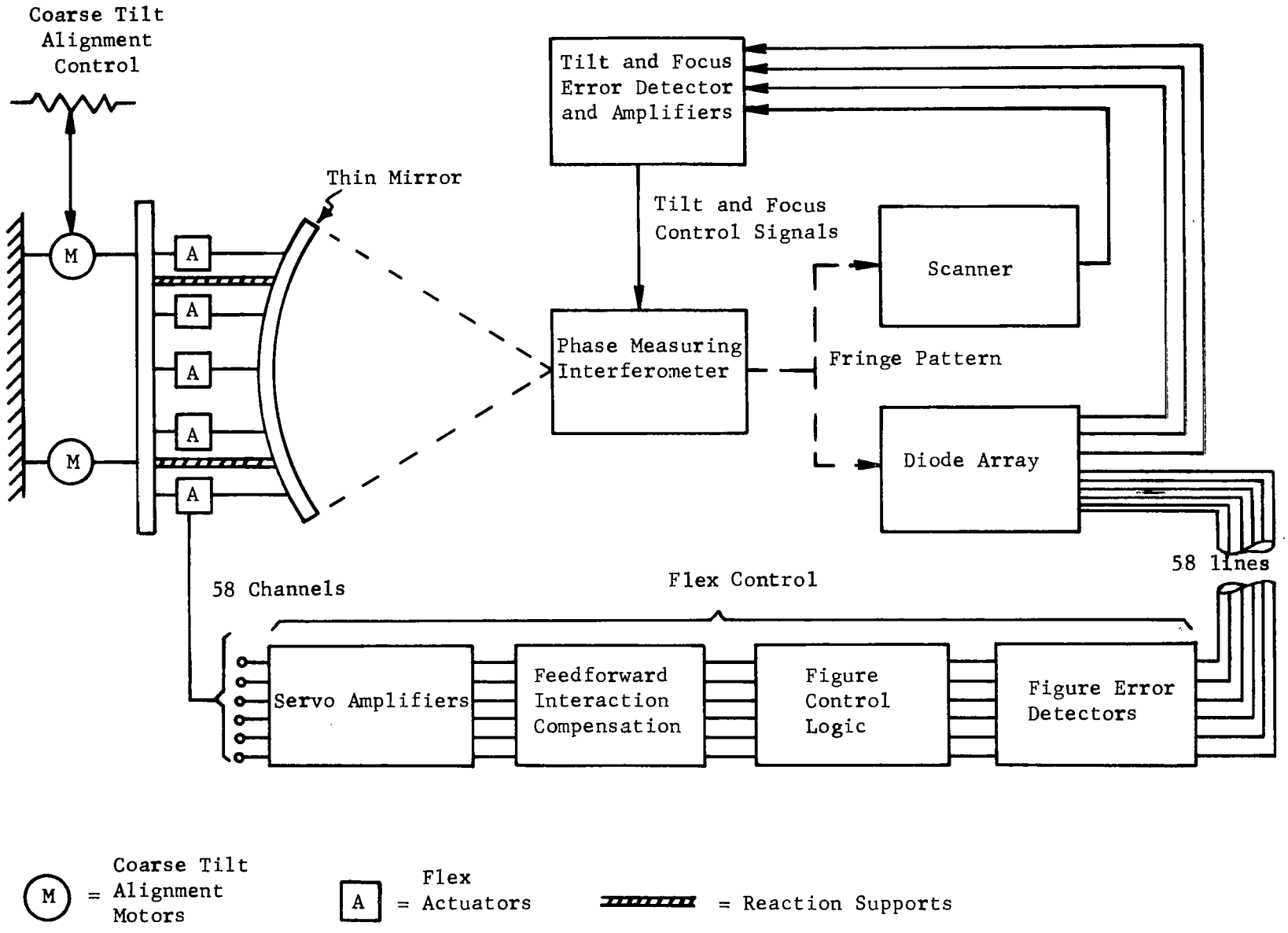

Figure 31. Control System Block Diagram

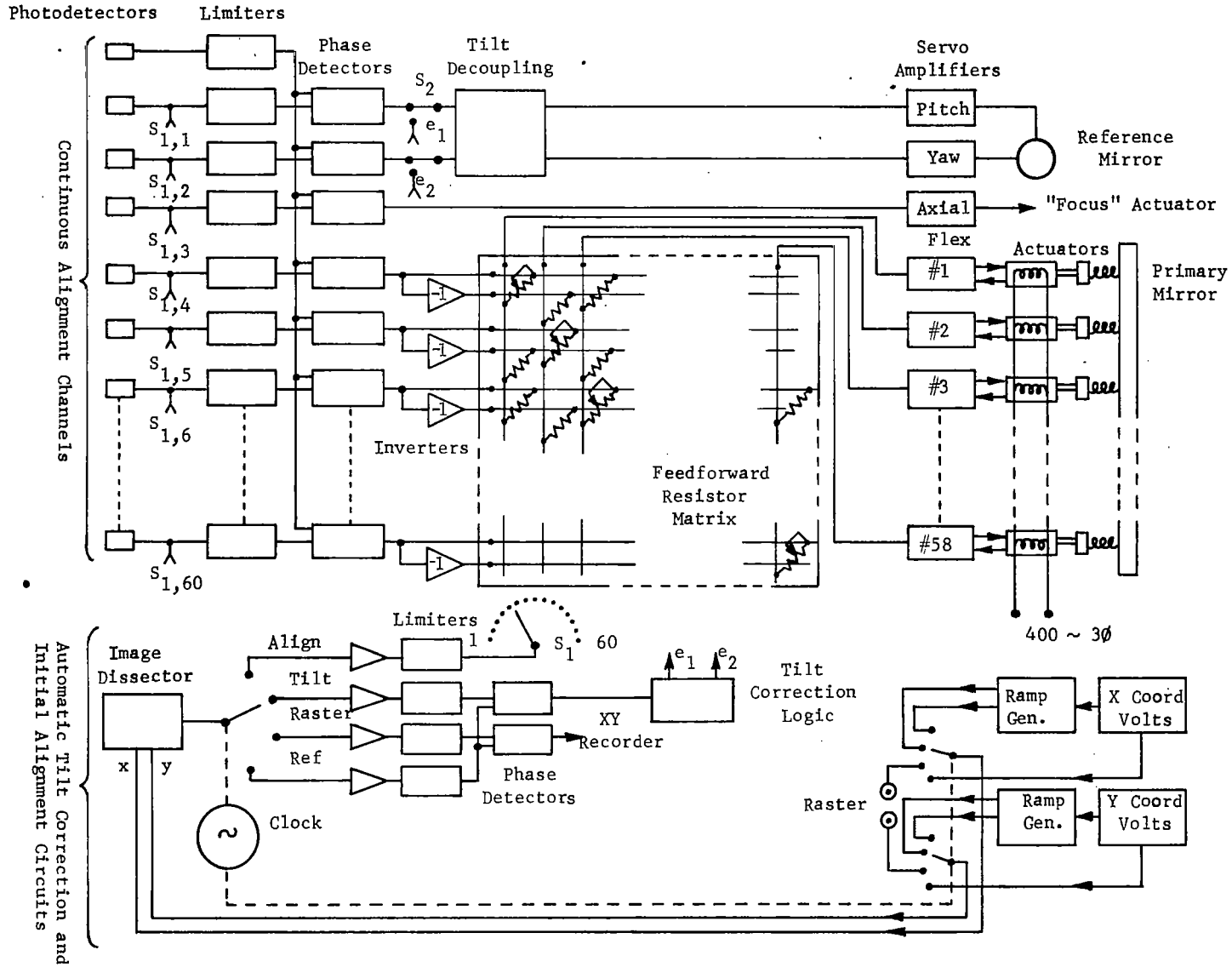

Figure 32. Functional Diagram of Closed Loop Control System for Thin Deformable Mirror

For initial alignment, a switching arrangement is provided that allows the input to each channel to be taken from a movable pre-programmed position on the image dissector face plate instead of from the Fotofet detectors. This allows each channel to be aligned by sweeping the movable spot from a nearby aligned channel to the channel being aligned and then switching the input to the signal from the individual Fotofet detector. This step is necessary because of the possibility of integral fringe displacements existing initially between actuator locations.

Control loop design.- The design of an individual control channel suffices for all control channels since they are assumed to be identical. The system design approach was to design a single loop in the classical way for the range of eigenvalues, assuming that only direct feedforwards with no crossfeeds would be used, i.e., the feedforward matrix was taken to be equal to the identity matrix.

It was determined from the stability study that the system would be absolutely stable even without a compensating feedforward matrix for simple integrator loops and second-order loops. However, the spread of eigenvalues as obtained from the computer analysis of the mirror's influence coefficient matrix led to a set of widely dispersed transient response modes. Even without calculating the amplitudes of these transient modes, the design could be carried out in terms of the closed-loop damping ratio and the natural frequency for each channel and its associated loop. Having established an acceptable design which accommodated the uncompensated or natural spread in transient response modes, the use of a compensating feedforward matrix then served to reduce this natural spread. Ideally, if an exact inverse resistance matrix is employed, then all modes degenerate to a single mode with a well-established transient performance. In the actual case, because of tolerances, the ideal is not achieved but, after appropriate adjustment to insure that the effect of the tolerances does not result in instability, the transient performance is improved over the uncompensated case for which the system was originally designed. The adjustment consisted of decreasing the resistance values of the diagonal elements of the feedforward matrix approximately 10% to increase the driving point

gains. This increases control channel interaction somewhat but protects against the possibility of positive feedback due to a worst case pile up of tolerances.

A typical single-loop design procedure (uncompensated case): Consider the block diagram for a typical channel and its associated feedback loop as shown in figure 33. The known quantities are listed in table I. It is required to determine the values of the parameters K_A, which establish the loop gain, and the time constant τ, which together with K_A establishes the loop dynamics. The value of the motor transfer constant K_N is not required since it cancels out in the loop gain expression as a result of the use of tachometric feedback.

TABLE I

CONTROL SYSTEM PARAMETERS

Device	Parameter	Units	Value
Phase Detector	Sensitivity, K_ϕ	Volts/rad	$16/\pi$
Chopper	Gain, K_C	V, rms/volt, DC	0.896
Tachometer	Sensitivity, K_T	V, rms/rad/sec	2.42×10^{-3}
Gear Train	Gear ratio, n	---	93
Lead Screw	Pitch factor K_p	in/rad	3.98×10^{-3}
Soft Spring	Stiffness, k	lb/in	4.0
Mirror	Influence coefficient at point i, α_{ii}	μin/lb	87 (center) - 576 (edge)
Figure Sensor	Sensitivity, K_{FS}	rad/μin	$4\pi/24.91$ @ $\lambda = 0.6328$Å

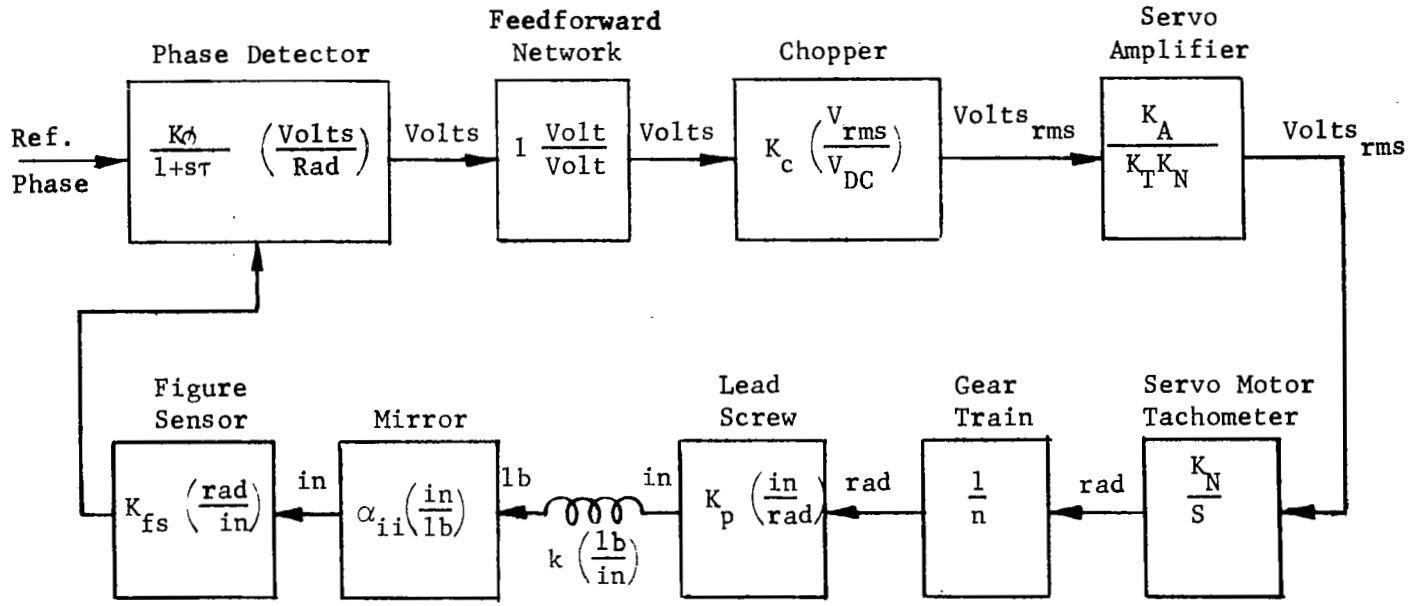

Figure 33. Typical Single-Loop Control System

The loop gain expression, using the data of table I, is:

$$K(S)\Big|_{\alpha_{ii}=87} = \frac{14.167K_A}{S(1 + S\tau)}$$

The poles of the closed-loop transfer function are found from the relation that

$$\frac{K(S)}{\alpha_{ii}} = -\frac{1}{\lambda_i}$$

for each eigenvalue λ_i. From NASA's and Perkin-Elmer's joint efforts, it was found that

$$\lambda max = 3224 \frac{\mu - in}{lb}$$

$$\lambda min = 1 \frac{\mu - in}{lb}$$

The roots of the characteristic equation are the zeros of

$$1 + \frac{K(S)}{\alpha_{ii}} \lambda_i = 0$$

which are also the zeros of

$$S^2 + \frac{S}{\tau} + \frac{C}{\tau} \lambda_i = 0$$

using $K(S) = \frac{C}{S(1 + S\tau)}$. Thus, the damping ratio and natural frequency for the i-th channel are:

$$\xi_i = \frac{1}{2} \sqrt{\frac{1}{\lambda_i C \tau}}$$

$$fn_i = \frac{1}{2\pi} \sqrt{\frac{\lambda_i C}{\tau}}$$

Numerically, using the center influence coefficient as a reference value, we find

$$\xi_i = \frac{1}{2}\sqrt{\frac{1}{0.16284\ K_A\lambda_i\tau}}$$

$$fn_i = \frac{1}{2\pi}\sqrt{\frac{0.16284\ K_A\lambda_i}{\tau}}$$

Consider the extremum value of ξ and fn from the extremum value of λ_i. A bar placed over the quantity denotes a maximum and a bar placed under the quantity denotes a minimum so that:

$$\underline{\xi} = \frac{1}{2}\sqrt{\frac{1}{524.99\ K_A\tau}} \approx \frac{1}{50\sqrt{K_A\tau}}$$

$$\overline{f_n} = \frac{1}{2\pi}\sqrt{\frac{524.99\ K_A}{\tau}} \approx 4\sqrt{\frac{K_A}{\tau}}$$

$$\overline{\xi} = \frac{1}{2}\sqrt{\frac{1}{0.16284\ K_A\tau}} \approx \frac{1}{0.8\sqrt{K_A\tau}}$$

$$\underline{fn} = \frac{1}{2\pi}\sqrt{\frac{0.16284\ K_A}{\tau}} \approx 0.064\sqrt{\frac{K_A}{\tau}}$$

Thus $\overline{\xi}/\underline{\xi} = \overline{fn}/\underline{fn} = 62.5$

At this point it is necessary to invoke the use of an appropriately large time constant in order to reduce the phase detector output ripple due to the presence of the carrier to an acceptable minimum. From experimental investigation it appears that τ must be 1.0 second or greater so that

$$\underline{\xi} = \frac{0.02}{\sqrt{K_A}} \qquad \overline{\xi} = \frac{1.25}{\sqrt{K_A}}$$

$$\overline{fn} = 4\sqrt{K_A} \qquad \underline{fn} = 0.064\sqrt{K_A}$$

Since it is highly undesirable to have a damping ratio less than 0.1, choose $K_A = 0.0004$ so that

$\underline{\xi} = 0.1$ $\qquad$ $\overline{\xi} = 6.25$

$\overline{fn} = 0.8$ Hz $\qquad$ $\underline{fn} = 0.015$ Hz

Thus, the most underdamped loop will ring at a period of 1.25 seconds for several cycles when subjected to a step command, and will take 5 to 10 seconds to stabilize. The most sluggish loop will take several minutes to stabilize but with no overshoot.

With the loop compensated properly by use of the feedforward matrix to obtain a local deformation at each point, the eigenvalues are identical. If these are assumed to be 12.5μin/lb then the identical characteristic equation for each loop will be

$$1 + \frac{\frac{(14.167)(12.5)\ K_A}{87}}{S(1 + S\tau)}$$

or

$$s^2 + s\,\frac{1}{\tau} + 2\,\frac{K_A}{\tau} = 0$$

For a gain $K_A = 0.04$ and time constant $\tau = 1$ second

$$s^2 + s + 0.08 = 0$$

This establishes the damping ratio and natural frequency of the compensated system as:

$\xi = 1.77$ $\qquad$ $fn = 0.045$ Hz

Determination of Feedforward Network

The decoupled control loop approach, employing a matrix of feedforward resistors, required an evaluation of the multipoint interaction of the mirror to determine the number of matrix elements required and their values.

A finite element computer program was utilized by J.F. Creedon at the NASA Langley Research Center to provide data on the static mirror behavior in response to actuator loads. A 12-inch-diameter, 0.125-inch-thick, f/2.5 spherical plate glass mirror was studied experimentally to establish the ability of the computer program to describe the mirror behavior. The calculated displacements obtained from the analysis of a mirror of the same dimensions as the test mirror were compared to the experimental displacements, and it was concluded that the results were sufficiently compatible to warrant predicting the behavior of the 30-inch-diameter mirror with the computer program. A detailed description of the above analysis and experimental investigation is found in reference 3.

The results of the analysis were used to obtain actuator force configurations that would provide local displacements of the mirror at any one of the actuator control points. The analytically derived force configurations gave the forces to be applied to every one of the 58 actuation points for each local displacement desired. However, the forces were observed to diminish rapidly with distance for actuator locations removed from the driving point (i.e., the point where local displacement is desired). A close approximation to the effects of the full set of forces could be made by a limited number of forces close to the driving point. In fact, it was estimated that a 19-point* configuration was the maximum useful array around each driving point since the forces outside this array were smaller than the uncertainty in the calculated values. Nineteen-point force configurations were then obtained by disregarding points outside the first two adjacent rings of actuators around each driving point and adjusting the remaining values so that they met three requirements: first, that the sum of the forces around each driving point equal zero; second, that the sum of the moments of the forces around each driving point equal zero; and third, that the 58 sets of force configurations fit rows and columns of a 58-by-58 matrix [F] such that $F_{ij} = F_{ji}$.

*Nineteen points were used for interior actuator locations. Locations near the mirror edge required fewer points.

Two of the resultant sets of force configurations are shown in figures 34 and 35.for an interior point and an edge point, respectively. The numbers shown indicate the relative force applied at each point. The absolute values were determined from analysis of the loop gain desired.

Figure 36 shows the total matrix of feedforwards and gives the actual resistor values used in the experiment.

SYSTEM HARDWARE

Thin Mirror Fabrication

The first step in the fabrication procedure was to process a 30-inch diameter, 4-inch thick, fused silica mirror blank, which had been selected for low uniform strain relief, to obtain a high quality spherical surface on one side. Since the techniques for producing a spherical mirror surface on a thick blank are well established, this operation did not involve any new procedure. The next step was to reduce the thickness of the mirror to 1/2 inch by removing material from the back. The amount of warping due to released stress in the material was expected to be small since the material was relatively strain free. The procedure for removing material was: first, to cut off a slab 2 inches thick and then to remove the remainder by grinding. The 2-inch slab was cut by a moving wire that carried a grinding slurry. Most of the remaining material to be removed was taken off on a surface generator, but the final operation to remove the last millimeter of material utilized a polishing tool as shown in figure 37. Successively finer grits of grinding compound were used to remove any local strains introduced in the coarse grinding process.

The mirror was first tested after the spherical front surface had been generated but before the thickness was reduced. An interferogram of the mirror surface at this stage is shown in figure 38. Evaluation of the interferogram yielded the contour map shown in figure 39.

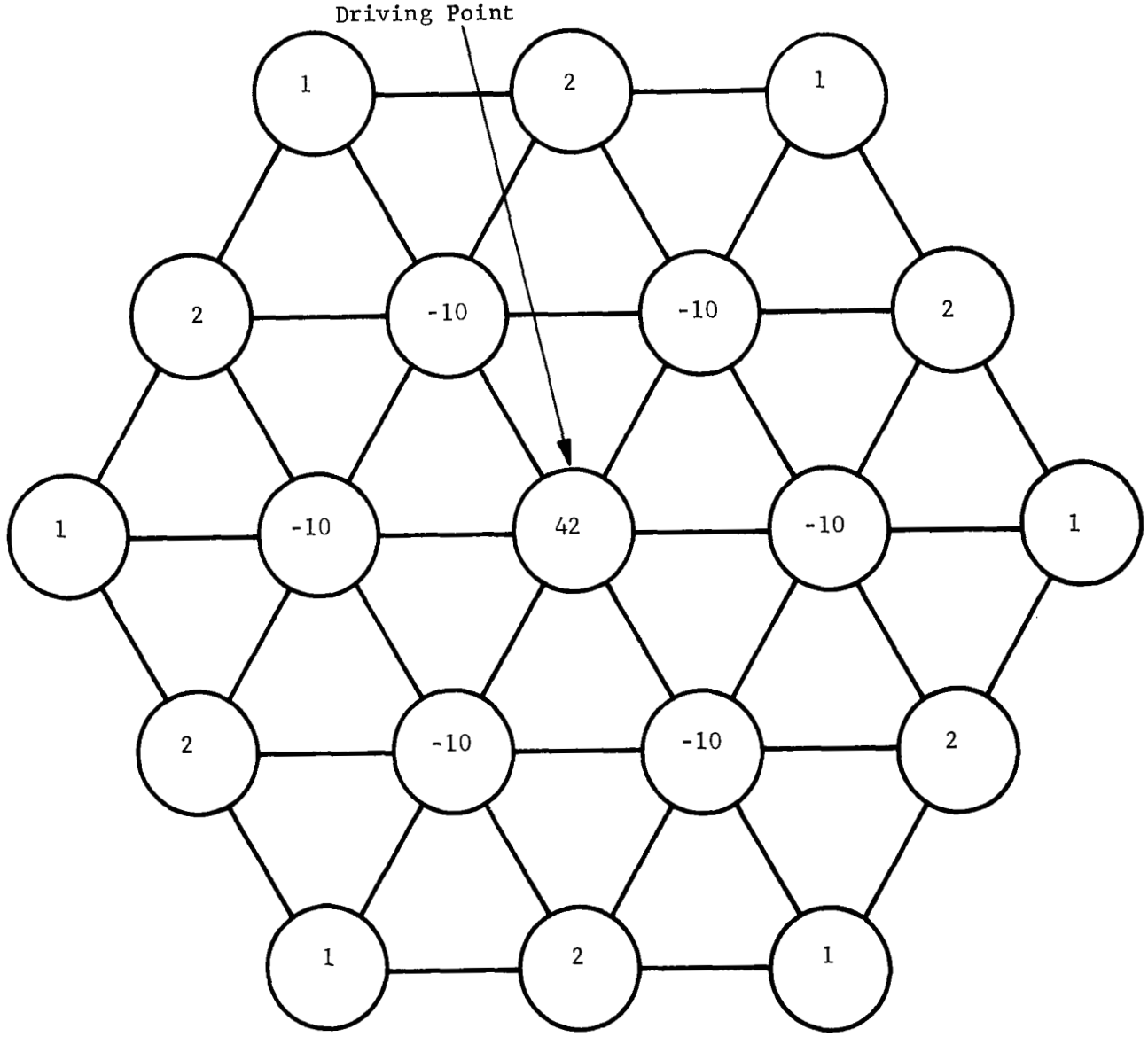

Figure 34. Nineteen-Point Force Configuration to Obtain Local Displacement at Interior Actuator Locations (Numbers indicate relative forces)

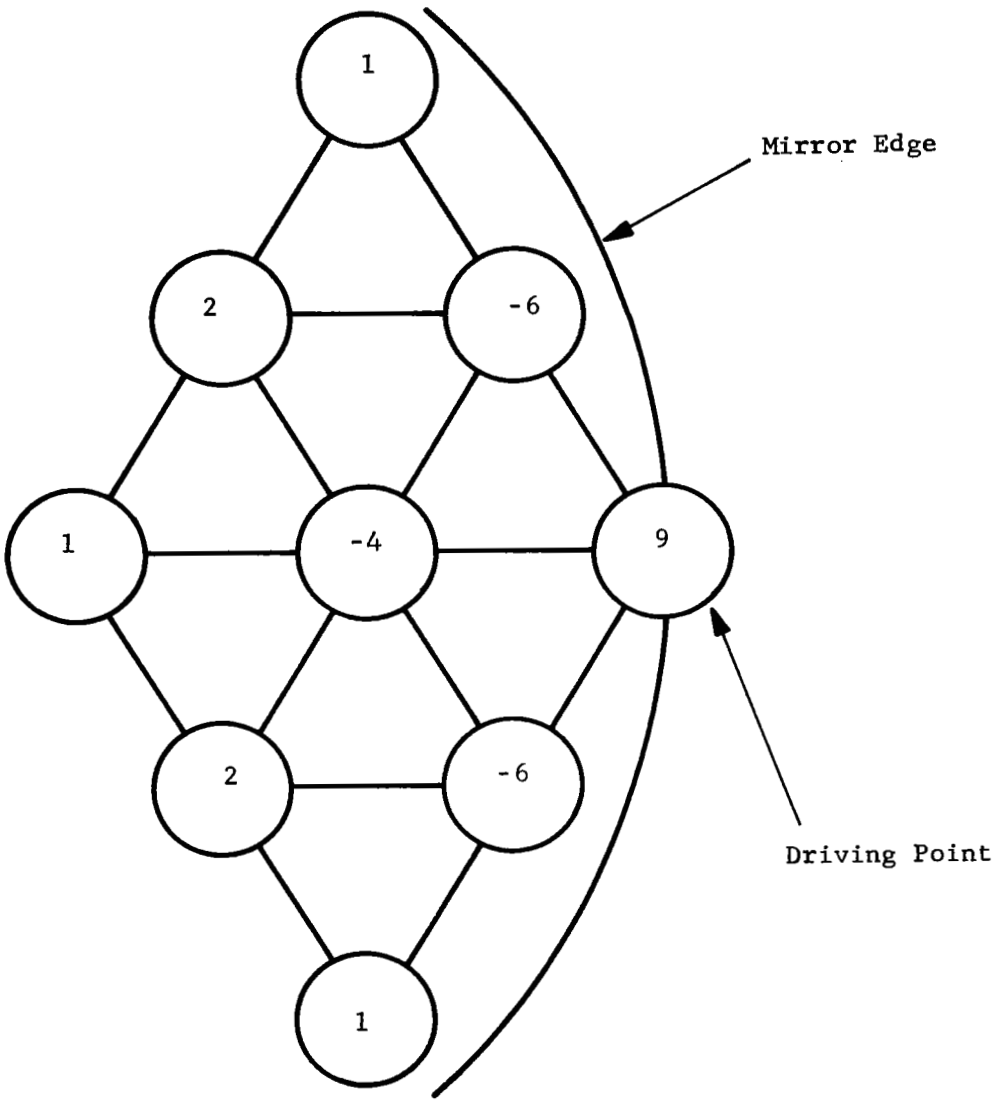

Figure 35. Force Configuration to Obtain Local Displacement at Edge Actuator Location (Numbers indicate relative forces)

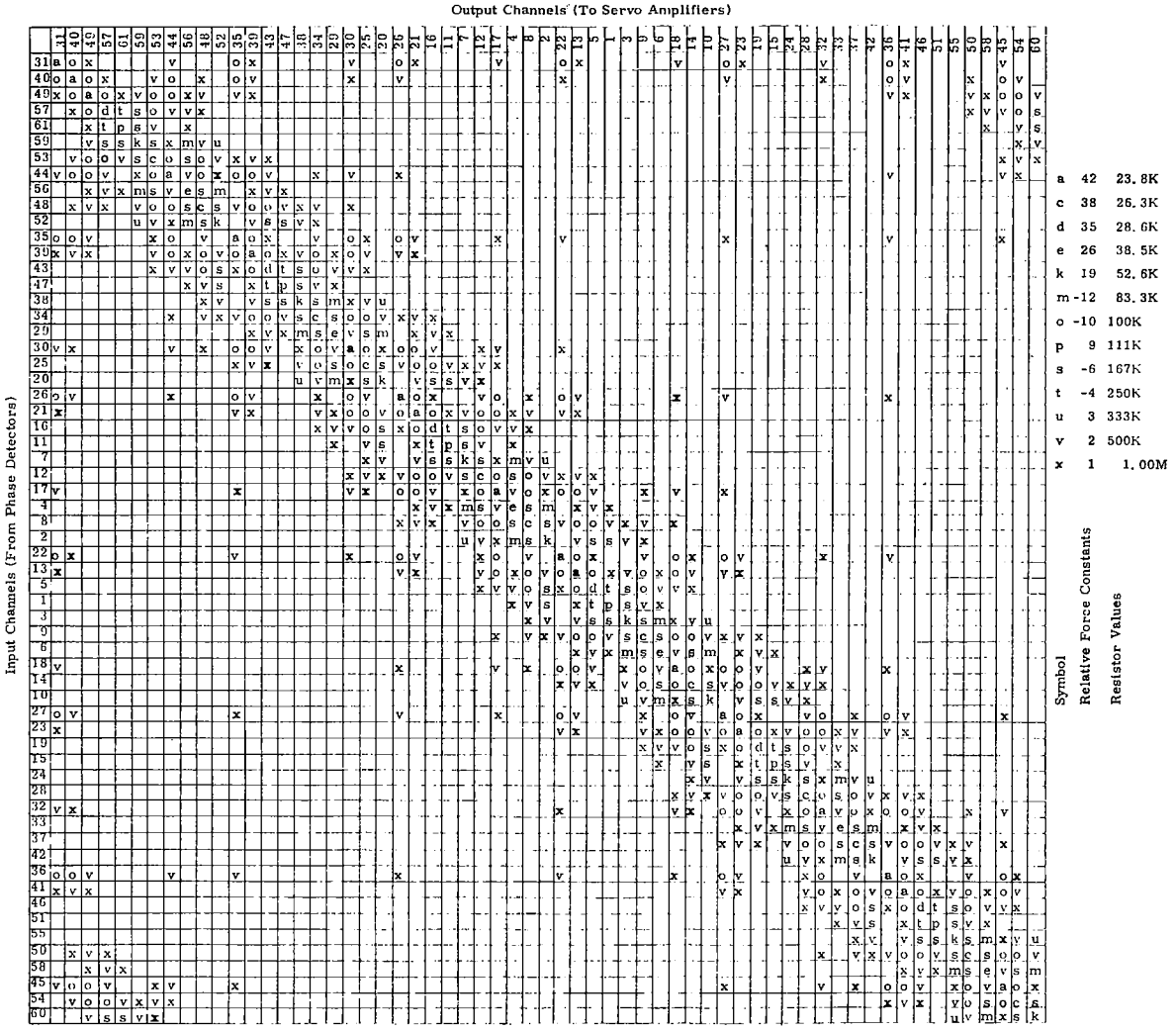

* See figure 2 for channel numbering code.

Figure 36. Feedforward Matrix of Resistors for Counteracting Mechanical Interactions of Thin Mirror

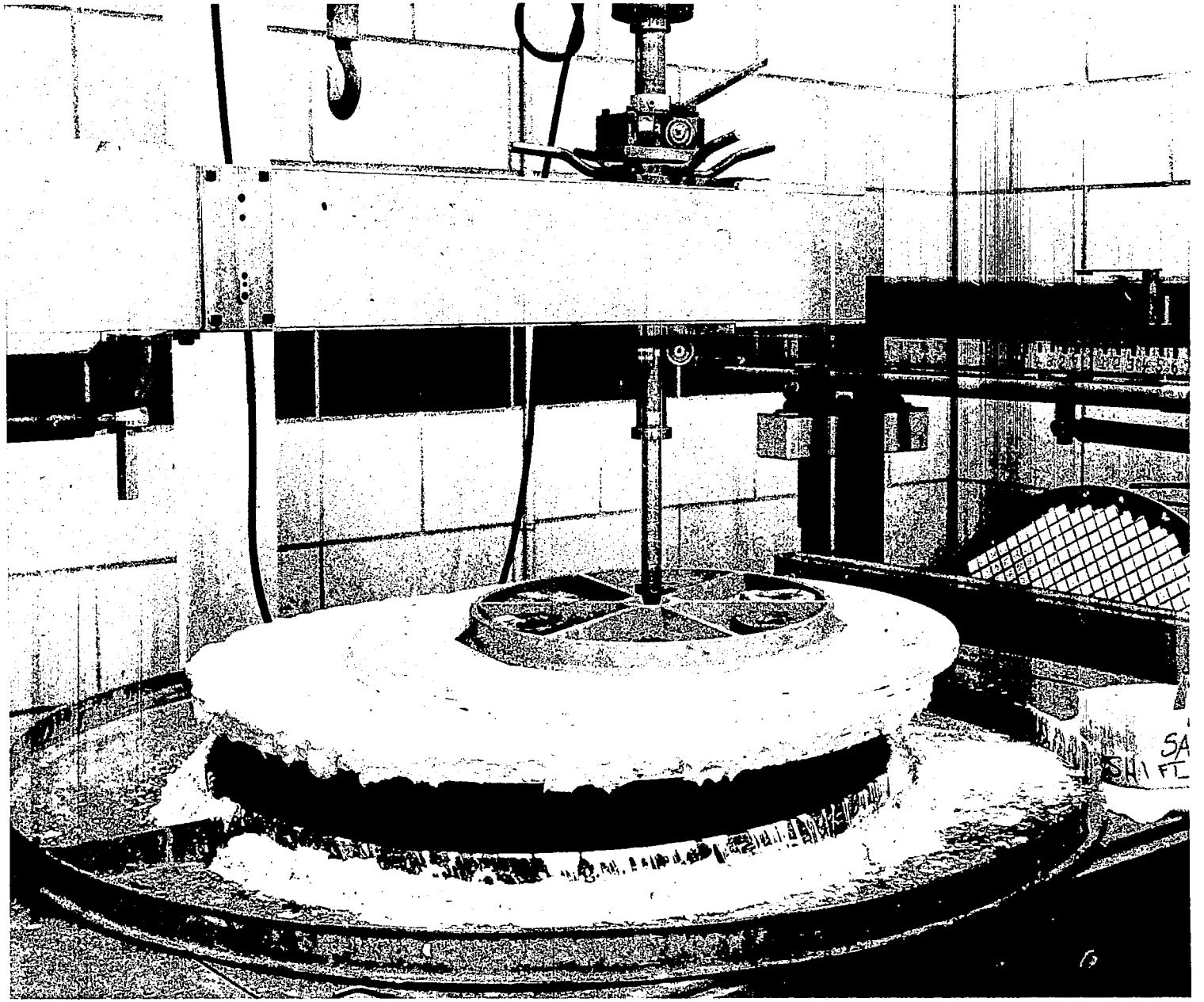

Figure 37. Final Grinding to Reduce Mirror Thickness

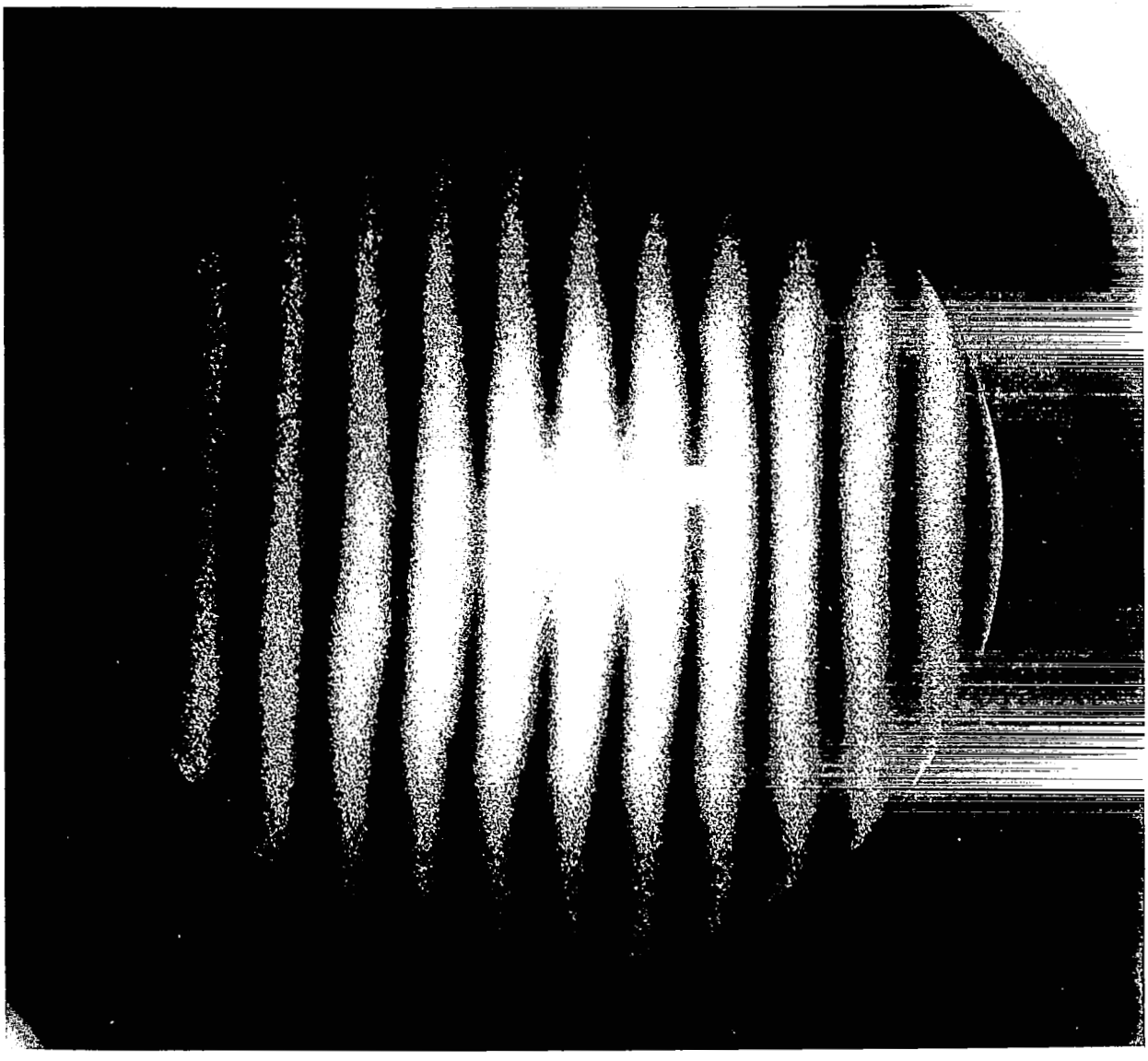

Figure 38. Scatterplate Interferogram of Mirror Before Thickness Reduction

Figure 39. Contour Map of 30-Inch Deformable Mirror Before Thickness Reduction (Contours show departures from a best-fit sphere)

The largest peak deviations of the mirror from a best fit sphere are observed to be +0.06 wavelength and -0.04 wavelength. The mirror therefore was within the tolerances of 1/10 wavelength peak-to-peak that had been desired at this stage. This does not include approximately 1/2 inch of edge around the mirror, which was observed to be somewhat rolled off. This rolling off might have been further reduced in order to bring this 1/2-inch zone within the desired tolerances but little overall improvement in performance of the actively controlled system could be expected for the effort involved.

The test of the 1/2-inch-thick mirror to obtain its figure in an unstressed condition involved considerably more delicacy in the supporting arrangement than did the test of the thick mirror. The rigidity of the mirror is a function of the thickness cubed so that the amplitude of deflection due to a local non-distributed force is on the order of 8^3 times as great for the 1/2-inch thick mirror compared to the deflection produced by the same force on the 4-inch thick mirror. A noncompensated local force of less than an ounce can produce a bending of the 1/2-inch mirror of a wavelength.

The method used to support the mirror during test was an air support technique recently developed at Perkin-Elmer for use with large optical elements and provided a uniform pressure distribution much as the air bag technique does but with fewer problems of pressure control.

The evaluation was performed using a scatterplate interferometer at the center of curvature. The mirror was mounted in a vacuum tank that was evacuated to 2 to 3 inches of mercury absolute pressure, with the optical axis vertical. The interferometer was mounted at the top of the tank just above a vacuum window and, therefore, at atmospheric pressure for convenience of operation.

Measurements of the surface topography of the mirror were performed for several orientations of the mirror relative to the support system. This was done to indicate how much of any observed distortion was caused by the mirror itself and how much was caused by any small nonuniformities in support pressure.

Some variations of figure were observed in the different support positions, introducing an astigmatism on the order of 1/2 wavelength in addition to the distortions that were observed to rotate with the mirror.

The mirror was finally tested while mounted with its axis horizontal on the weight and reaction support system with which it was actually used. Interferograms were obtained with the phase measurement interferometer. The figure observed in this condition was very close to the average of those measured on the pneumatic support, within the plus or minus 1/2 wavelength variation described in the preceding paragraph.

The interferogram and contour map in figures 40 and 41 show the surface figure of the mirror while supported on the weight and reaction support system used in the closed-loop experiment. There are approximately 2 wavelengths of astigmatism plus a kidney-shaped plateau of approximately 1 wavelength amplitude. Although this was more than twice the amplitude initially desired, it was still expected to be within the range of amplitude that could be removed with the designed actuator spacing to obtain a final alignment with less than 1/20 wavelength rms error.

Main Structural Plate

The main plate consists of a 3/4-inch-thick piece of cast aluminum tooling plate with appropriate cutouts to mount actuators, the reaction support system, and the weight support system. Figure 42 shows the backing plate. Since force actuators are to be used, it is not required that the backing plate be extremely rigid, so that the material removed to allow mounting of the actuators and support hardware does not affect the performance of the system. Four safety support arms are mounted on the backing plate as shown in figure 43. These support arms have several important functions: 1) they hold the mirror in position until the spring supports have been attached; 2) they provide support for the mirror while the assembly is being moved so that vibrations will not put an excessive strain on the three locating rods; and 3) they serve as safety snubbers for the mirror in the unlikely event that the support system should fail to hold the mirror. The mirror is mounted on these support arms,

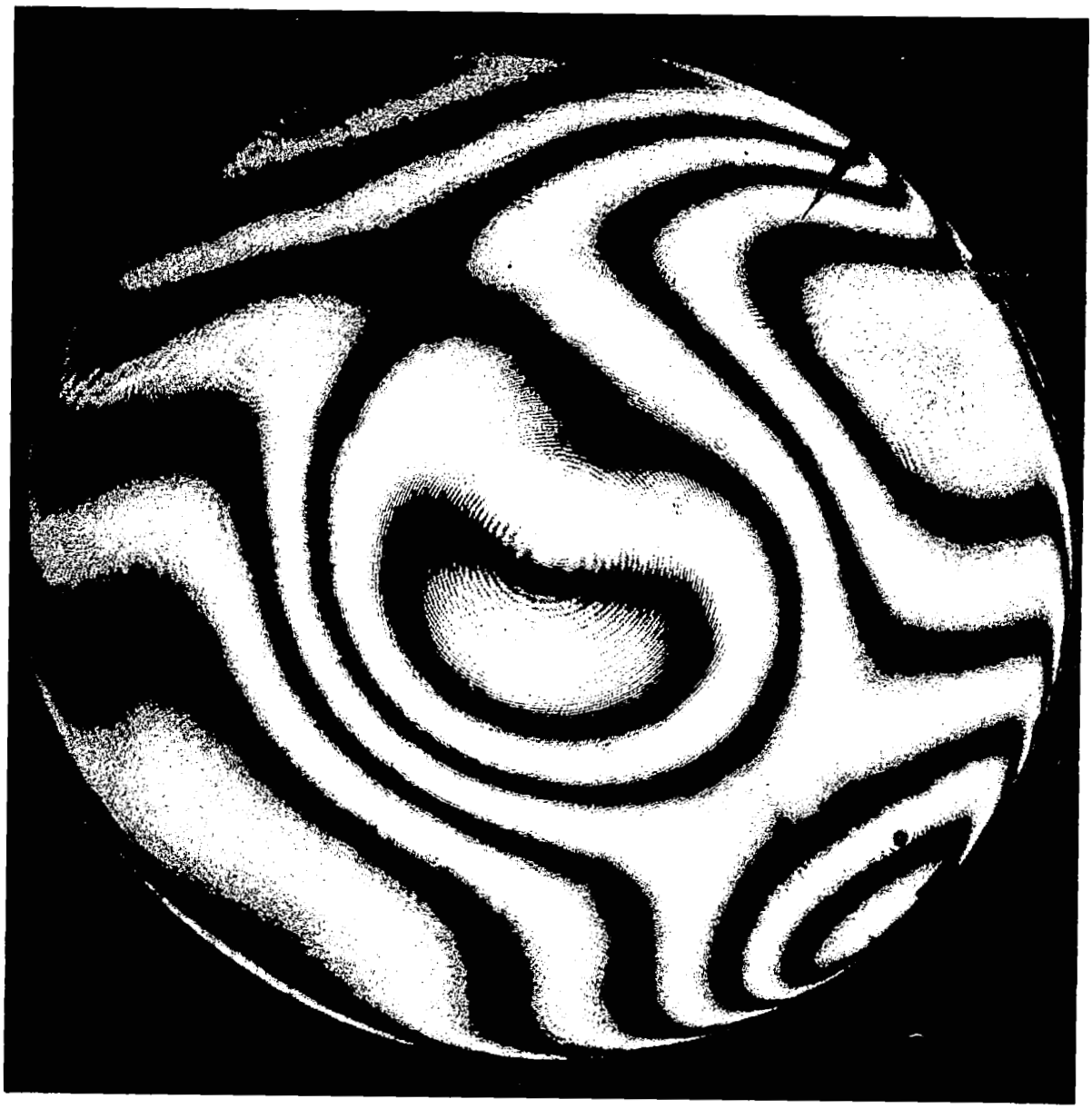

Figure 40. Interferogram of Thin Mirror Before Active Correction (Compare with figure 38)

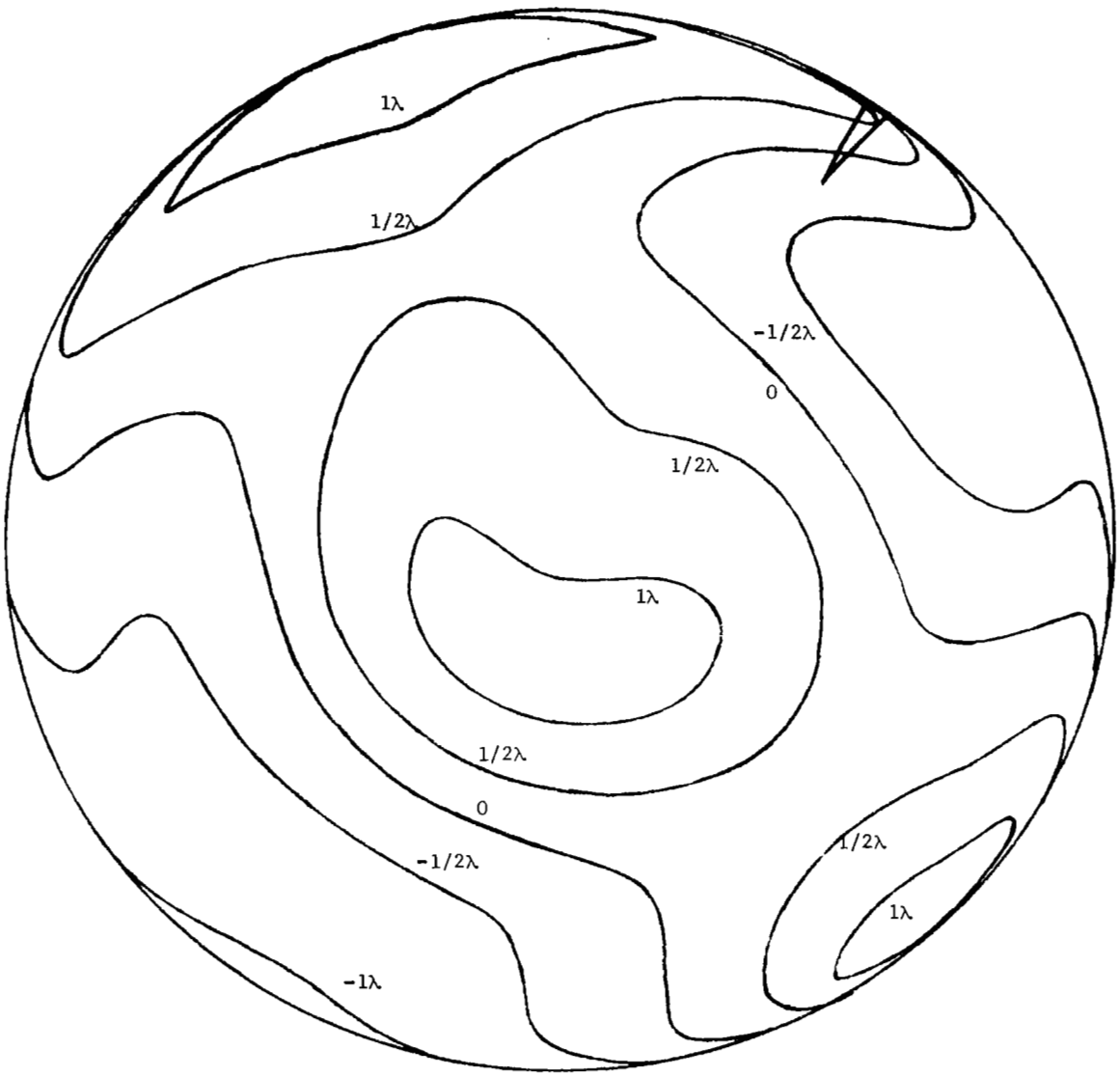

Figure 41. Contour Map of Mirror Surface Showing Deviation in Wavelengths from a Best-Fit Sphere

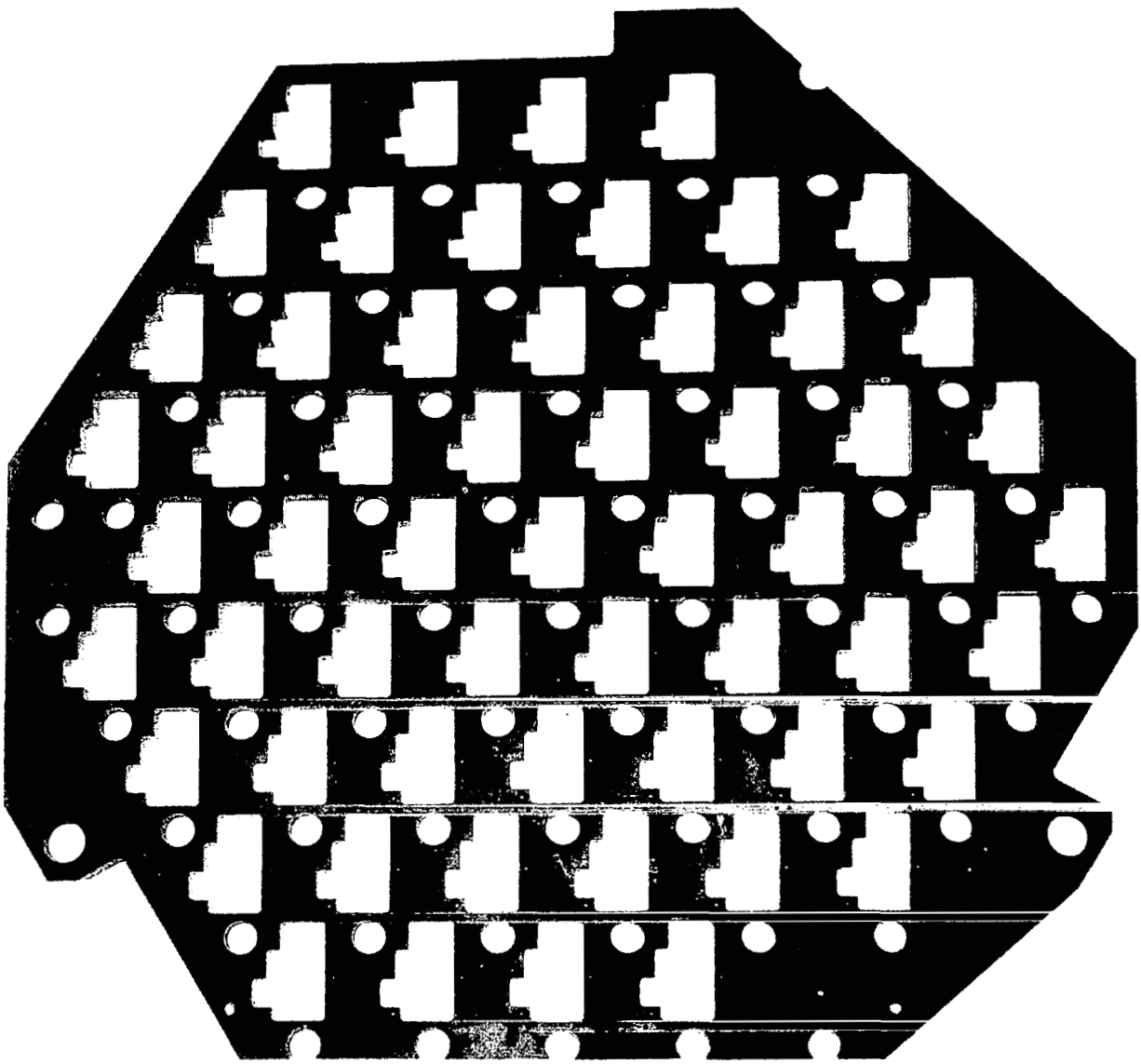

Figure 42. Typical Main Structural Plate

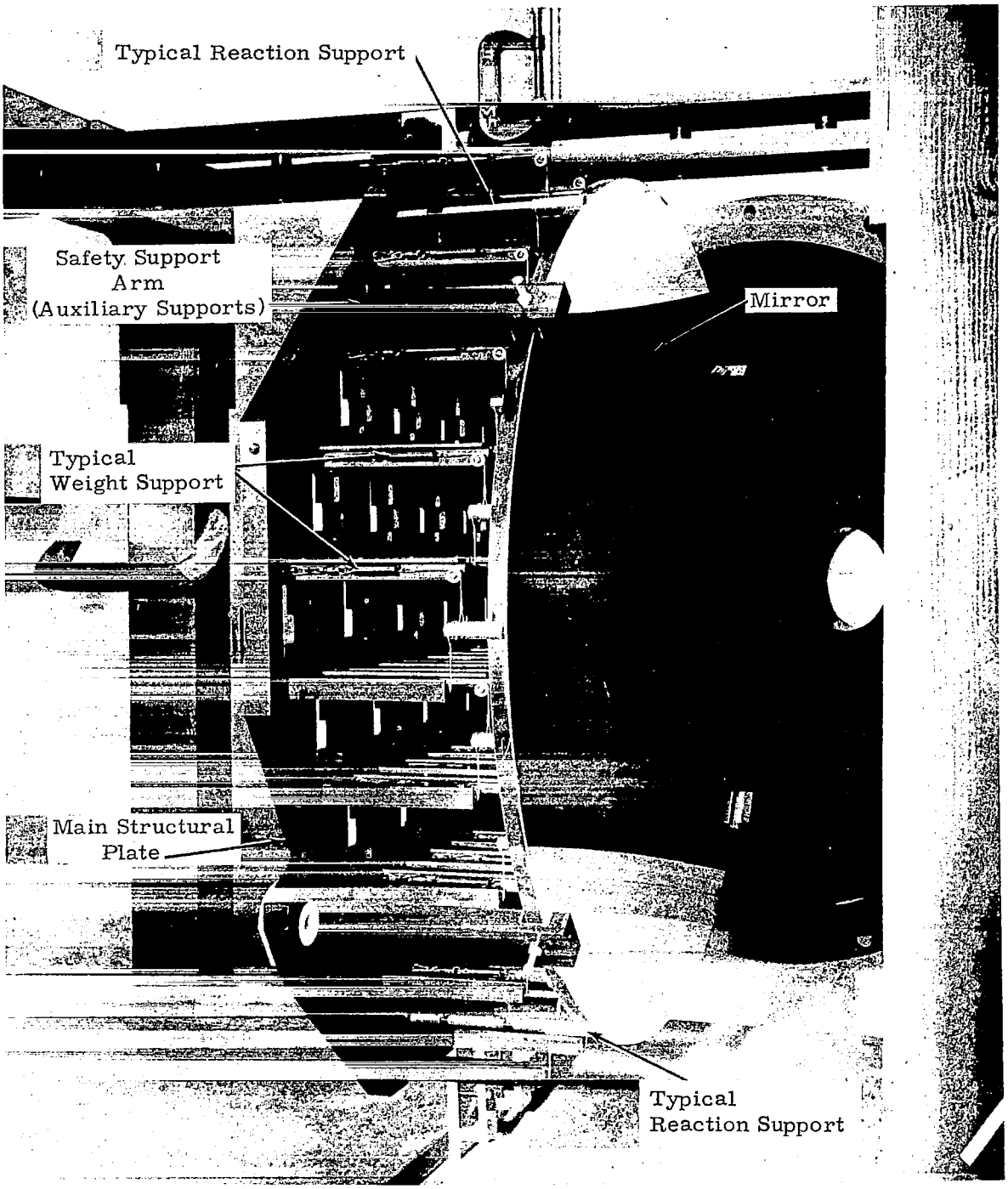

Figure 43. 30-Inch Deformable Mirror and Mirror Support System

resting on nylon-tipped screws. The three locating rods that provide a kinematic mount for the mirror are attached between the mirror and the backing plate. The spring support brackets are attached to the backing plate, and the wires from the springs are looped over Invar plugs into retaining grooves provided in the plugs. Two springs are attached to each plug to provide a moment as well as a lift, in order to balance out the moment that is created as a result of the center of gravity of the mirror being ahead of the points of attachment of the support wires. The tension on each spring is set to precalculated values by adjustments of screws that control the extension of the springs.

Reaction Support System

Attached to the main plate and tied into the mirror is the reaction support system. Its principle of operation is shown in figure 44, and its function is to locate the mirror and react to residual uncompensated actuator loads.

If there were no manufacturing tolerances to consider, the supports could simply be three rigid members. However, since this is not the condition, the mount is designed to be "kinematic" (non-overconstraining) yet rigid in tension or compression.

Each of the three supports (A, B, and C) contains one circular compliant member giving it a rotational degree of freedom. One of the supports (A) contains no other compliant members, a second (B) contains an additional circular compliant member, and a third (C) contains a leaf compliant member.

The circular member permits two-axis rotation, and the leaf member permits one-axis rotation. The axis that is perpendicular to the compliant axis of the leaf is set to pass through another support permitting translation in that direction. Thus, as set up, the supports with two members permit translation to accommodate the fixed position of the one-member support. The leaf acts as a system torsional restraint. The system can now react to the axial imposed loads. The design is geared to the worst case where all actuators act

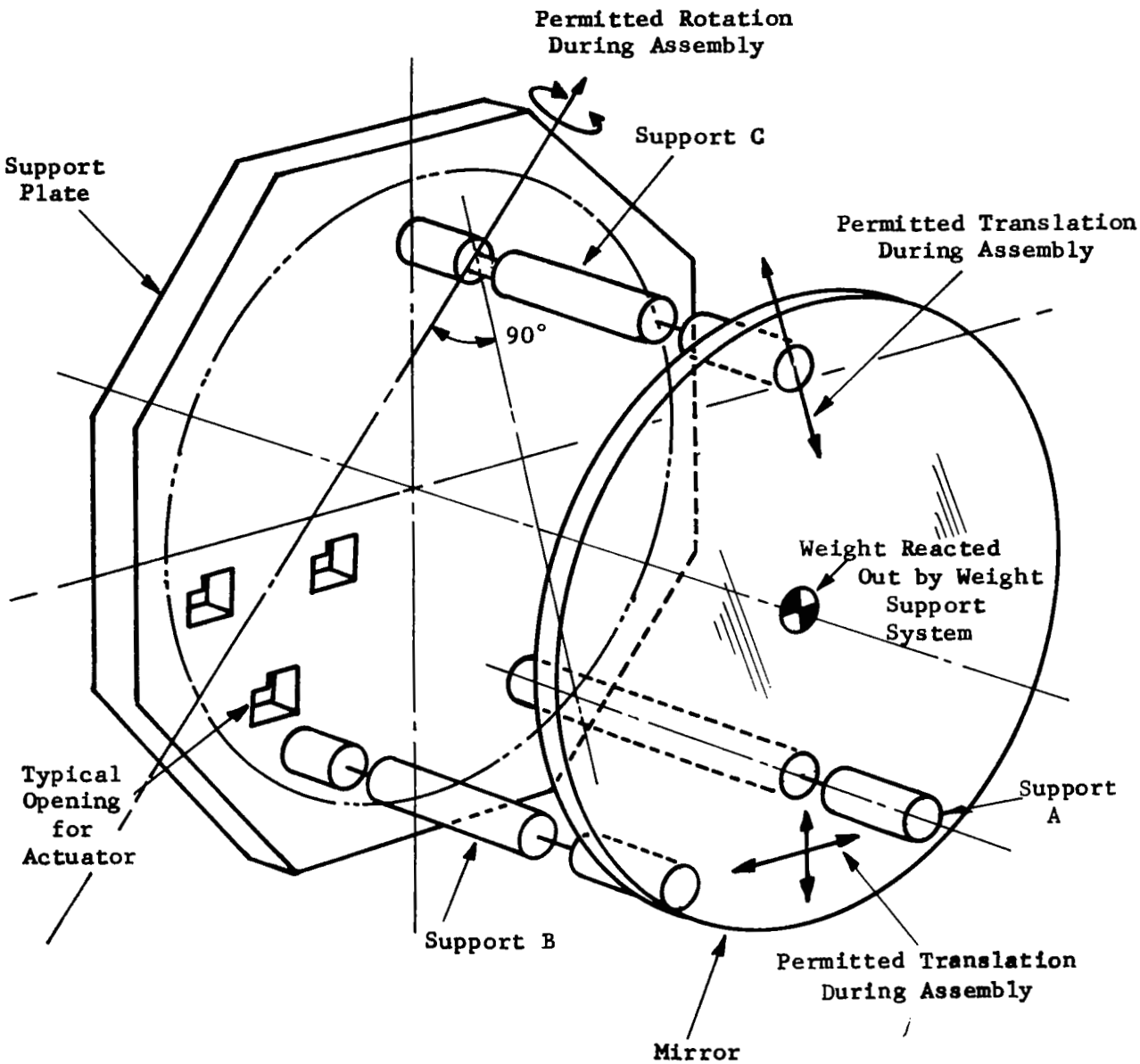

Figure 44. Reaction Support System

simultaneously with maximum load in the same direction. It was found by experience that small misalignments between the locating rods and the backing plate could introduce considerable moments to the edge of a mirror. The mounting therefore incorporates a connection between the locating rods and the backing plate by means of an epoxy cement that is allowed to harden while the mirror is in a comparatively strain-free condition.

Mirror Mounting and Weight Support Arrangement

The connection between mirror and actuators is made by Invar plugs that are fastened to the mirror with epoxy cement. The plugs are made of Invar to reduce shear stresses at the interface caused by differences in thermal expansion coefficients, and the plug cross section is kept small (1/2-inch diameter) to minimize the effect of any stresses set up in the cement. Each plug has a receptacle hole and setscrews to receive and hold the short wire and cylinder at the tip of the actuator which transmits the force. To accurately position the plugs on the mirror, an alignment fixture is used. Figure 45 shows the 30-inch mirror resting on part of its alignment fixture, after the Invar plugs had been fastened in place with epoxy.

The technique used to support the mirror is very similar in several ways to techniques currently being used in other applications at Perkin-Elmer. Figure 46 shows a system consisting of a thin deformable mirror, main structural plate, weight support system, and actuator. An interferogram of the mirror of this system shows an astigmatism of about 2 wavelengths. (As shown in figure 40.) The amplitude and direction of the astigmatism are quite close to those measured in the tests of the mirror on a special air bag support. This shows that the distortion introduced by the support system itself is quite small and well within the range that the actuator system is capable of removing. The figure shows an arrangement using springs for counterbalancing the mirror.

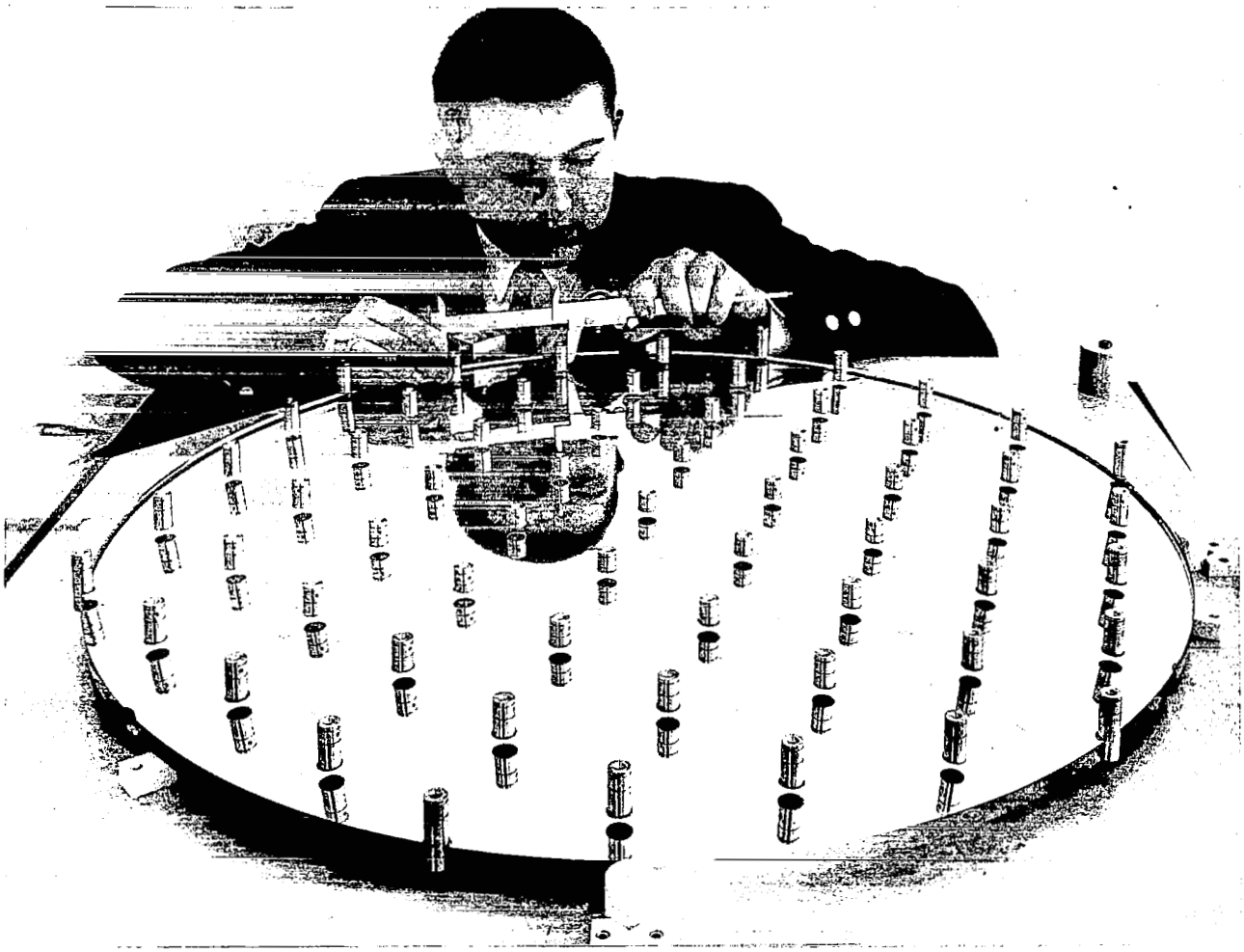

Figure 45. Deformable Mirror with Bonded-on Invar Plugs

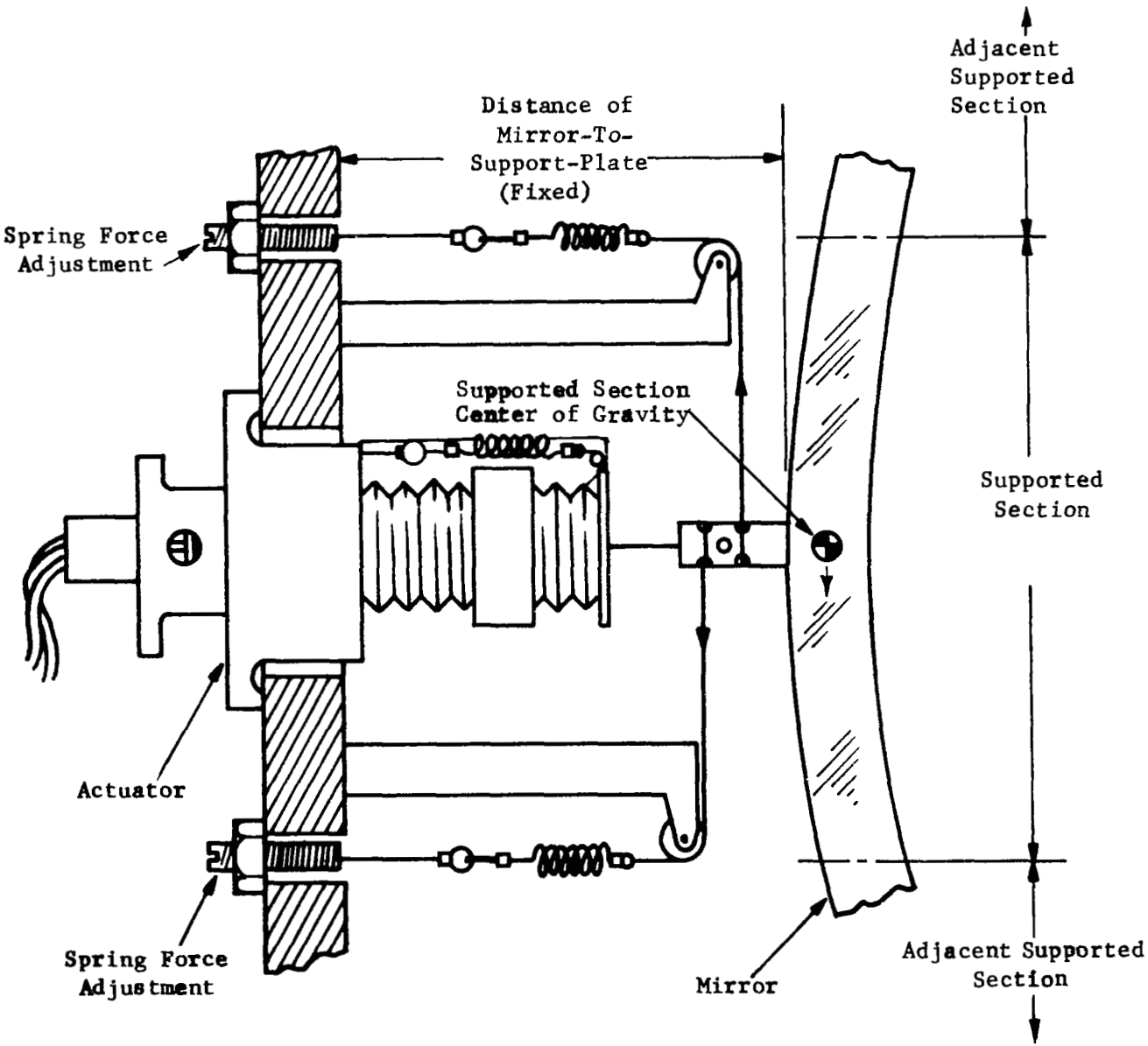

Figure 46. One of Sixty-one Horizontal Weight Supports

Flex Actuator

The Active Optics actuator is shown in figure 47. It is capable of exerting any force up to 2 pounds in either direction on the mirror. An exploded view is shown in figure 48 and two views of the assembly are shown in figure 49.

General characteristics.- The essential parts of the flex actuator are the drive motor, coupling, readout potentiometer, bearing countershaft and leadscrew, translating nut, preload spring, bidirectional force spring assembly, main casting, and minimum moment coupling. The leadscrew is "simply supported" in two places by a pair of preloaded flanged bearings and is driven through a torsionally stiff misalignment coupling by a geared-down motor. The leadscrew passes through a nut that is constrained in rotation by a pin in a precision slot and is loaded from both sides with springs of different spring constants. As the leadscrew is rotated, the nut is translated, simultaneously displacing the two springs. Since the bidirectional force spring is attached to the high-spring-rate, small-displacement mirror, the total force on the mirror can be considered to be governed by the relationship:

$$F = \pm (k\,x)$$

where

F = force on mirror (lbs)

k = "Bidirectional force spring" spring constant (lbs/in.)

$\pm x$ = translation of end of spring

In this manner it is possible to exert either a tension or a compression force on the mirror, depending on leadscrew rotation. In the initial state, no force is exerted on the mirror. However, the translating nut always experiences a unidirectional force of a magnitude never less than that on the mirror. The result is a constantly applied, varying value preload always in the same direction. This is essential to insure that the backlash between the nut and the leadscrew is preloaded out of the servo system. The position of the nut on the leadscrew is monitored by the readout potentiometer.

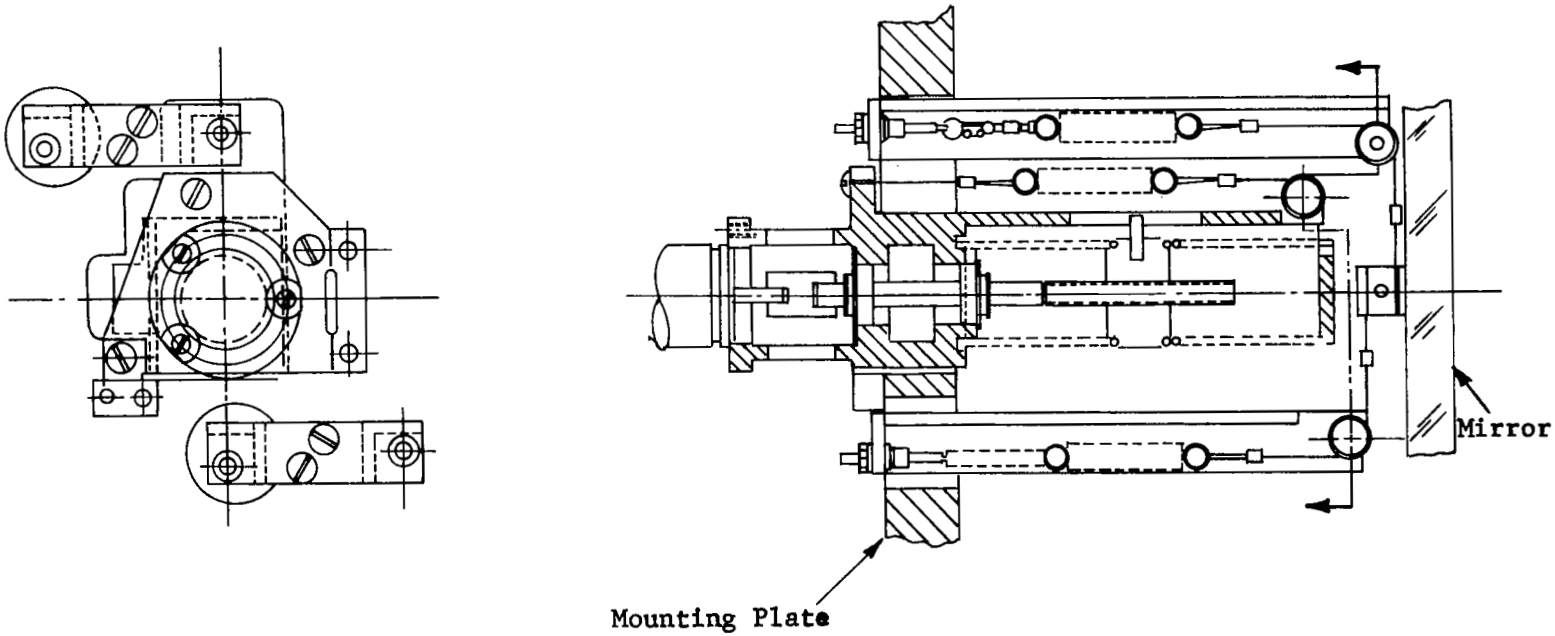

Figure 47. Linear Actuator (Deformable Mirror) Layout

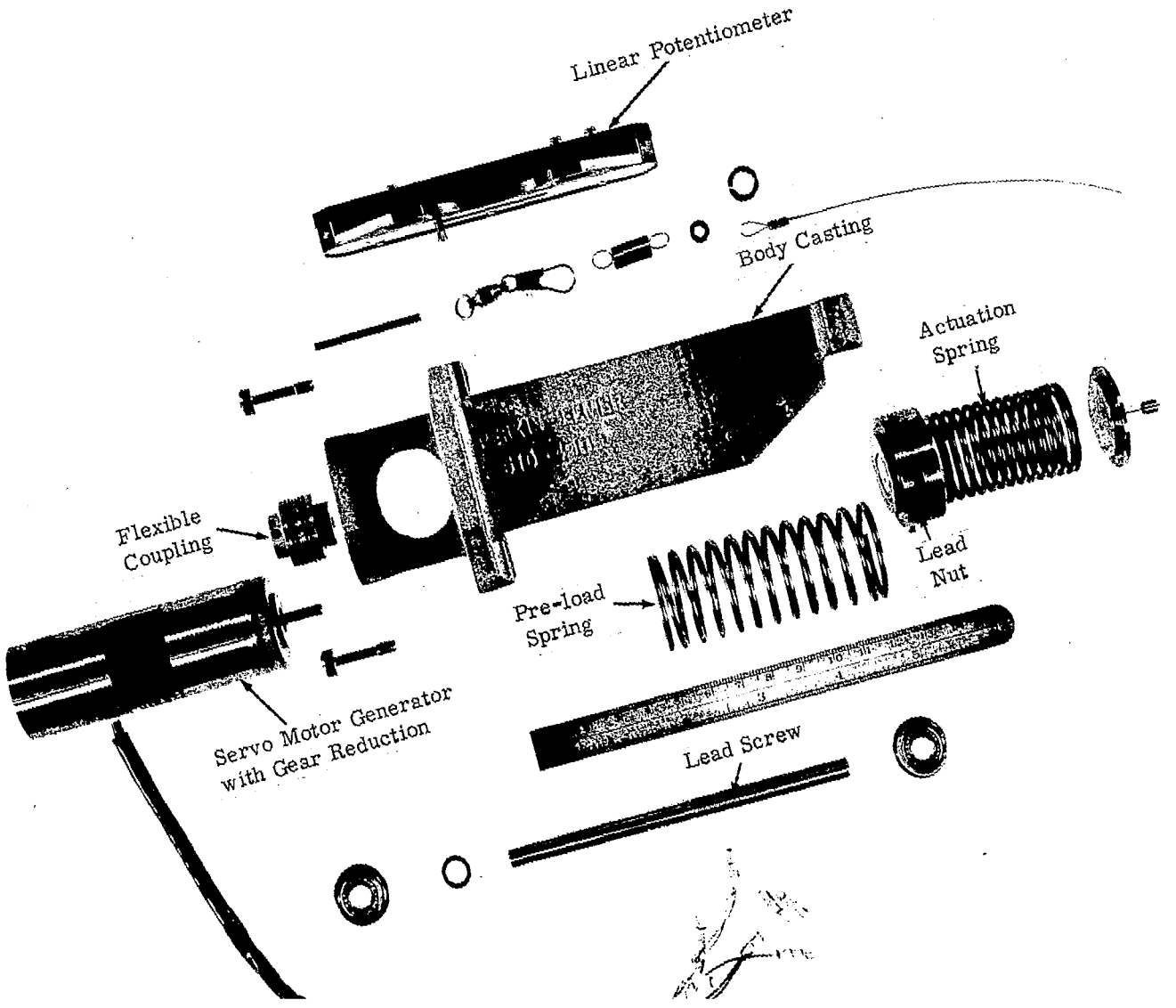
Linear Potentiometer
Body Casting
Actuation Spring
Flexible Coupling
Lead Nut
Pre-load Spring
Servo Motor Generator with Gear Reduction
Lead Screw

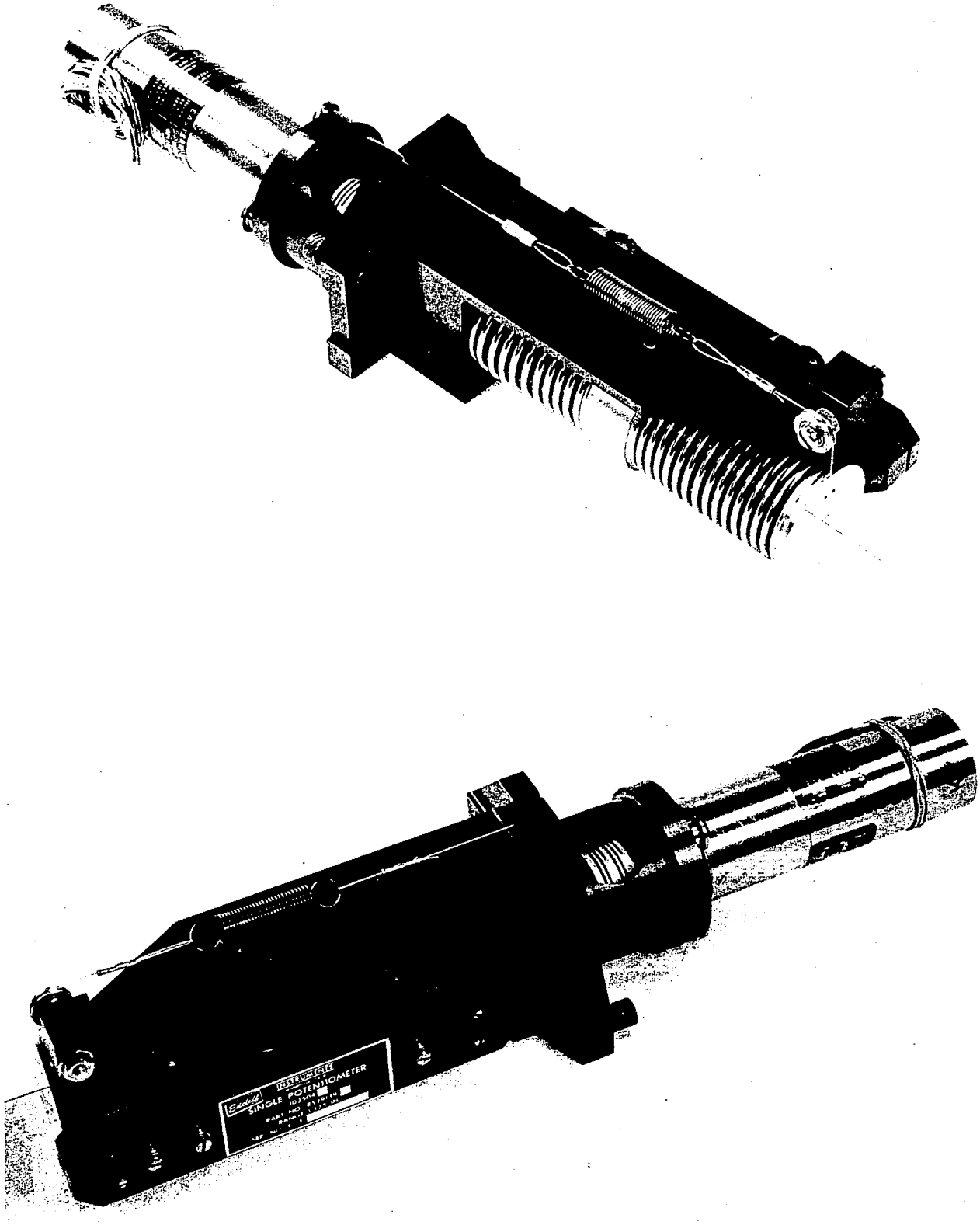

Figure 49. Two Views of a Flex Actuator

The nut will always see a net force in one direction, with the magnitude varying between 1.5 and 12.5 lbs. The mirror will see a force exerted on it varying between 2 lbs tension and 2 lbs compression, passing through zero at the neutral position.

Coupling.- The coupling of the actuator to the mirror is designed to transmit the actuation load axially but to be compliant in bending so as to minimize the initial stress resulting from manufacturing tolerances and misalignment. At the mirror's back surface, the load is distributed over a circular area to eliminate high localized stresses.

The actuator coupling was analyzed to find the minimum diameter (0.010 inch) that would support the maximum load without buckling, and yet would have a low working stress in tension and compression.

Actuator characteristics.- Tests on the actuator in the 30-inch-diameter thin mirror system show that the minimum resolvable motion at the most sensitive area of the mirror, near the edge, is less than 1/250 wavelength at 6328Å or approximately 0.1×10^{-6} inch. The dynamic range is better than plus or minus 25 wavelengths at the same point.

The motion of this actuator is reversible and does not require power to maintain its position since it effectively locks when power is turned off. The actuator has been used in a vacuum chamber and similar actuators have remained in a vacuum of less than 1 mm of Hg for periods of several months with no apparent deterioration in operation. Some modification and selection of materials would undoubtedly have to be performed to insure reliability in a very hard vacuum for extended periods of time, but the principle of operation is compatible with space use.

The linearity of the actuator is the product of the linearity of the servo motor output as a function of the servo amplifier input and the linearity of the spring force as a function of the motor shaft position. The linearity of the spring force as a function of motor shaft position is essentially dependent on the linearity of the spring itself. The coefficient of displacement

for the spring configuration being used stays constant over the operating range to within ±0.02 percent. The servo amplifier uses feedback from a tachometer on the servo motor to maintain the linearity of the rate of change of the motor shaft position as a function of the amplifier input. The linearity of the servo motor shaft rate is essentially determined by the linearity of the tachometer response since the open loop amplifier gain is high. The tachometer linearity is given by the manufacturer as ±0.07 percent. The rate of change of force developed by the actuator as a function of input voltage to the servo amplifier is therefore linear to approximately 0.1 percent over the full range of the actuator.

Actuator assembly.- The actuators were aligned in a separate fixture (figure 50) to a predetermined position to circumvent the necessity of fabricating all mating parts to very high tolerances. Each actuator was placed in its appropriate location on the main structural plate and banked against prealigned registration surfaces. This resulted in very accurate alignment and negligible residual external forces on the mirror.

Mirror, Mirror Support, and Actuator Assembly

Figures 51 and 52 are different views of a completed 30-inch deformable mirror assembly ready for installation into a vacuum tank.

The function of the coarse alignment system (figure 53) is to align the assembly close to the final desired tilt angle. The system consists of two motor-driven leadscrews, each passing through a Teflon bushing in the lower half of the main support plate. The main support plate is pivoted from a captivated 1/2-inch diameter ball, forming both a vertical axis and a horizontal axis of rotation. If each of the servo motors driving the leadscrews rotates in the same direction, the assembly will "pitch", and if each rotates in opposite directions, the assembly will "yaw". This technique gives all the desired adjustments, and provides a rigid link from "ground" to the main plate when not in use.

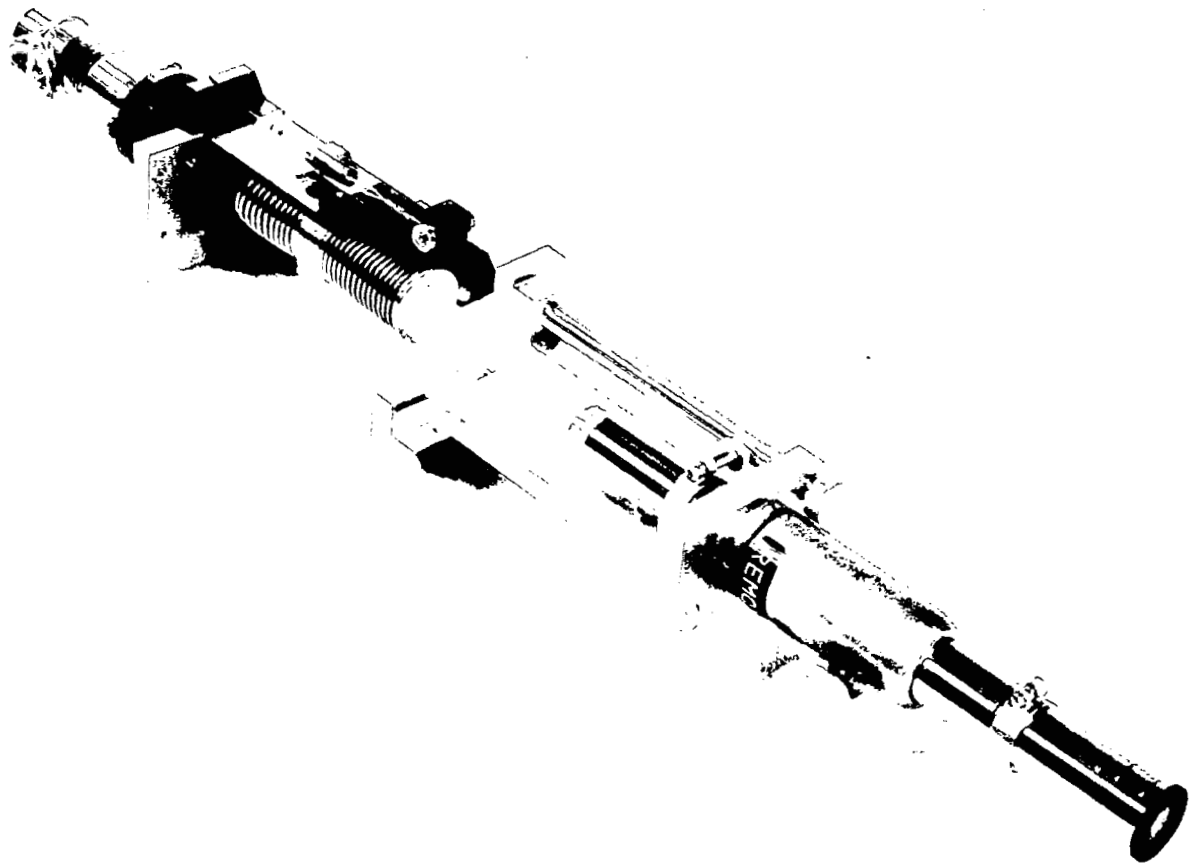

Figure 50. Flex Actuator Aligned in Fixture

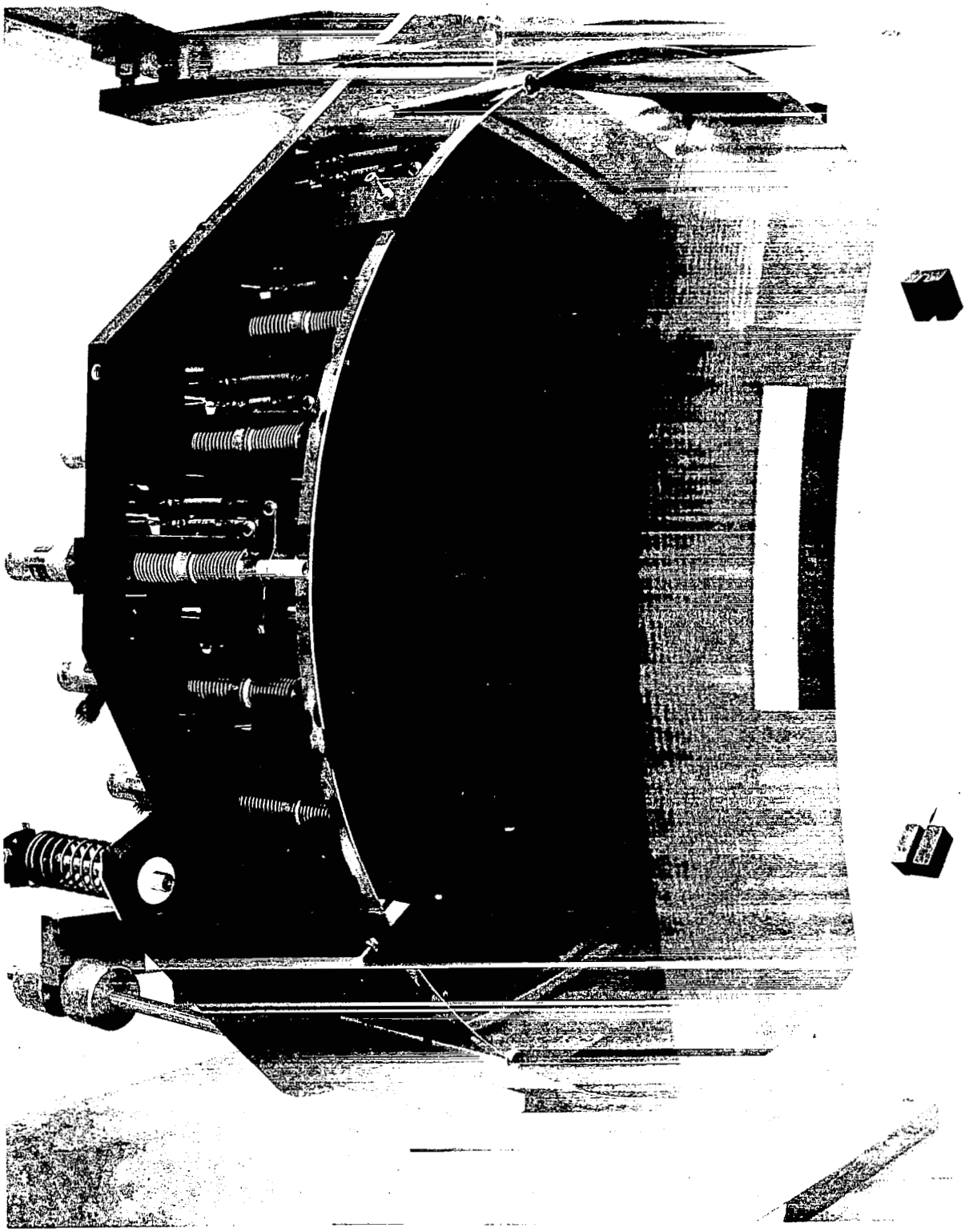

Figure 51. 30-Inch Deformable Mirror Assembly, Front View

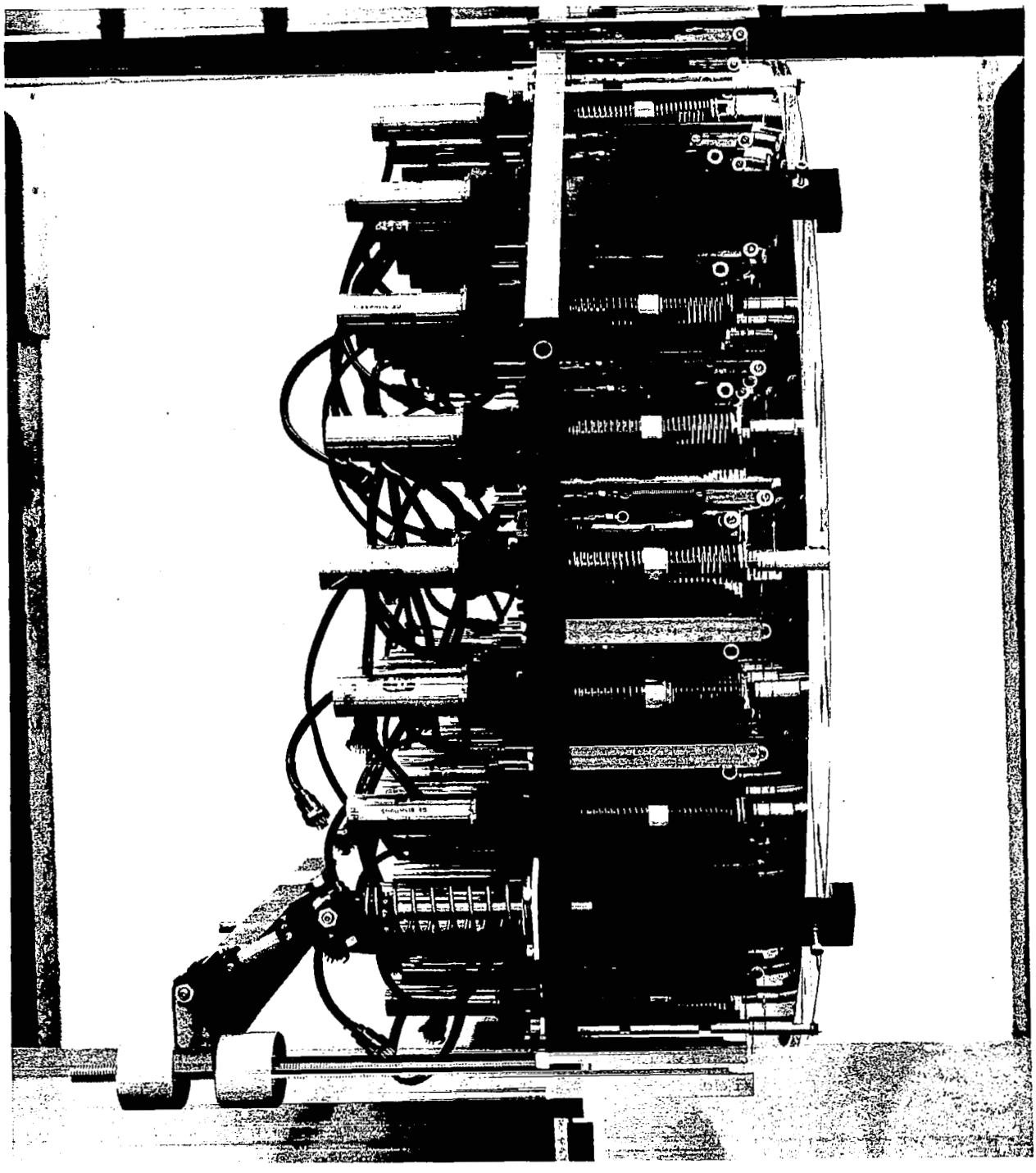

Figure 52. 30-Inch Deformable Mirror Assembly, Side View

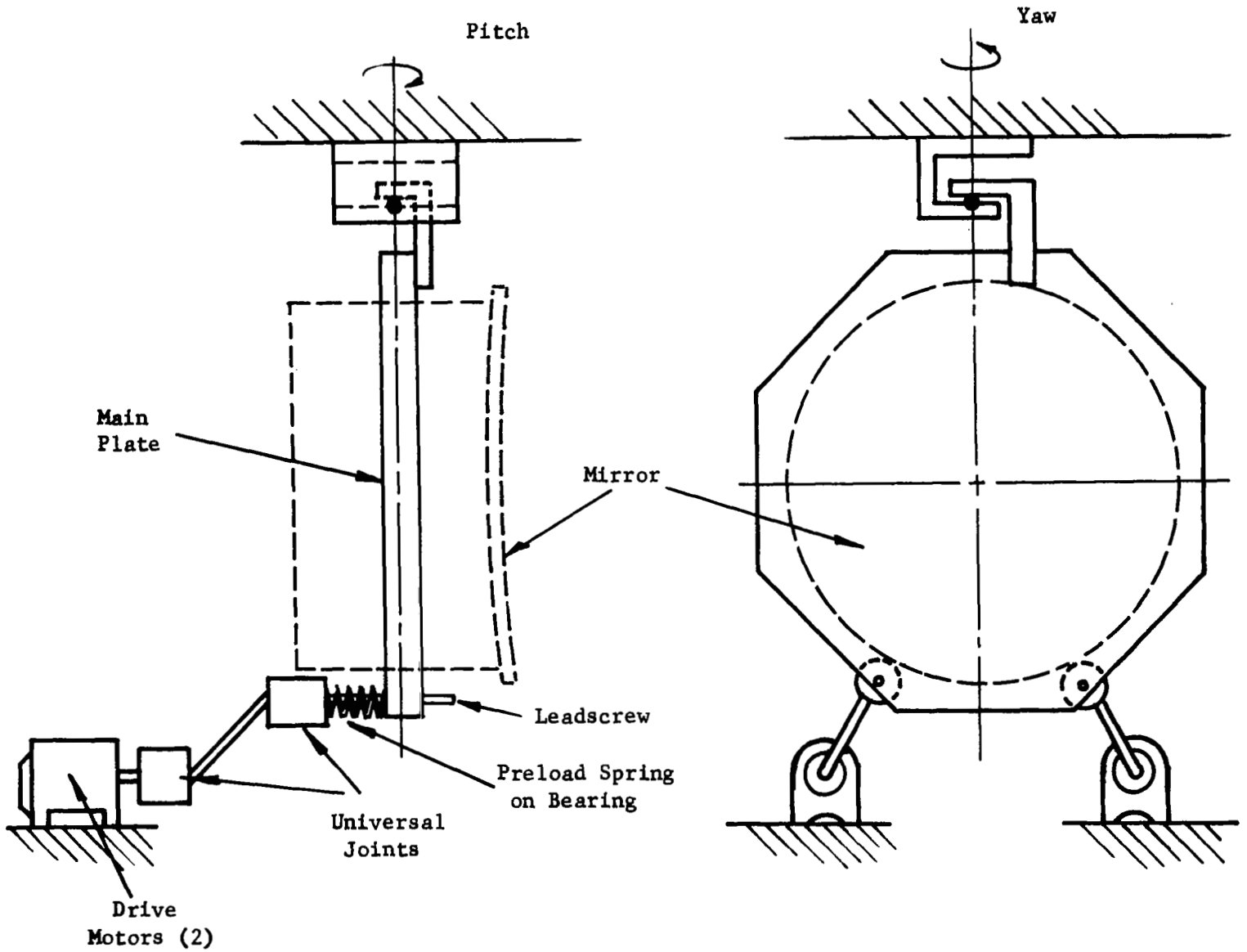

Figure 53. Coarse Alignment System

Figure Sensor

Figure 54 shows a schematic of the figure sensor including the components required to image the mirror on the photodiode matrix as well as on the image scanner. Figure 55 shows a photograph of the hardware. The interferometer assembly uses essentially the same components as the original segmented Active Optics experiment. There are two additional optical mounts, one for the decollimating lens (Lens #1) and one for the reference mirror mount. These permit focus control voltages to position Lens #1 axially, and tilt control voltages to rotate the reference mirror about two axes perpendicular to the optical axis. A beamsplitter diverts 70 percent of the light at the output of the phase measurement interferometer to the photodiode array. The remaining 30 percent of the light is incident upon the image scanner, which now has an S-20 detector surface and a 0.003-inch-diameter pinhole, the combination of which increases its sensitivity by a factor of approximately 40. With the loss of 70 percent to the photodiode array, there is still an overall increase of signal to the image scanner by a factor of 10 over the previous setup used with the segmented optics. The improvement in the signal-to-noise ratio at the output of the image scanner is significant. The light that is diverted to the photodiode matrix passes through a reimaging lens that enlarges the image by a factor of 2.5 to cover the diode array. A mirror flat is employed to fold the optical path to keep the arrangement compact. The beamsplitter, reimaging lens, folding flat, and diode array are shown in figure 55. In the axial alignment actuator arrangement the axial position of the decollimating lens of the phase measurement interferometer is controlled by moving one stage of an XYZ micropositioner with a 400-Hz servo motor connected through a series of gear reductions. A clutch allows manual displacement of the decollimating lens as well as positioning by the servo motor.

The reference mirror tilt control unit is shown in figure 56 and consists of a mirror supported from four piezoelectric bender elements and is driven in two axes of tilt by these elements. The bender elements are mounted in a micrometer-adjusted gimbal suspension for coarse and manual alignment. The mirror is held in a cell to facilitate removal and replacement in the event

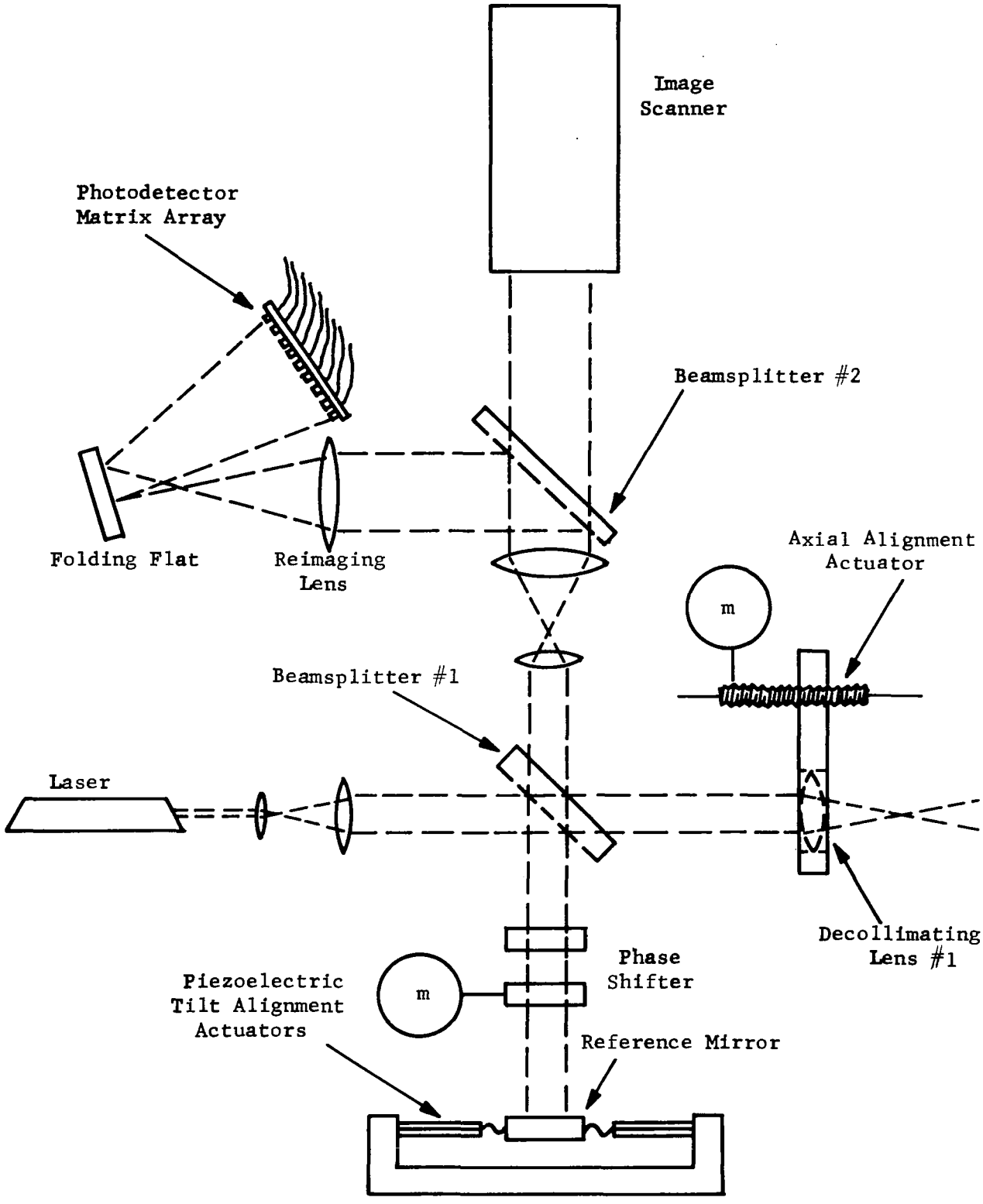

Figure 54. Figure Sensor Schematic

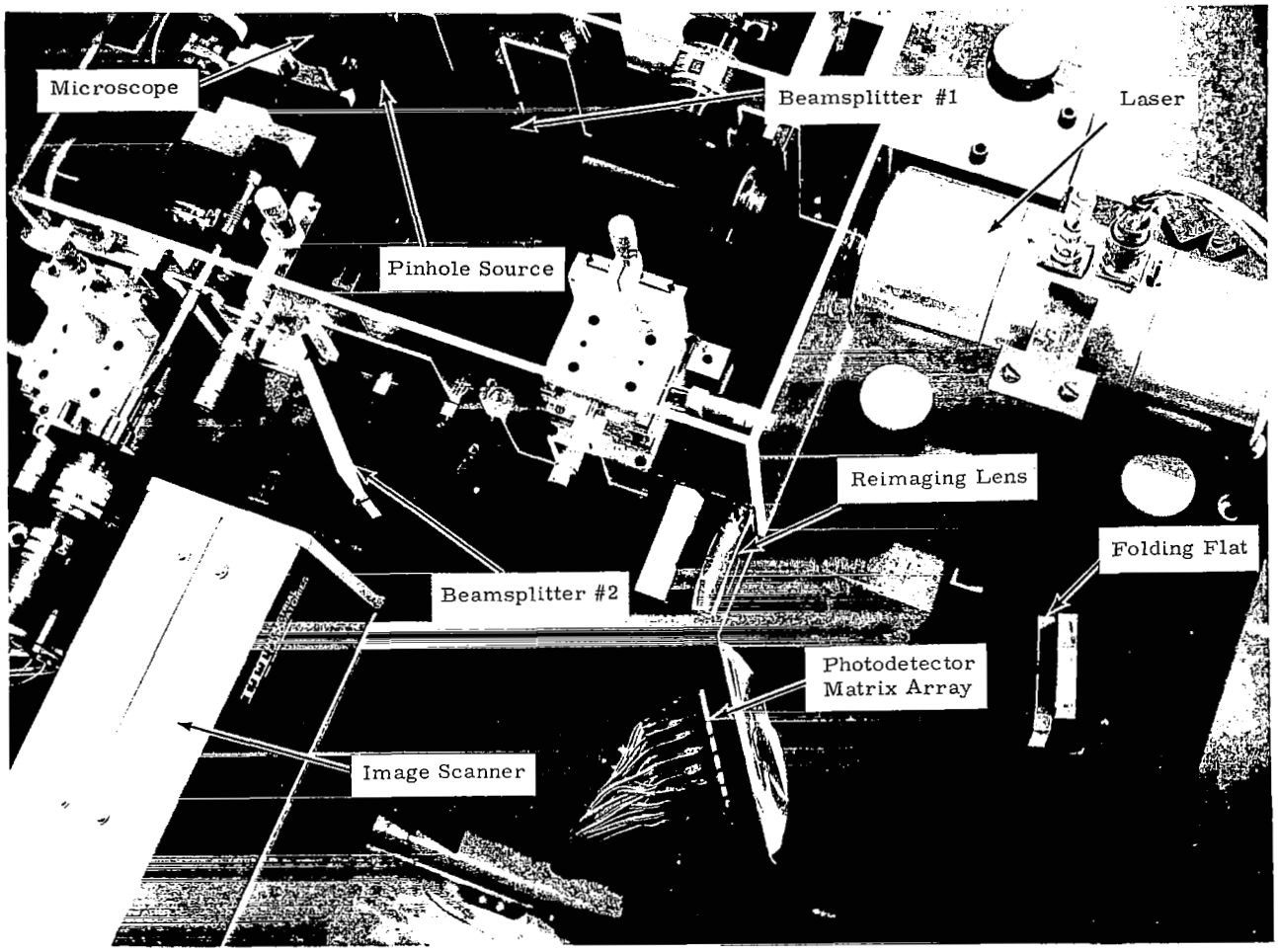

Figure 55. Figure Sensor Hardware

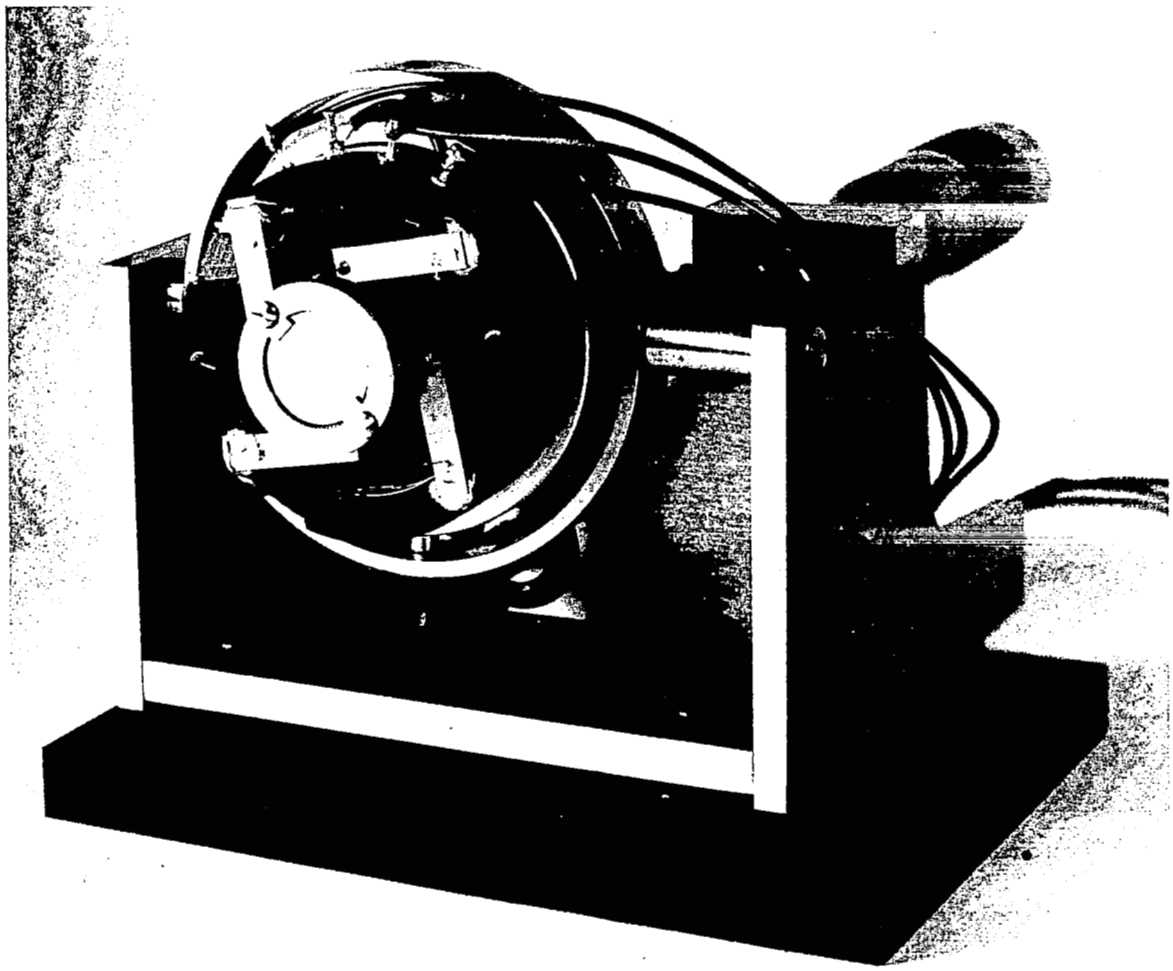

Figure 56. Reference Mirror Tilt Control Unit

that cleaning or substitution is desired. The cell is mechanically connected to the ends of the bender elements by 0.25-inch length, small diameter steel wires that act as flexible couplings in tilt yet are highly rigid in axial translation. The benders are driven in pairs by two identical electronic systems. Each system includes a long time constant electronic integrator and a high voltage amplifier with sufficient gain to raise the output voltage of the integrator to the level required to drive the benders as desired.

Electronics, Feedforward Network, and Alignment Controls

Fotofet detectors.- Rather than use the image dissector with a complex time storing system for 61 channels, it was decided to use a phototransistor detector matrix. This approach is simpler in circuit construction, operates with a lower level of photon noise, is free from crosstalk in signal transmission and behaves without the inherent phase shift introduced by a sample and hold multiplexing system. The image dissector is used as a supplementary detector to provide the scanning ability required for initial alignment and can be used for automating alignment sequencing for automatic correction of large figure errors. Figure 57 shows the circuit devised to increase sensitivity and overcome the effect of variation in the Fotofet detectors by adding simple components to produce adequate output signal level. This circuit arrangement not only makes the circuit nearly independent of parameter change, but also provides gate bias stabilization and moderate automatic gain control.

Servo amplifiers.- The servo amplifier schematic is shown in figure 58. By cascading a push-pull power stage with an operational amplifier, the servo amplifier provides substantial power with a convenient summing network at the input.

As shown in figure 58, the dc error signals are summed by an Analog Device Model 107A operational amplifier. Since many input signals are expected to be summed in the deformable mirror system, a high gain amplifier with low drift was chosen to insure good gain stability. Two chopper transistors, which are driven by a subminiature transformer, are alternately biased on and off to

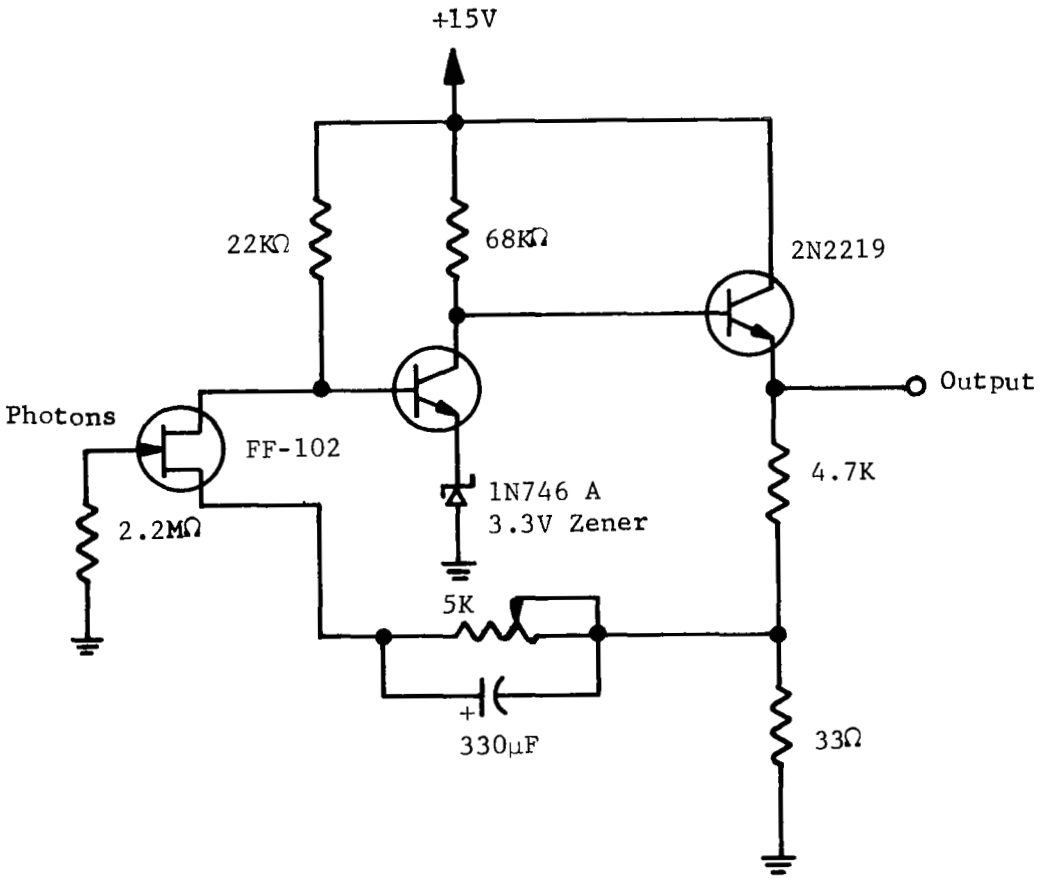

Figure 57. Fotofet Detector and Preamplifier

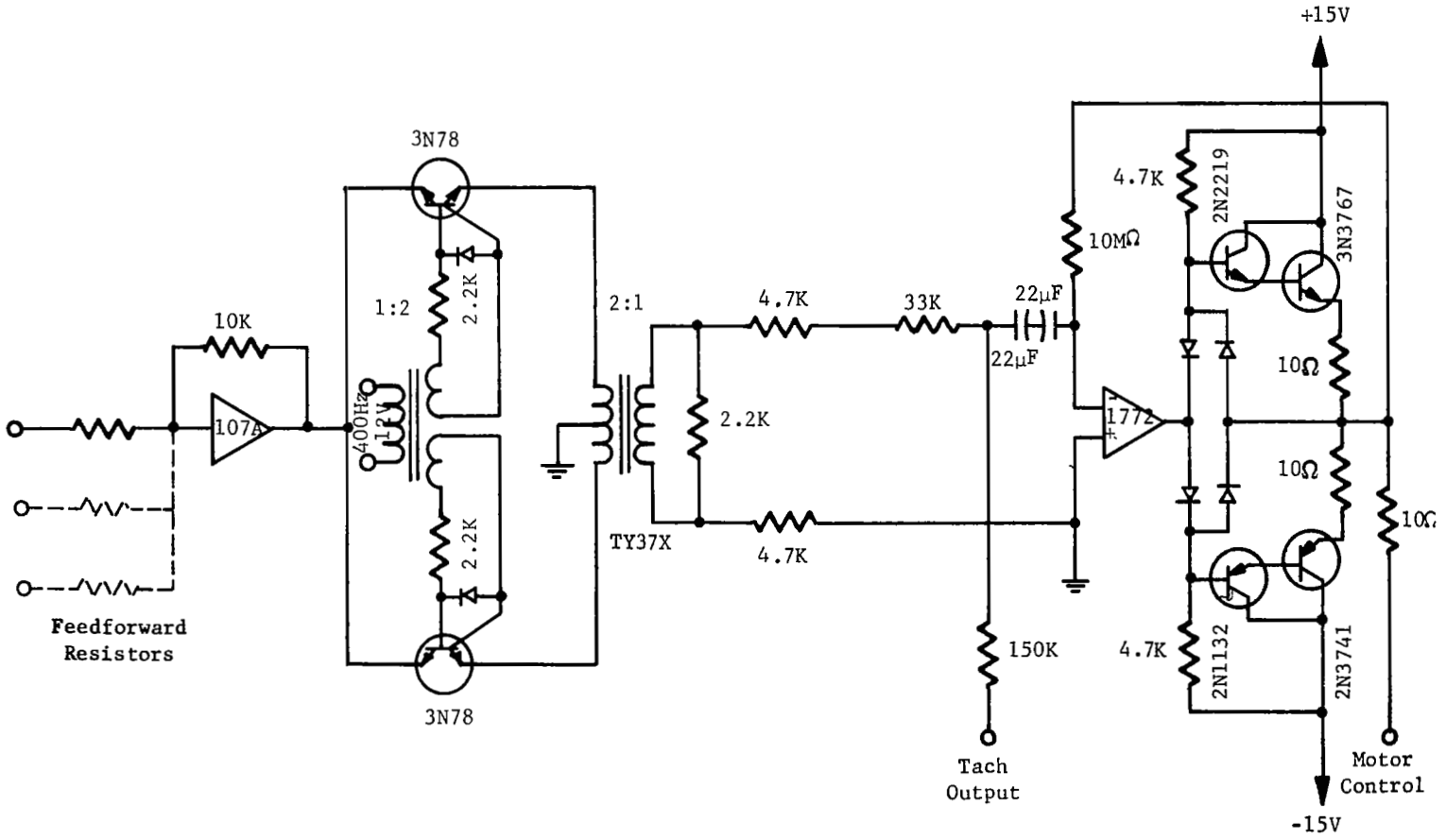

NOTE: All Diodes are 1N483B.

Figure 58. The Perkin-Elmer Servo Amplifier

obtain ac voltage that is proportional to the dc signal in amplitude and whose phase reverses 180 degrees when the signal polarity is reversed. The dual emitter choppers are used to insure a constant offset voltage over a wide range of noise. To insure long life expectancy, it was decided to use a solid state chopper instead of its mechanical counterpart.

A center-tapped transformer with a 2:1 turn ratio is used to provide isolation between the preamplifier and the main amplifier.

The main amplifier consists of an FET wideband operational amplifier, Model 1772, and a class-B power stage. A unity dc feedback insures a good dc stability so that no blocking capacitor is needed in the output. The wideband amplifier provides sufficiently high forward loop gain at 400 Hz. The output current is purposely limited to approximately 100 mA for this application to avoid excessive current drain when many units are in operation. A 10Ω resistor is added in series with the load for further protection of the circuit and to avoid possible instability.

Each servo amplifier is assembled on a printed circuit board for ease in fabrication. Another printed circuit board contains the limiter, phase demodulator, and inverter for each channel. The two printed circuit board assemblies are shown in figure 59.

Feedforward network.- Figure 60 shows the layout of the feedforward network. The resistors are plugged into receptacles on two large printed circuit boards that have the inputs from its phase detectors applied to horizontal conductors on the side shown and that have the outputs to the servo amplifiers connected to vertical conductors on the hidden side. This provides a two-dimensional layout for convenient checking and correlation with the design matrix and allows interchangeability of components for trying different networks. The diagonal elements are the driving point resistors that determine the driving point gains and are multiple turn potentiometers to allow precise gain adjustment.

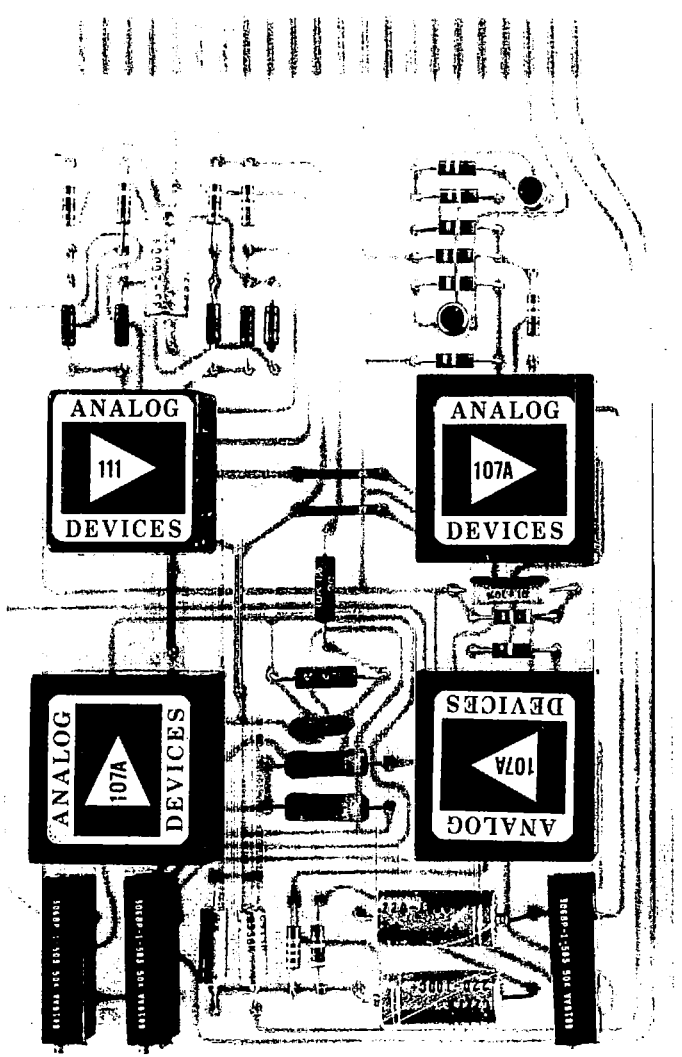

Servo-Amplifier

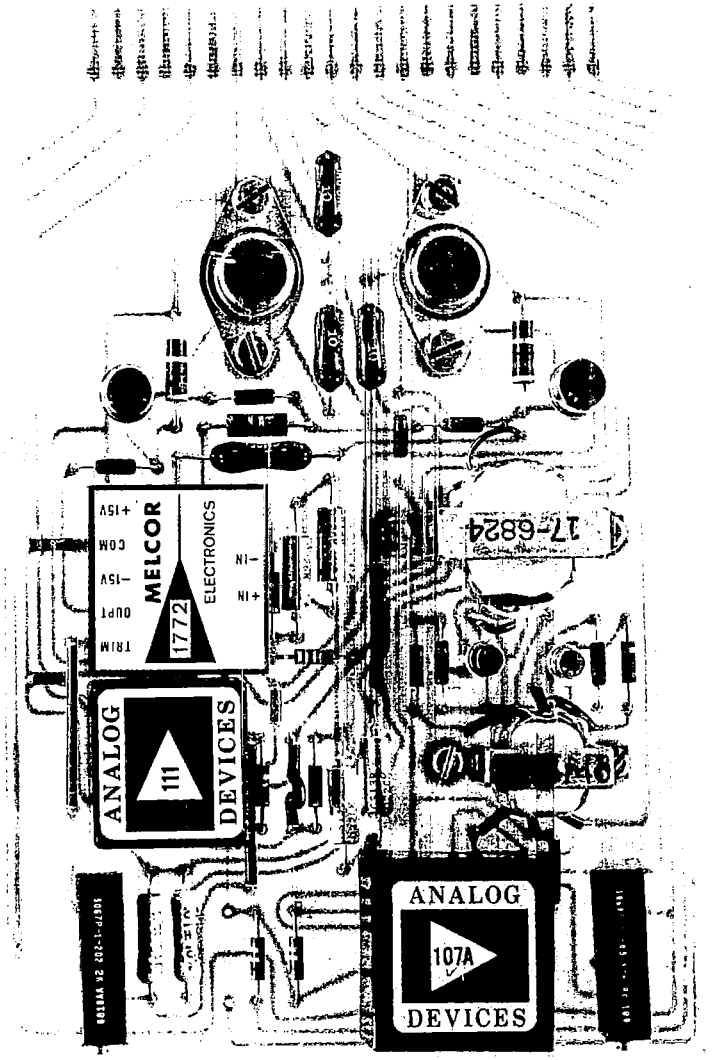

Limiter, Phase Detector, and Inverter

Figure 59. Printed Circuit Board Assemblies

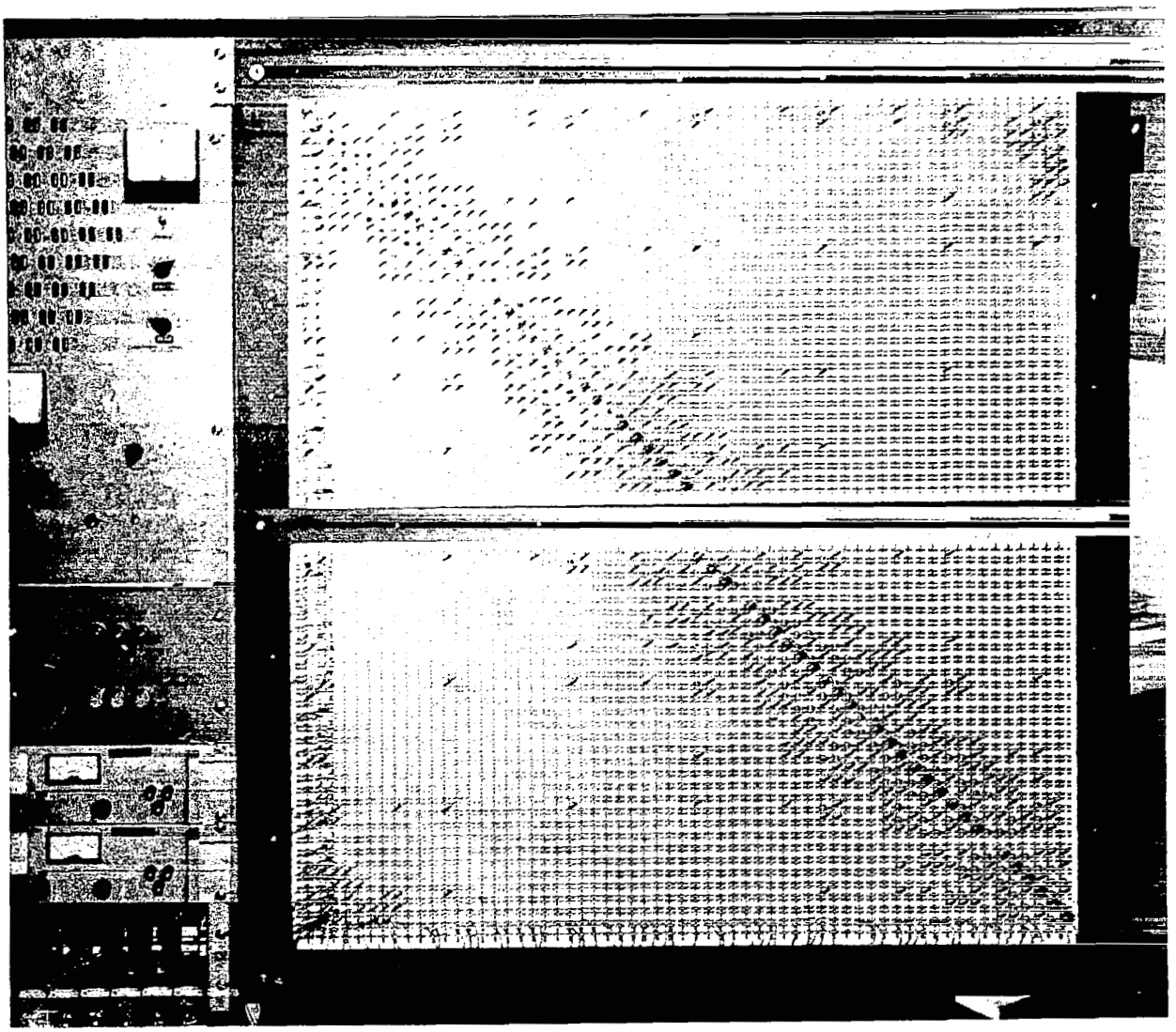

Figure 60. Feedforward Resistor Network Mounted on Printed Circuit Panels

Alignment Controls.- Figures 61 and 62 show the two control panels for test and alignment of the system. The control panel shown in figure 61 has an array of pairs of indicator lights arranged in the pattern of the actuators. These lights give a qualitative indication of the location of the nut on each actuator leadscrew. When an actuator is at its midrange or initial position, there is no force applied by it against the mirror and no voltage across its indicator lights. As the nut moves, causing a force to be applied against the mirror, one or the other of the pair of indicator lights, depending on the direction of the displacement, begins to glow. The intensity of the glow is proportional to the nut displacement from the midposition and hence to the force being applied. The pattern of forces being applied at any instant is therefore evident from the light display. A warning buzzer indicates when any actuator reaches more than 95 percent of its available displacement in either direction. The voltage from the linear potentiometer on each actuator, which operates the indicator lights and the warning buzzer, can be monitored quantitatively on the SERVO POSITION meter. The SERVO SELECT switches determine the channel to be monitored.

Manual control of the position of the actuators is possible by insertion of a dc voltage at the summing points of the amplifiers. The actuator to be controlled is determined by the INDIVIDUAL CHANNEL SELECTOR switches and the amplitude and polarity of the voltage are controlled at the VOLTAGE ADJUST potentiometer and the POLARITY switch.

Manual displacement of a local zone on the mirror is possible by insertion of a dc voltage at the input of the feedforward matrix board. The MODE switch determines whether the voltage is applied at the input of the feedforward matrix or at the input of the individual servo amplifiers, since the same power supply is used in both cases. The LOCAL CHANNEL SELECTOR switches determine the local zone to be displaced and, again, the amplitude and polarity of the voltage are controlled at the VOLTAGE ADJUST potentiometer and the POLARITY switch. The 0 to 6 switch selects the tens digit and the 0 to 9 switch selects the units digit for each of the switch pairs for the LOCAL CHANNEL SELECTOR, the INDIVIDUAL CHANNEL SELECTOR, and the SERVO SELECT.

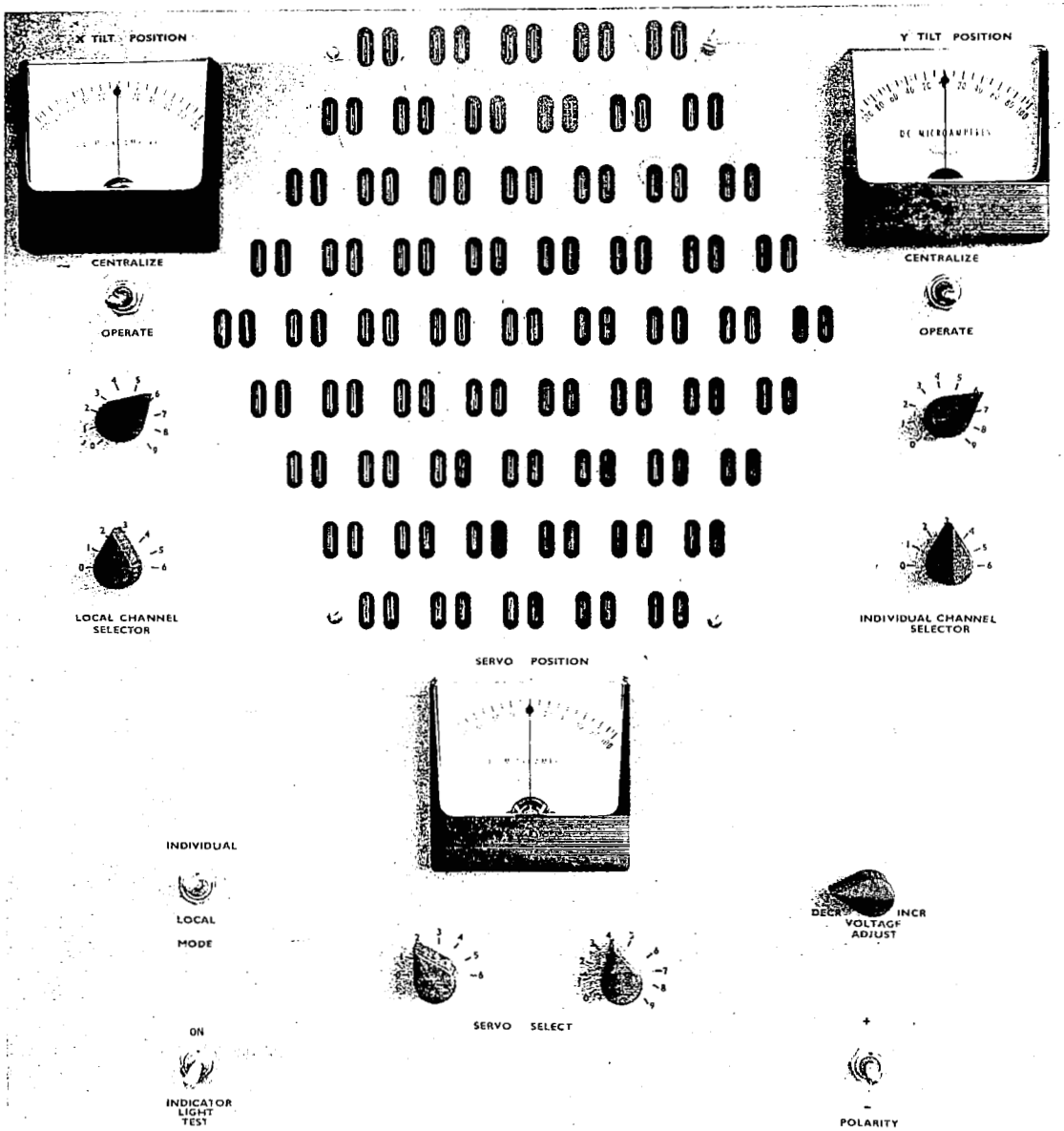

Figure 61. Actuator Control and Indicator Panel

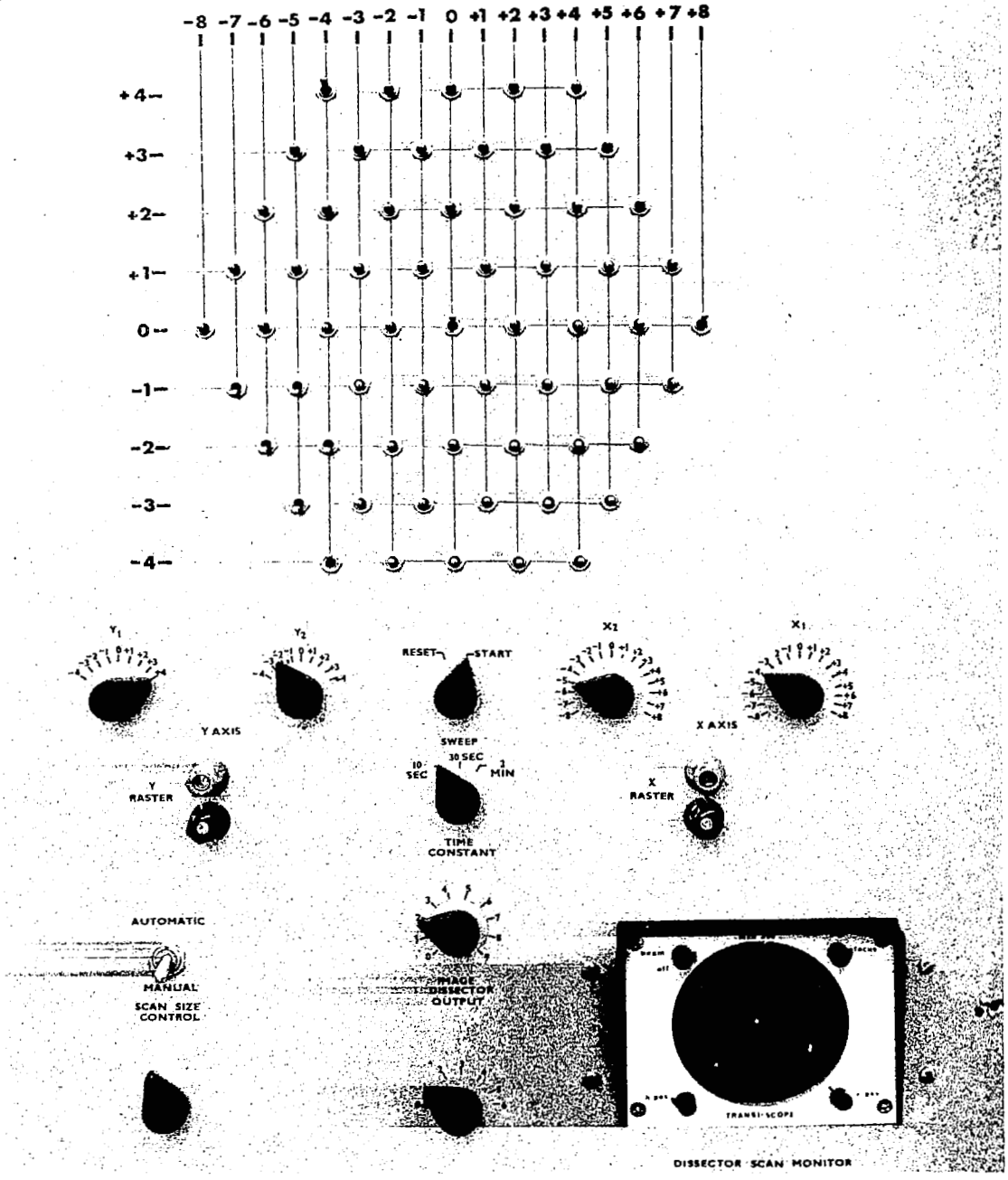

Figure 62. Alignment Control and Indicator Panel

The control panel shown in figure 62 contains the controls for initial alignment of the mirror. The sequencing of operation is manual to allow flexibility for experimentation at this point of development but could be automated. A matrix of three-position switches controls the input to the phase detector of each individual channel. Each switch can be moved from the "up" position where the input to the phase detector is neutral and the output of the phase detector is zero, to the "middle" position where the input to the phase detector comes from the image dissector, and to the "down" position where the input to the phase detector comes from the photodetector array.

The image dissector is time shared between four set of deflection voltages that are coordinated with four outputs. The multiplexing frequency is 6144 Hz so that each of the four points is sampled approximately 1,529 times per second. One of these points is located at the reference coordinates. The second is a movable point that can be scanned between coordinate points determined by the X_1Y_1 and X_2Y_2 coordinate selector switches. The scan starts at the X_1Y_1 coordinate and sweeps to the X_2Y_2 coordinate. The scan rate can be varied by the TIME CONSTANT switch. The third point is used for making raster scans, and its position is determined by external voltages applied at the X RASTER and Y RASTER input jacks. The fourth multiplexed point moves in a continuous circle, the radius of which can be automatically controlled by the amount of tilt existing in the mirror. The deflection voltages applied to the image scanner are also applied to the DISSECTOR SCAN MONITOR scope so that the position of the raster and alignment scanning spots and the amplitude of the tilt scan circle can be visually monitored.

CONCLUSIONS

An Active Optics control system has been designed and constructed, and initial tests have demonstrated that it has achieved an accuracy of control of the figure of a 30-inch-diameter thin mirror to better than 1/50 wavelength rms at visible wavelengths. This exceeds the 1/20-wavelength design goal set for this experiment and meets the requirement of 1/50 wavelength commonly cited as the design goal for a "diffraction-limited" system.

Analysis of the control system response and experimental verification of the analytical predictions indicate that the techniques used in the present system can be applied successfully to the active control of much larger primary mirrors to obtain diffraction-limited performance.

The Perkin-Elmer Corporation,
Norwalk, Connecticut, February 13, 1970

REFERENCES

1. H.J. Robertson: Active Optical System for Spaceborne Telescopes, Perkin-Elmer Corp., Norwalk, Conn., NASA CR 66297, October 14, 1966.

2. H.J. Robertson: Active Optical System for Spaceborne Telescopes, vol. II, Perkin-Elmer Corp., Norwalk, Conn., NASA CR 66489, December 7, 1967.

3. J.F. Creedon and H.J. Robertson: Evaluation of Multipoint Interaction in the Design at a Thin Diffraction-Limited Active Mirror, IEEE Trans. on Aerospace and Electronic Systems, vol. AES-5, no. 2, March 1969, pp. 287-293.

4. R. Crane, Jr.: An Experimental Twenty-Inch Segmented Active Mirror, IEEE Trans. on Aerospace and Electronic Systems, vol. AES-5, no. 2, March 1969, pp. 279-286.

NASA-Langley, 1970 —— 14 CR-1593